

Air Force Institute of Technology

AFIT Scholar

Theses and Dissertations


Student Graduate Works

3-9-2009

Demonstration and Verification of a Broad Spectrum Anomalous Dispersion Effects Tool for Index of Refraction and Optical Turbulence Calculations

J. Jean Cohen

Follow this and additional works at: <https://scholar.afit.edu/etd>

 Part of the [Atmospheric Sciences Commons](#), [Atomic, Molecular and Optical Physics Commons](#), and the [Statistical Models Commons](#)

Recommended Citation

Cohen, J. Jean, "Demonstration and Verification of a Broad Spectrum Anomalous Dispersion Effects Tool for Index of Refraction and Optical Turbulence Calculations" (2009). *Theses and Dissertations*. 2436. <https://scholar.afit.edu/etd/2436>

This Thesis is brought to you for free and open access by the Student Graduate Works at AFIT Scholar. It has been accepted for inclusion in Theses and Dissertations by an authorized administrator of AFIT Scholar. For more information, please contact richard.mansfield@afit.edu.



**DEMONSTRATION AND VERIFICATION OF A BROAD SPECTRUM
ANOMALOUS DISPERSION EFFECTS TOOL FOR INDEX OF REFRACTION
AND OPTICAL TURBULENCE CALCULATIONS**

THESIS

J. Jean Cohen, Captain, USAF
AFIT/GAP/ENP/09-M03

**DEPARTMENT OF THE AIR FORCE
AIR UNIVERSITY**

AIR FORCE INSTITUTE OF TECHNOLOGY

Wright-Patterson Air Force Base, Ohio

APPROVED FOR PUBLIC RELEASE; DISTRIBUTION UNLIMITED

The views expressed in this thesis are those of the author and do not reflect the official policy or position of the United States Air Force, Department of Defense, or the United States Government.

AFIT/GAP/ENP/09-M03

**DEMONSTRATION AND VERIFICATION OF A BROAD SPECTRUM
ANOMALOUS DISPERSION EFFECTS TOOL FOR INDEX OF REFRACTION
AND OPTICAL TURBULENCE CALCULATIONS**

THESIS

Presented to the Faculty

Department of Engineering Physics

Graduate School of Engineering and Management

Air Force Institute of Technology

Air University

Air Education and Training Command

In Partial Fulfillment of the Requirements for the

Degree of Master of Science in Applied Physics

J. Jean Cohen, BS

Captain, USAF

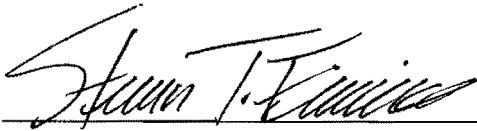
March 2009

APPROVED FOR PUBLIC RELEASE; DISTRIBUTION UNLIMITED

**DEMONSTRATION AND VERIFICATION OF A BROAD SPECTRUM
ANOMALOUS DISPERSION EFFECTS TOOL FOR INDEX OF REFRACTION
AND OPTICAL TURBULENCE CALCULATIONS**

J. Jean Cohen, BS
Captain, USAF

Approved:



Steven T. Fiorino (Chairman)

20 Feb 09

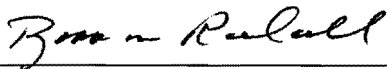
Date



Michael A. Marciniak (Member)

20 Feb 09

Date



Robb M. Randall (Member)

18 FEB 2009

Date

Abstract

An atmospheric optical turbulence strength, C_n^2 , model with a broad wavelength range of 355nm (ultraviolet) to 8.6m (radio frequencies) has been created at AFIT and implemented into the High Energy Laser End-to-End Operational Simulation (HELEEOS) tool. This modeling and simulation tool is a first principles atmospheric propagation and characterization model. Within HELEEOS lies the High-Resolution Transmission Molecular Absorption (HITRAN) database, containing 1,734,469 spectral lines for 37 different molecules as of version 12.0 (2004). HITRAN affords HELEEOS incredible accuracy for electromagnetic (EM) propagation prediction.

A full understanding of C_n^2 is needed to successfully predict EM radiation propagation, particularly within the application of high energy laser weapon systems. Existing models for C_n^2 do not encompass wide ranges of wavelengths, nor do they include anomalous dispersion effects. Both of these additions have been incorporated into AFIT/CDE's new optical turbulence strength model. This thesis's objective is to verify and demonstrate the C_n^2 prediction tool. This tool enables predictions to occur in notoriously difficult regions of the spectrum to measure (i.e. Terahertz). One can measure C_n^2 at one wavelength and accurately determine C_n^2 at a different wavelength based on the relation of the vertical gradient of the index of refraction, $(\frac{\partial n}{\partial z})^2$, to C_n^2 .

Acknowledgements

Thanks to God - from whom all good knowledge and wisdom is gained.

~~~~~

I would like to express my sincere appreciation to my faculty advisor, Lt Col Fiorino for his guidance and support throughout the course of this thesis effort. His energy and motivation are truly rare and valuable qualities. To Dr. Marciniak and Maj Randall, thank you for providing me the foundation of knowledge I needed that allowed me to produce this work. To Chris Rice, thanks for paving the way for me, giving me guidance, and working with me to build the laboratory scintillometer. Thanks to my coworkers Seth Marek, Mike Dexter, Frank Echeverria, and Jonathan Spaulding for being sounding boards. Thanks to Larry & Julie Matthews for the mentorship provided and the use of your work truck for the field experiments. Finally, thanks to the irreplaceable laboratory technicians: Jeff Sitler, Mike Ranft, and Greg Smith. I could not have done any of the experiments without them. They were there for me, helping me troubleshoot problems.

~~~~~

Special thanks go to my family: my husband and our two miniature doxies. To my husband, for his infinite patience, strength, and prodding to get this done, and to Brownie and Barley for taking in stride the many belly scratches denied while working on this thesis.

J. Jean Cohen

Table of Contents

	Page
Abstract.....	iv
Acknowledgements.....	v
List of Figures.....	viii
List of Tables.....	x
List of Symbols.....	xi
List of Equations.....	xii
I. Introduction.....	1
Motivation.....	1
Refraction and Refractivity.....	2
Anomalous Dispersion.....	3
Index of refraction structure function, C_n^2	5
Hypothesis.....	6
Objective of Research.....	6
Approach.....	7
Document Outline.....	9
II. Literature Review.....	10
Turbulence Theory.....	10
Structure Functions.....	14
Anomalous Dispersion from Liou.....	16
Optical Turbulence Methods.....	17
<i>Intensity Variation Method</i>	17
<i>Scintillation Index Method</i>	20
<i>Vertical Gradient of the Index of Refraction Method</i>	21
<i>Radar Method</i>	23
III. Methodology.....	27
Overview.....	27
McClung-Tunick Variable Sensitivity Charts.....	28
Weather Station.....	31
Temperature Sensors Calibration.....	33
Field Experiment Set-Up.....	36
AFIT Scintillometer.....	40
Communication Laser Sensitivity Study.....	43

	Page
IV. Analysis and Results.....	51
AFIT Laboratory Built Scintillometer.....	56
Field Experiments.....	58
<i>Weather Station and BLS900</i>	58
<i>Thermocouples and BLS900</i>	62
Laser Communications Sensitivity Study	65
<i>HUMID</i>	65
<i>MID-LATITUDE</i>	68
<i>DESERT</i>	71
V. Conclusions and Recommendations	76
Conclusions	76
Recommendations for Future Work	79
Appendix A.....	81
MatLab source code for runTunickModel.m.....	81
MatLab source code for tunickGUI2.m.....	86
MatLab source code for McTunick.m.....	96
Appendix B.....	98
Appendix C.....	100
Appendix D.....	101
Bibliography	102

List of Figures

Figure	Page
1. Normal dispersion in the visible spectrum with a prism.....	3
2. Real and imaginary parts of refractivity	4
3. Power versus wavenumber from air jet experiment.	12
4. Kolmogorov's cascade theory of turbulence.	13
5. Mathar curves showing anomalous dispersion	19
6. McClung-Tunick Graphical User Interface.	23
7. Percent error introduced in to C_n^2	29
8. Optical turbulence sensitivity to weather factors.....	30
9. Refrigerator calibration of temperature sensors.....	34
10. Reaction time of weather station temperature sensors.....	35
11. Delta T (T1-T2) data from weather temperature sensors.....	36
12. Field experiment location, mowed grassy field at WPAFB.	37
13. BLS900 receiver and transmitter from left to right.	38
14. Scintillometer receiver looking down the path	38
15. Davis Vantage Pro2 Plus weather station	39
16. Thermocouple tripod station for two levels of temperature.....	39
17. Laboratory built scintillometer experimental set-up.....	42
18. Normal dispersion curve from 760nm – 1560nm	47
19. GPS coordinates of scintillometer location available through Google.....	50
20. Example of reflectivity data from weatherTAP radar analysis model.....	50
21. Theorized refractivity of tunable wavelength laser #1	51
22. Theorized refractivity of tunable wavelength laser #5.	52
23. Theorized refractivity of BLS900 scintillometer.....	52
24. Recreation of Mathar curve from 1 to 6 microns.....	53
25. Recreation of Mathar curve from 0.3 – 30 microns.....	54
26. Broad spectrum view of refractivity from UV to RF.....	55

Figure	Page
27. AFIT scintillometer showing optical turbulence versus time	56
28. AFIT scintillometer with all four hot plate temperatures.	57
29. 23 Oct 08 BLS900 compared to McClung-Tunick model.....	59
30. Zoomed-in 23 Oct 08 BLS900 compared to McClung-Tunick model	60
31. 6 Nov 08 BLS900 compared to McClung-Tunick model.....	61
32. 21 Nov 08 BLS900 compared to McClung-Tunick model using Type K.....	62
33. 30 Dec 08 BLS900 compared to McClung-Tunick model using Type T.....	63
34. 31 Dec 08 BLS900 compared to McClung-Tunick model using Type T.....	64
35. Humid, Eglin AFB, 3D irradiance (all effects) plot of the laser beam.	66
36. Humid, Eglin AFB, FL scenario at 1200-1500 in June	67
37. Humid, Eglin AFB, FL scenario at 1200-1500 in January	68
38. 3D irradiance plot (all effects) of the laser beam for the mid-latitude WCS.....	70
39. Optical turbulence vertical profile for mid-latitude, January 0900-1200	71
40. 3D irradiance plot (all effects) of the laser beam for the desert WCS.....	73
41. Optical turbulence vertical profile for desert, January 1200-1500	73
42. 6 Nov 08 BLS900 data compared to weather radar method.....	74
43. 21 Nov 08 BLS900 data compared to weather radar.....	75
44. 21 Nov 08 with overlay of Type K thermocouple.	75

List of Tables

Table	Page
1. Run matrix for desert scenario at Nellis AFB, NV	44
2. Run matrix for mid-latitude scenario at WPAFB, OH.	44
3. Run matrix for humid scenario at Eglin AFB, FL.	45
4. Complex index of refraction for water at various temperatures.	49
5. Optical turbulence values for humid Eglin AFB, FL environment	65
6. Laser characterization for worst case scenario (WCS) in humid environment	66
7. Optical turbulence values for mid-latitude WPAFB, OH environment.....	69
8. Laser characterization for worst case scenario (WCS) for mid-latitude.....	69
9. Optical turbulence values for desert Nellis AFB, NV environment	72
10. Laser characterization for worst case scenario (WCS) for desert environment.....	72

List of Symbols

Symbol		Page
n	index of refraction.....	1
m_r	real portion of the complex index of refraction.....	1
m_i	imaginary portion of the complex index of refraction.....	1
c	speed of light in a vacuum.....	2
N	refractivity.....	2
λ	wavelength.....	3
α_n	anomalous dispersion region.....	4
C_n^2	index of refraction structure parameter / optical turbulence strength.....	4
K_H	turbulent exchange function.....	5
ε	energy dissipation rate.....	5
$\frac{\partial n}{\partial z}$	vertical gradient of the index of refraction.....	5
L_o	outer scale (of eddy size).....	11
l_o	inner scale.....	11
κ	wavenumber.....	11

List of Equations

Equation	Page
1. Relationship between C_n^2 and the vertical gradient of the index of refraction.	5
2. Structure function, separation vector, and structure function parameter.	14
3. Structure function parameter for wind, where ε is the eddy dissipation rate.	14
4. Structure function and structure function parameter for the index of refraction.	14
5. Power spectral density for refractive index fluctuations.....	14
6. Tatarski's power spectral density for the index of refraction into dissipation range. ..	15
7. Real part of the complex index of refraction as a function of frequency.	16
8. Imaginary part of the index of refraction as a function of frequency.	16
9. Radar reflectivity as a function of radar system specifications.	24
10. Optical turbulence strength relation to radar reflectivity.	24
11. Reflectivity (dBz) relation to Z_e	25
12. Z_e relation to reflectivity.....	25
13. K_w relation to the complex index of refraction for water.....	26
14. Optical turbulence strength related to dBz with wavelength in units of meters.	48
15. Relationship between C_n^2 and the vertical gradient of the index of refraction.	22
16. Log-normal amplitude intensity variation method of deriving optical turbulence.	17
17. Scintec's log-normal amplitude intensity variation.....	18
18. Scintillation index relation to intensity.	20
19. Optical turbulence strength relation to scintillation index.....	20
20. Correction factor for scintillation index if $D/2 > \sqrt{L/k}$	21

DEMONSTRATION AND VERIFICATION OF A BROAD SPECTRUM ANOMALOUS DISPERSION EFFECTS TOOL FOR INDEX OF REFRACTION AND OPTICAL TURBULENCE CALCULATIONS

I. Introduction

Motivation

Accurately predicting electromagnetic (EM) radiation performance through the atmosphere, particularly for high energy laser (HEL) weapon systems, is important to the Air Force and the Department of Defense (DoD). Large under-predictions can result in a mission failure, whether that is the inability to destroy a target, image properly, or communicate effectively. Large over-predictions inefficiently use limited energy sources. In order to obtain high accuracy in prediction, a precise characterization of the index of refraction of the atmosphere is required. It is with this variable we know how much light is bent and distorted by our atmosphere.

The index of refraction of the atmosphere, n , is a function of wavelength, temperature, pressure, and humidity. It is a complex value, having a real part, m_r , associated with the propagation speed of the EM radiation, and an imaginary part, m_i , associated with absorption of the EM energy. A full understanding of the index of refraction and the effects of its variations across the EM spectrum enhances not only performance predictions for HEL weapons, but also for many other applications such as imaging, wireless communication, and astronomy.

In the past, the index of refraction's wavelength dependence in air has been considered unimportant and n was commonly given a value very near unity (~ 1.0003) for all wavelengths, even at sea level densities. This assumption has worked well for applications of the past, but with the emergence of EM devices which stretch across many wavelengths or are used at wavelengths far beyond the visible region, the near unity assumption is invalid. There are two ways in which wavelength impacts the index of refraction: normal and anomalous dispersion. Normal dispersion is the downward curve and leveling off of the index of refraction as wavelength increases. Anomalous dispersion, to be discussed in detail in its own section, occurs at strong absorption lines. For example, the terahertz (THz) spectral region contains numerous absorption lines, thus many occurrences of anomalous dispersion are present.

A disregard of wavelength dependence in n could directly impact performance predictions for HEL weapon systems since the systems are often comprised of multiple lasers at different wavelengths. One laser measures refractive index variation, allowing the system to correct for atmospheric distortion, while a second laser is the actual weapon. For example, the Airborne Laser's (ABL) HEL, a chemical oxygen iodine laser (COIL), lases at a 1.315 micron wavelength, and its beacon and tracking solid state laser (SSL) lases at a 1.06 micron wavelength.

Refraction and Refractivity

Refraction is a measure of the speed at which EM radiation travels through a medium relative to the speed at which it would travel in a vacuum (the speed of light, c). Refractivity, N , is $(n - 1)$, and is usually multiplied by a factor of 10^6 and used in place

of refraction since, as mentioned previously, n is ~ 1.0003 . Refractivity allows one to look at the changes which occur from 1. The following are a few illustrations of the concept of refraction. For two mediums of the same length (i.e. glass and air), it will take light (at non-normal incidence) a longer time to travel through a high refractive medium (glass) than a low refractive medium (air). The higher refractive medium will cause the light to bend further and travel a longer distance, thus explaining the longer time. A prism is a great example of normal dispersion within the visible region of the spectrum. In this region, as wavelength increases, refraction decreases. This is seen in Figure 1 below as the shorter wavelengths (violet) are bent at a greater angle than the longer wavelengths (red) of light.

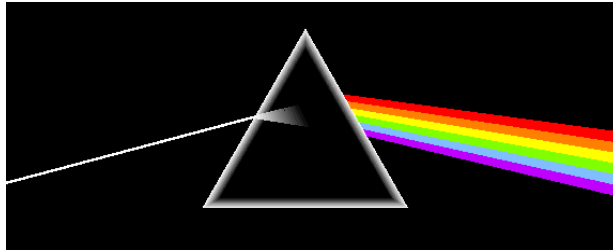


Figure 1. Normal dispersion in the visible spectrum with a prism. (Morgan, 2006)

Anomalous Dispersion

Anomalous dispersion, as opposed to normal dispersion, occurs when n increases with increasing wavelength, $\frac{\partial n}{\partial \lambda} > 0$. Another way to describe anomalous dispersion is by Dr. Liou in Appendix D of his book, An Introduction to Atmospheric Radiation (2002). It occurs when the real part of complex refractivity, $(m_r - 1)$ decreases with increasing frequency. Liou defines the real part of the complex refractivity $(m_r - 1)$

using the Lorentz-Lorentz equation. The imaginary part of refractivity due to absorption is defined by Born and Wolf (1975), discussed further in the literature review section.

Absorption due to various molecules or aerosols in the air alters the atmosphere's complex index of refraction (or refractivity) by affecting the peak of the imaginary, and the anomalous dispersion of the real. Stronger absorption correlates to stronger anomalous dispersion. Below is an illustration by Liou, depicting the Lorentz-Lorentz equation (similar in effect to Kramers-Kronig relations) showing the real (solid) and imaginary (dashed) portions of refractivity as a function of frequency (Liou, 2002). Interestingly, refractivity sharply decreases immediately preceding the anomalous dispersion region, α_N . This implicates that very near absorption lines, EM radiation travels faster than c . However, it should be noted that this is the light's phase velocity, not overall group velocity that travels faster than c .

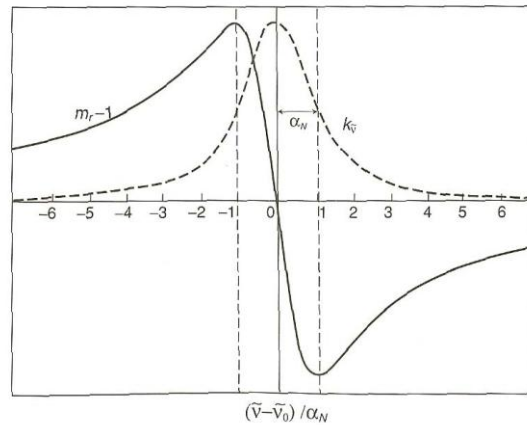


Figure 2. Real and imaginary parts of refractivity as a function of frequency encountering absorption.

Index of refraction structure function, C_n^2

Optical turbulence strength, also known as the index of refraction structure function, C_n^2 , can be derived using several methods. Variations in log-normal amplitude (intensity), scintillation index, radar reflectivity, and the vertical gradient of the index of refraction are some of these methods. This thesis will discuss all of the methods mentioned, but will particularly focus on the vertical gradient of the index of refraction method. This relationship between optical turbulence strength and the index of refraction was theorized by Tatarski in 1971 with the following equation (Panofsky, 1968; Tatarski, 1971; Tunick, 2003):

$$C_n^2 = b \frac{K_H}{\varepsilon^{1/3}} \left(\frac{\partial n}{\partial z} \right)^2 \quad (1)$$

Equation 1. Relationship between C_n^2 and the vertical gradient of the index of refraction.

Where b is a constant, usually 3.2, K_H is the turbulent exchange function for heat diffusion, and ε is the energy dissipation rate.

Similarity theory (Rachele et al., 1995) can be used to determine surface heat and moisture flux through a layer of the atmosphere, although this layer must be within the first 50 meters off the ground. This information can be used to determine the index of refraction of the surface boundary layer, since n is dependent on both temperature and moisture (i.e. relative humidity). With the index of refraction of a layer of atmosphere known, its vertical gradient can be calculated, and optical turbulence derived. Optical turbulence, like the index of refraction, has a wavelength dependence that needs to be investigated and incorporated into predictive models for accurate predictions.

Hypothesis

It can be verified and demonstrated through a modified similarity theory model that C_n^2 can be measured at one wavelength, and known accurately at another wavelength. This accuracy is attained by the incorporation of anomalous dispersion effects, made possible through the HITRAN database (Rothman et al., 2005). Additional knowledge needed for this high accuracy in optical turbulence is: the vertical gradient of the index of refraction, $(\frac{\partial n}{\partial z})^2$, and similarity theory used to determine $(\frac{\partial n}{\partial z})^2$ within the lowest 50m of the atmosphere.

Objective of Research

The objective of this research is to verify the theory behind and demonstrate the usefulness of the index of refraction and optical turbulence model, the McClung-Tunick model (McClung et al., 2008) incorporated into the High Energy Laser End-to-End Operational Simulation (HELEEOS) tool. As of publication date, this model contains the most accurate description of both the index of refraction and optical turbulence from wavelengths 355nm (ultraviolet) – 8.6m (radio frequencies) for any inertial subrange atmospheric environment. This tool can be built upon to be used as an operational tool, enhancing performance predictions for HEL weapon systems.

This research pertains to the adaptive optics within the ABL. If there are large dispersive differences between the wavelength of the beacon laser (the one being sent out first determining atmospheric distortion) and the wavelength of the larger COIL laser, the C_n^2 calculator will automatically update and correct. This enables the COIL beam to

accurately adapt to the atmosphere it is lasing through, resulting in a less dispersed beam. Additionally, this research opens up the potential capability for a three dimensional range-gated optical turbulence strength network, made possible through common and readily available weather radars. This optical turbulence strength “mapping” could be uploaded to the ABL or any future laser harboring aircraft.

Ultimately, the objective of this research is to verify and demonstrate an optical turbulence predictive tool, which can forecast times and environmental scenarios in which to best use a high energy laser weapon. Future work includes the creation of a real-time C_n^2 calculator, exploiting the availability and abundance of common weather radar information.

Approach

Existing models for either the index of refraction or optical turbulence of the atmosphere do not encompass wide ranges of wavelengths across the EM spectrum, nor do they include anomalous dispersion effects. These additions have been made into the Air Force Institute of Technology Center for Directed Energy’s (AFIT/CDE) HELEEOS version 3.0. HELEEOS is a first principles atmospheric propagation and characterization model. Within HELEEOS lies the High-Resolution Transmission Molecular Absorption (HITRAN) database (Rothman et al., 2005). This database contains 1,734,469 spectral lines for 37 different molecules (with files for two more in a separate supplement) as of version 12.0 (2004). This database affords HELEEOS incredibly accuracy for EM propagation prediction.

The refractivity and C_n^2 calculator that has been added to HELEEOS is the McClung-Tunick model. Theory behind this model will be investigated and verified and its theoretical modeling and simulation capability to predict refractivity across a broad spectrum will be demonstrated. A scintillometer will be built at AFIT using a tunable wavelength laser and qualitatively demonstrated. This will be a first step towards validation, beyond mere verification of the anomalous dispersion and broad spectrum capability of the model.

Holding wavelength constant at 880nm, the McClung-Tunick model will be compared against scintillometer field measurements, using Scintec's BLS900 scintillometer. Questions about spectral and measurement limitations of scintillometers and the model will be investigated. For example, limitations in scintillometers are artificial floors and ceilings due to path range restrictions. From previous papers by Tunick (2003, 2005) it appears that commercial scintillometers cannot measure the smallest values of C_n^2 that his model predicts due to an artificial floor.

In addition to the model's theory being verified, demonstrations of the tool's usefulness is also a part of this thesis's approach. A sensitivity study for the Air Force Research Lab's Sensors Directorate (AFRL/RYSM) is completed, showing how C_n^2 varies with geographic location, time of day, season, and its implication on laser communication performance. Information on optical turbulence, laser irradiance on target, spot size, and power in the bucket is provided. A taste of future work with weather radar is also provided. Optical turbulence is derived from common 10cm

wavelength radar. Theoretically, turbulence derived from radar could be related back to any other wavelength desired via the McClung-Tunick model.

Document Outline

This document is organized in the following manner. Chapter two is an in depth literature review over turbulence, optical turbulence, and the methods by which it is derived. Commercial scintillometer measuring techniques and optical turbulence theory used in industry and academia are investigated. Theory behind the vertical gradient of the index of refraction method (McClung-Tunick) C_n^2 model is explored. Chapter three describes methodology used to prove or disprove the stated hypothesis. Chapter four contains results, discussion, and analysis of the model's theoretical capability, the AFIT built scintillometer, the Scintec BLS900 scintillometer field measurements, and the demonstrative studies aforementioned. Chapter five contains conclusions and a summary of research performed.

II. Literature Review

Turbulence Theory

Turbulence, the “curious and beautiful natural phenomena” according to physicist Tom Faber, has a rich history of inquiry. Over the last hundred years, many scientists have made major contributions to turbulence theory to include, but not limited to L.F. Richardson in the early 1900s, A.N. Kolmogorov in the 1940s, V.I. Tatarski in the 1970s, and Andrews & Phillips, and Arnold Tunick in our modern time. The term, theory, is dubiously associated with turbulence for reasons more eloquently explained by professor emeritus Peter Bradshaw. “‘Theory’ belongs in quotes because turbulence, the nearly random fluid motion that mixes the cream in your coffee and the clouds in the sky, is governed by the Navier-Stokes equations... (Bradshaw, 1996).”

The highly complex conservation of momentum Navier-Stoke’s equations have no analytic solution, only numerical at a computationally expensive price. Because of this, it is impossible to solve turbulence’s nonlinear, near-random processes with first principle physics equations. Out of this dilemma arose Kolmogorov’s classical theory of turbulence in the 1940s. Andrews & Phillips wrote of this in their book, Laser Beam Propagation Through Random Media (2005:59).

Turbulence is fundamentally a nonlinear process as described by the governing Navier-Stokes equations. Because of mathematical difficulties in solving these equations, Kolmogorov developed a statistical theory of turbulence that relies heavily on dimensional analysis and additional simplifications and approximations. Thus, turbulence theory as we know it today is not derived from first principles.

Before going further and discussing how Kolmogorov addressed the dilemma, a clarification of basic terms is required for turbulence, eddies, cells, turbules, optical

turbulence, scintillation, and C_n^2 . Turbulence is classically defined as random wind fluctuations in the atmosphere, or stated another way: “fluctuations in the velocity field of a viscous fluid” (Andrews & Phillips, 2005). Sources of turbulence arise from convection off hot surfaces, wind shear, and weather systems, which form and break up eddies (also called cells or turbules). Most people think of turbulence as the bumps on an airplane that jostle passengers around. This type of turbulence is caused by large scale eddies whose lengths are on the order of 10s of meters, although other sources such as Wallace and Hobbs (2006) refer to “large scale” eddy size as 2km. Opposite of large scale turbulence is optical turbulence, caused by smaller eddies only 0.1-1cm to 10s of meters in size. These smaller cells “bump” around the micron sized optical wavelengths. Also commonly used in turbulence theory is the term, scintillation. Scintillation refers to fluctuations in image brightness due to optical turbulence in our atmosphere, as seen by the twinkling of stars. A scintillometer is a device used to measure optical turbulence strength and is discussed further under “Intensity Variation Method” (Scintec, 2008).

Optical turbulence and C_n^2 are generally used interchangeably. Yet to be as accurate as possible, the two terms should be viewed as related rather than equal. As a structure function, C_n^2 has no wind component. Technically, one could observe little or no wind, yet measure strong C_n^2 because of high humidity or temperature gradients. The terms are linked because it is physically impossible to have a temperature gradient arise without winds that follow. C_n^2 is a mathematical construct from dimensional analysis and is solely related to the fluctuations in the index of refraction. Structure functions will be discussed in depth further. C_n^2 should be viewed as optical turbulence *strength*.

Now that basic terms are clarified, turbulence statistical theory can be discussed more in depth. Kolmogorov predicted a statistical consistency that linked large turbules to smaller ones within what is called the inertial subrange. He maintained the assumption that within this inertial subrange, turbulence was statistically homogenous, isotropic, and stationary in time, and modern lab experiments have agreed with this assumption (Max, 2008). The below figure from a UC Santa Cruz lecture series on optical turbulence showing a constant slope within the inertial subrange during a 10cm diameter air jet experiment. Credit for figure is given to Gary Chanan of UCI (Max, 2008:20).

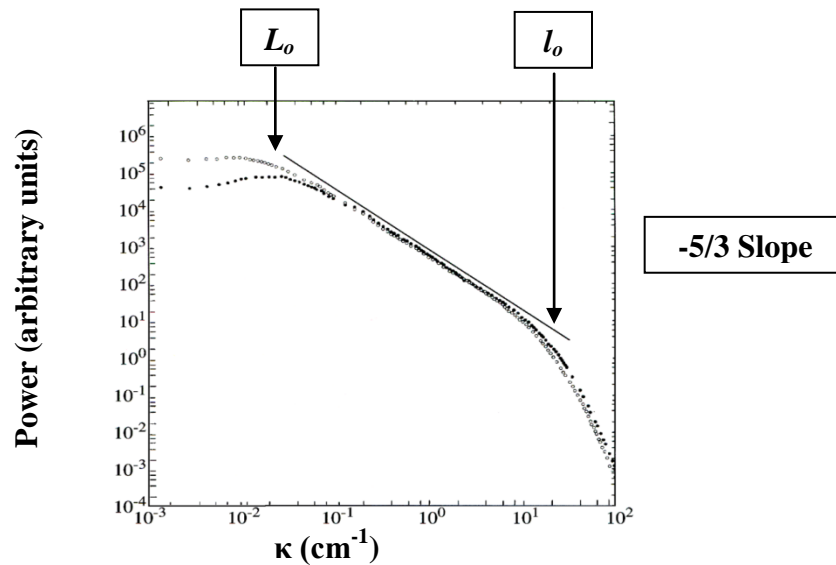


Figure 3. Power versus wavenumber from air jet experiment.

Aiding in the visualization of Kolmogorov's statistical turbulence theory, L.F. Richardson developed the energy cascade theory of turbulence. Larger eddies break up into smaller ones and so on down in size. Eddies at the outer scale size, L_o , and larger are dominated by wind shear or convection. Their structure is not well defined because they are so large (Andrews & Phillips, 2005; Wallace & Hobbs, 2006). Eddies at the inner scale, l_o and smaller, break up into even smaller cells and eventually dissipate as heat.

Within the inertial subrange, between L_o and l_o , it is assumed that energy loss does not occur (i.e. through heat loss). Energy is neither created nor dissipated in this range. Rough estimates of eddy size within the inertial subrange are between 100m and 1mm. According to the department of astrophysics at the Universite de Nice-Sophia in France, the generalized seeing monitor (GSM) has measured the outer scale to be approximately 16-45m, depending on whether one measures in night or daytime conditions (Martin et al., 2000). Figure four below is an illustration out of Andrews and Phillips showing Richardson's energy cascade diagram (Andrews & Phillips, 2005:60). Interestingly, an ambulance driver for France during WWI, Richardson did much of his initial work in turbulence and meteorology in-between transporting wounded soldiers during the war.

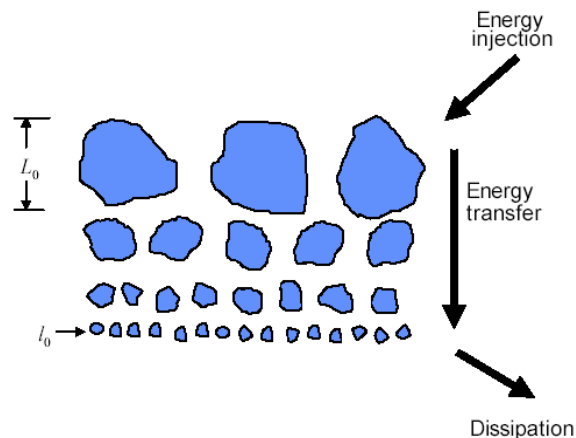


Figure 4. Kolmogorov's cascade theory of turbulence.

“Big whirls have little whirls that feed on their velocity;
Little whirls have lesser whirls, and so on to viscosity.”

– L. F. Richardson

Structure Functions

Kolmogorov used dimensional analysis to come up with a relationship between the structure function, separation vector, and structure function parameter, see Equation 2 (Andrews & Phillips, 2005). Two points are taken within the inertial subrange and the vector parallel to those points satisfies the 2/3 power law. Equation 3 is the structure function parameter for wind.

$$D_{rr}(R) = \langle (V_1 - V_2)^2 \rangle = C_v^2 R^{2/3}, l_o \ll R \ll L_o \quad (2)$$

Equation 2. Structure function, separation vector, and structure function parameter relationship.

$$C_v^2 = 2\varepsilon^{2/3} \quad (3)$$

Equation 3. Structure function parameter for wind, where ε is the eddy dissipation rate.

The structure function parameter for the index of refraction is C_n^2 , shown below in Equation 4 using the 2/3 power law again. Equation 5 is the Kolmogorov power-law spectrum, showing how the power spectral density for refractive index fluctuations relates to the refractive index structure function parameter, C_n^2 . This equation works well for visible wavelengths and again, only within inertial subrange.

$$D_n(R) = 2[B_n(0) - B_n(R)] = C_n^2 R^{2/3}, l_o \ll R \ll L_o \quad (4)$$

Equation 4. Structure function and structure function parameter for the index of refraction.

$$\Phi_n(\kappa) = 0.033 C_n^2 \kappa^{-11/3}, 1/L_o \ll \kappa \ll 1/l_o \quad (5)$$

Equation 5. Power spectral density for refractive index fluctuations.

V. I. Tatarski extended the use of the above Kolmogorov power spectrum beyond the inertial subrange into the dissipation range (the range of eddies smaller than l_o), using a Gaussian function truncating at low wavelengths. Novikov was the first to propose this

type of function for velocity fluctuations and Tatarski applied it to the index of refraction (Tatarski, 1971; Andrews & Phillips, 2005:67).

$$\Phi_n(\kappa) = 0.033C_n^2\kappa^{-11/3} * \exp\left(-\frac{\kappa^2}{\kappa_m^2}\right), \kappa \gg 1/L_o, \kappa_m = 5.92/l_o \quad (6)$$

Equation 6. Tatarski's power spectral density for the index of refraction into dissipation range.

There are more proposed spectrum density models such as Von Karman, modified atmospheric spectrum, and exponential that will not be discussed in this thesis.

Optical Turbulence, Index of Refraction, & Wavelength Dependence

As stated previously, Andrews and Phillips are major contributors to the field of optical turbulence. This thesis uses their definitions of turbulence and optical turbulence. Fluctuations in velocity (wind) define classical turbulence whereas fluctuations in the index of refraction define optical turbulence. It is a commonly held view that temperature is the driving variable influencing the atmospheric index of refraction. “We define *optical turbulence* as the fluctuations in the index of refraction resulting from small temperature fluctuations (Andrews & Phillips, 2005:58).” This is a true statement for the index of refraction within visible wavelengths and wavelengths where little absorption is present. However, at wavelengths where strong absorption lines occur, the index of refraction varies widely due to anomalous dispersion. Applications, current or future, which operate at or near strong absorption lines, need to take into account this strong wavelength dependence in the index of refraction, as it greatly distorts EM beam transmission.

Anomalous Dispersion from Liou

The complex index of refraction, dispersion of light, and Lorentz-Lorentz formula is described by Dr. Liou in Appendix D of his book. Starting from first principles, using the Lorentz force equation from introductory electromagnetic theory, a clear description is given of how the complex index of refraction behaves at absorption lines. Below is the Lorentz-Lorentz profile for the real portion of the index of refraction as a function of frequency (Liou, 2002:531):

$$m_r - 1 = - \frac{Ne^2}{4\pi m_e} \frac{\nu_0 - \nu}{(\nu_0 - \nu)^2 + \alpha_N^2} \quad (7)$$

Equation 7. Real part of the complex index of refraction as a function of frequency.

Where m_r is the real part of n , N is the number of dipoles, e is electron charge, m_e the mass of an electron, ν is the frequency (c/λ), ν_0 is the natural (resonant) frequency, and α_N is the half width of the natural broadening.

The absorption coefficient, k_v , dictates the behavior of the imaginary portion of the index of refraction (Born & Wolf, 1975; Liou, 2002).

$$k_v = \frac{4\pi \nu_0 m_i}{c} = \frac{S}{\pi} \frac{\alpha_N}{(\nu_0 - \nu)^2 + \alpha_N^2} \quad (8)$$

Equation 8. Imaginary part of the index of refraction as a function of frequency.

Where S is line strength equal to $\frac{\pi Ne^2}{m_e c}$ and m_i is the real part of n . Refer back to Figure 2 to see both Equations 7 and 8 graphed together.

Optical Turbulence Methods

The final sections of Chapter II present several methods of deriving optical turbulence. First, log-normal amplitude intensity variation is looked at in relation to commercial scintillometers. The scintillation index method, very similar to intensity variation, is evaluated and used later on to build a laboratory scintillometer from a tunable wavelength laser at AFIT. The vertical gradient of the index of refraction method (McClung-Tunick model) is discussed and some of the equations behind it are disclosed. Lastly, in regards to future work, the method of deriving turbulence from weather radar is shown.

Intensity Variation Method

Commercial scintillometers like Scintec's BLS900 work because scintillation in the atmosphere causes fluctuation in intensity of a transmitted EM beam. In both the BLS900 manual and Tunick's recent journal article, "Optical turbulence parameters characterized via optical measurements..." (2008b), equations are given for this method, specifically known as log-normal amplitude intensity variation method. Equation 9 below provides the basis for this theory (Scintec, 2008; Tunick, 2008b).

$$C_n^2 = C\sigma^2 D_t^{7/3} L^{-3} \quad (9)$$

Equation 9. Log-normal amplitude intensity variation method of deriving optical turbulence.

Where $C = 4.48 D_r / D_b$, a ratio of the diameter of the receiver to the diameter of the transmitter (a value of 4.629 is used by Scintec for C), σ^2 is the log amplitude variance, D_t is the diameter of the transmitter, and L is propagation path length. Scintec refers to their log amplitude variance, σ^2 , as B_{11} and B_{22} because they have two Si photodiode

detectors in their receiver. This is valuable feature as it allows the user to check the accuracy of the detectors, since there should be little variation between detector 1 and 2. Equation 17 refers to how Scintec defines one their log-amplitude variances:

$$B_{11} = \frac{1}{4} Ln \left[1 + \frac{\sigma_{11}}{\langle I_1 \rangle^2} \right] \quad (10)$$

Equation 10. Scintec's log-normal amplitude intensity variation.

There are limitations to the intensity variation method as industry makes approximations when dealing with the wavelength dependence in refractivity. This is understandable when the application operates at wavelengths impervious to anomalous dispersion. Scintec's boundary layer scintillometer (BLS900) (Scintec, 2008) measures optical turbulence at a wavelength of 880nm +/- 20nm and allows the user to calculate what the optical turbulence would be at different wavelengths, up to 30µm. While in their manual, Scintec's theory section discusses some wavelength dependence in their equations, this discussion accounts for normal dispersion only. There are no equations taking into account absorption lines and thus anomalous dispersion. The stated wavelength range allowing the user to calculate other C_n^2 values is 0.1-30µm. This is indicative of the current views on anomalous dispersion and wavelength dependence in conjunction with refractivity.

The figure below is taken from Mathar's journal article, "Calculated refractivity of water vapor and moist air in the atmospheric window at 10µm", showing refractivity versus wavelength with absorption lines for eight molecules taken into account from 1-6µm and then again from 0-20µm (Mathar, 2004). The accessed HITRAN database,

(Rothman et al., 2005) enables such accuracy in his model. Mathar uses the 2001 version of HITRAN. Note the anomalous dispersion lines that are shown as predicted by the Lorenz-Lorenz equations when absorption lines in the atmosphere are encountered (Liou, 2002). The wavelength dependence, incorporated into the Scintec scintillometer, enabling one to measure C_n^2 at one wavelength and calculate it at another, is most likely the dotted line, only accounting for normal dispersion, in Figure 5. The dotted line (or small crosses) is calculated using the Ciddor equations for wet air. Ciddor equations are the accepted laboratory derived index of refraction equations for air. As one can see from the Mathar curves, calculating a second optical turbulence value at a different wavelength using the BLS900 would theoretically be incorrect if one requests a value near or at an absorption line.

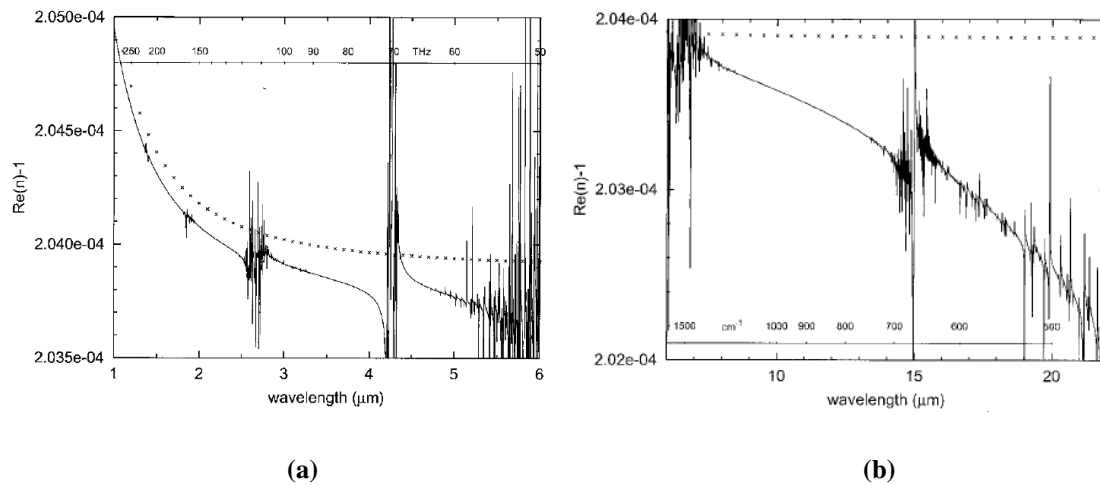


Figure 5. Mathar curves showing anomalous dispersion in refractivity for various wavelengths.

Ultimately, scintillometers are great tools to measure C_n^2 , so much so that this thesis will use one to verify AFIT/CDE's new optical turbulence model. However,

scintillometers do not currently take into account anomalous dispersion, a limitation to be aware of. Additional limitations of this method are:

- a scintillometer is expensive
- it takes a path average and does not “range-gate”
- path needs to be clear line of sight
- path is preferably over large homogenous (non-varying) terrain
- path has 500m min range without aperture reduction, max range of 2km (BLS900 only, other scintillometers may have longer or shorter ranges)
- has artificial floors and ceilings dependent on chosen range

Scintillation Index Method

The scintillation index method is very similar to log-normal amplitude intensity variation, however, it does not use a log-normal distribution. Tunick’s journal article (Tunick, 2008b) has a wealth of information, laying out the technique clearly. The following equations for the scintillation index method are below. Equation 11 shows the relation of the scintillation index, σ_I^2 , to signal intensity, I . Equation 12 depicts the relationship between the scintillation index and optical turbulence strength.

$$\sigma_I^2 = \frac{\langle I^2 \rangle - \langle I \rangle^2}{\langle I \rangle^2} \quad (11)$$

Equation 11. Scintillation index relation to intensity.

$$C_n^2 = 2k^{-7/6} L^{-11/6} \sigma_I^2 \quad (12)$$

Equation 12. Optical turbulence strength relation to scintillation index.

Where k is wavenumber, $k = 2\pi/\lambda$, and L is propagation path length. It is important to correct for aperture averaging if the radius of one’s receiving optics is larger than $\sqrt{L/k}$.

Tunick uses the multiplication correction factor, A, on the scintillation index for a point aperture. The below corrective factor, A, is for spherical waves.

$$A = \left[1 + 0.33 \left(\frac{kD}{4L} \right)^{5/6} \right]^{-7/5} \quad (13)$$

$$\sigma_I^2(D) = A\sigma_I^2(0)$$

Equation 13. Correction factor for scintillation index if $D/2 > \sqrt{L/k}$.

The scintillation index method has the same limitations as described for the intensity variation technique because they are so similar. Further ahead, this method is demonstrated qualitatively, being used to build a laboratory scintillometer at AFIT.

Vertical Gradient of the Index of Refraction Method

The vertical gradient of the index of refraction method, theorized by Tatarski (1971), was first developed into a code by Dr. Arnold Tunick of the Army Research Lab (ARL). AFIT/CDE's McClung-Tunick model is an offspring of his technical report, Army Overland Optical Turbulence (CN2) Model (Tunick, 2008a). Brandon McClung of AFIT with the help of Matt Krizo, Kenneth Moore, Thomas Harris, and Rick Bartell diligently took Tunick's equations from that report and wrote MatLab code from scratch. They debugged, troubleshot, linked it with the HITRAN database, and integrated it into the Center for Directed Energy's flagship code, HELEEOS version 3.0.

As stated previously, the basis of the code is Tatarski's theory. This is seen below by revisiting Equation 1 from the introduction chapter (Tatarski, 1971).

$$C_n^2 = b \frac{K_H}{\varepsilon^{1/3}} \left(\frac{\partial n}{\partial z} \right)^2 \quad (1)$$

Equation 1. Relationship between C_n^2 and the vertical gradient of the index of refraction.

Since the vertical gradient of the index of refraction is dependent on pressure, temperature, wavelength, and humidity, so is this tool dependent on vertical gradient weather information. Inputs to the C_n^2 tool are wavelength, pressure, surface boundary layer depth, and two levels of temperature, humidity, and wind speed. Figure 6 is a picture of AFIT/CDE's McClung-Tunick C_n^2 calculator. Here, one can see all the inputs previously mentioned and how the program graphs a vertical profile of optical turbulence, comparing it to the standard HV 5/7 profile. To the right of the optical turbulence graph is a vertical profile of refractivity (McClung et al., 2008).

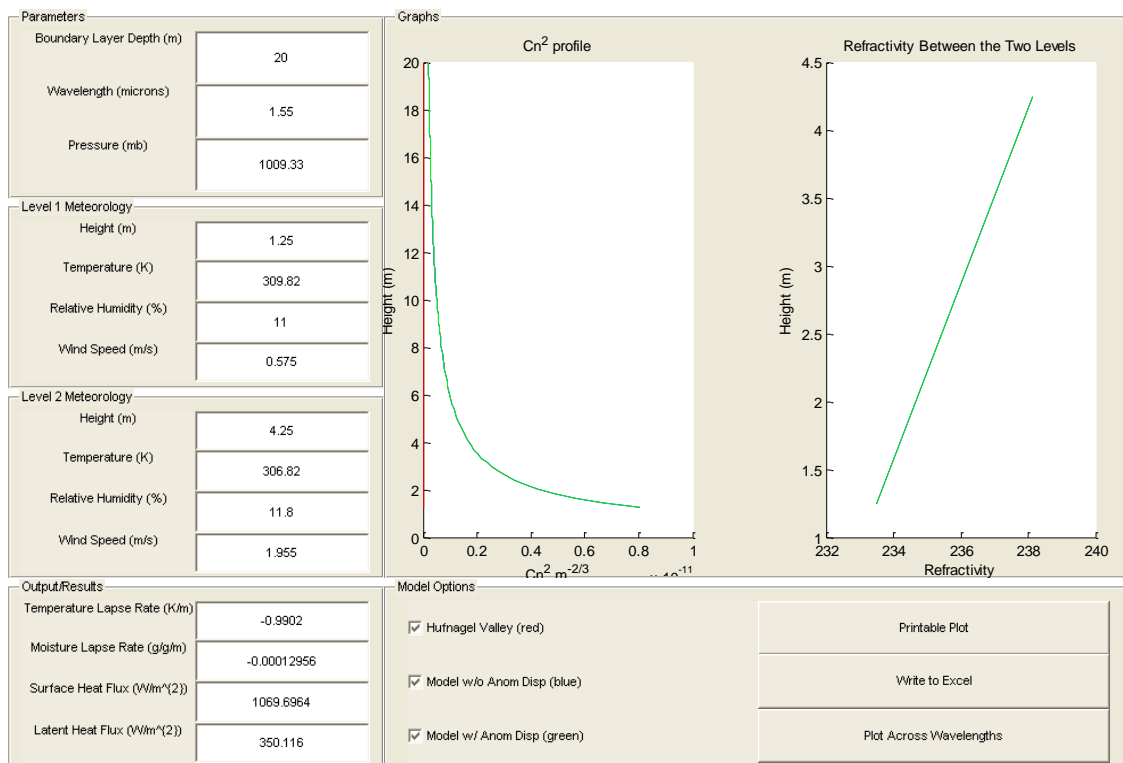


Figure 6. McClung-Tunick Graphical User Interface.

See Appendix A for the complete code, labeled: runTunick.m, McTunick.m, and tunickGUI2.m. The first .m file “runTunick” is the basis for the “tunickGUI2” shown above, while the “McTunick” allows an advanced user to input a large Excel database to plot optical turbulence over time. This provides for an apples-to-apples comparison with a scintillometer. Additionally, in the beginning of the results section, graphs similar to the Mathar curves which demonstrate the ability to plot across wavelengths are shown.

Radar Method

Doviak and Zrnica in their book, Doppler Radar and Weather Observations, mimic much of what Andrews and Phillips state over optical turbulence, but from a weather

perspective instead of an electro-optics imaging perspective (Doviak & Zrnic, 1993). Like Andrews and Phillips, they discuss Kolmogorov theory, cascade theory, and structure functions. In fact, they delve deeper into describing structure functions.

An interesting aspect of radar applications relevant to measuring optical turbulence is its capability of “range-gating” layers of the atmosphere. Unlike scintillometers, which take a path average, radar is able to range-gate due to Bragg scattering effects. Radar “sees” range when the back scatter off of its original signal comes back. Below is the equation for the expected scattering cross section per unit volume, otherwise known as reflectivity (Doviak & Zrnic, 1993:452).

$$\eta = \frac{(SNR)\alpha^2 P_T A_e \Delta r}{9\pi r^2 kTB} \quad (14)$$

Equation 14. Radar reflectivity as a function of radar system specifications.

SNR	= signal to noise ratio
α	= antenna efficiency
P_T	= peak pulse power
A_e	= effective antenna aperture
Δr	= range resolution
r	= range
k	= Boltzmann’s constant
T	= receiver system temperature
B	= receiver bandwidth

Optical turbulence is directly related to reflectivity in Equation 15 (Doviak & Zrnic, 1993:452).

$$C_n^2 = (\eta / 0.38)\lambda^{1/3} \quad (15)$$

Equation 15. Optical turbulence strength relation to radar reflectivity.

Units are important to keep track of when attempting to derive optical turbulence strength from reflectivity. S-band (10cm) weather radars, like Wilimington Ohio's WSR-88D Nex-Rad provide reflectivity in units of dBz, which is logarithmically related to the number of drops per unit volume and their diameter to the sixth power. Logically, this is because weather radars are engineered to look at water droplets in the atmosphere. However, even if there is no precipitation, weather radar will still provide reflectivity information. This being so, with no precipitation, a weather radar is in "clear air mode" and can be used to measure optical turbulence. The Wilmington's Nex-Rad radar information is easily accessed with a subscription to www.weatherTAP.com. The radar information provided from weatherTAP is given in units of dBz. Below is the equation relating dBz to drop diameter to the sixth power per unit volume.

$$dBz = 10 \text{Log}_{10} Z_e \quad (16)$$

Equation 16. Reflectivity (dBz) relation to Z_e .

Z_e is in units of $(\text{mm}^6)\text{m}^{-3}$, where mm^6 refers to drop diameter and m^{-3} refers to volume.

Z_e is directly related to reflectivity in the following equation.

$$\eta = \frac{\pi^5}{\lambda^4} |K_w|^2 Z_e \quad (17)$$

Equation 17. Z_e relation to reflectivity.

K_w is related to the complex index of refraction for *water* in the following manner:

$$K_w = \frac{m_w^2 - 1}{m_w^2 + 2} \quad (18)$$

Equation 18. K_w relation to the complex index of refraction for water.

The radar method will be delved into further in the methodology chapter. Optical turbulence will be derived from weather radar and compared to the other methods described.

III. Methodology

Overview

This section outlines the logic used to verify and demonstrate the index of refraction method of deriving optical turbulence. Theory, modeling and simulation, experimental lab work, and experimental field work are combined to comprehensively examine this method.

First, holding wavelength constant, a deeper look into the McClung-Tunick modeling and simulation tool is done to properly understand its “forcing variables” (most influential inputs). A small sensitivity study of the tool is performed to understand which factors in the model are the most influential on optical turbulence, and to ask the question “does this make sense?” This information in hand, experimental field equipment to include a weather station which provides data for each input needed for the model is chosen and calibrated. Calibration data of sensors for the most influential forcing variable at the 880nm wavelength, temperature, is shown.

Secondly, the set-up for the experimental field work is determined, and data is gathered in the field using weather equipment and the BLS900. For a meaningful comparison, data collection for both weather equipment and BLS900 is taken at the exact same time and location. Weather inputs are used to determine optical turbulence over time in the McClung-Tunick model after adjustments are made to the original algorithm. Optical turbulence values from the model are then compared to values taken by the BLS900 scintillometer.

Thirdly, with the intentions of varying wavelength, an experimental laboratory scintillometer is built at AFIT using a tunable wavelength laser. The AFIT scintillometer is qualitatively proven and is a first step towards validation of the anomalous dispersion portion of the McClung-Tunick model. Refractivity plots across wavelength, created using the model are investigated. Specifically, refractivity of the wavelength ranges of the AFIT tunable wavelength lasers are looked into.

Lastly, demonstrations of the tool's usefulness are presented in the form of a communication laser sensitivity study and a weather radar proof of concept.

McClung-Tunick Variable Sensitivity Charts

For any given modeling and simulation tool, it is important to find out which variables have the greatest influence on the code's outcome. This sanity check is part of a proper vetting of one's code. This effort reduces error and enables one to realize which sensors need to have what accuracy levels, regarding code validation. This has been done for the McClung-Tunick tool in the following small variable sensitivity study.

Figures 7 and 8 depict each factor's impact on C_n^2 , illustrating how pressure, temperature gradient, humidity gradient, and wind gradient affect optical turbulence. Wright-Patterson Air Force Base (WPAFB) November afternoon weather values were chosen as initial conditions as these values were part of a real data collection effort. The following were the initial values: pressure at 1010.4mb, temperature gradient at 0.8°C, wind gradient at 6.3m/s, and humidity gradient at 4%, along with a wavelength of 880nm, and height gradient of 1.79m (tripod limitations in the field). One variable at a time was changed a particular percentage while holding the rest constant at their control value.

Wavelength and height levels never varied. Wavelength was not varied since the scintillometer used in verification emits a fixed wavelength of 880nm +/-20nm.

Additionally, the following charts show no interactions of variables. Realistically, as one increases temperature, a decrease in pressure would follow, however, it is a much more complicated relation than merely the ideal gas law: $P = \rho RT$

. Local weather is not an absolutely closed system.

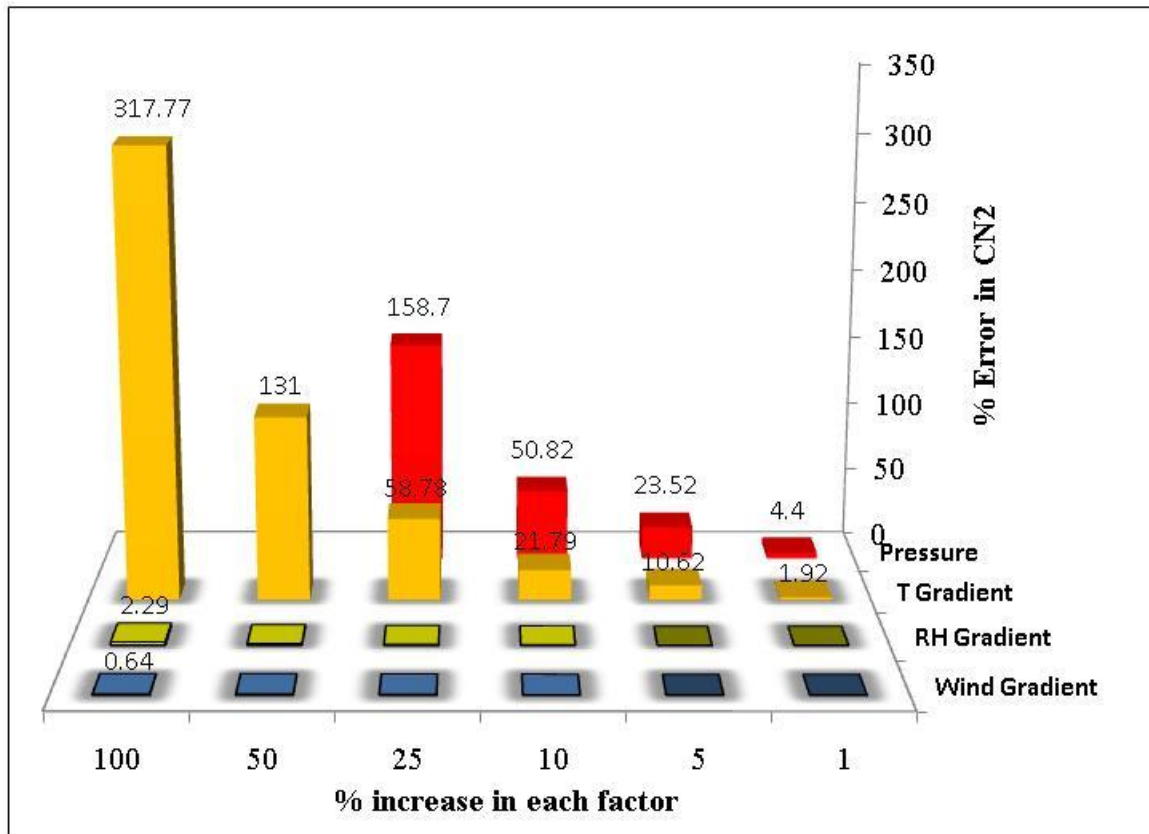


Figure 7. Percent error introduced in to C_n^2 when increasing each factor a particular percentage. At 880nm, pressure and temperature gradient are by far the most influential factors.

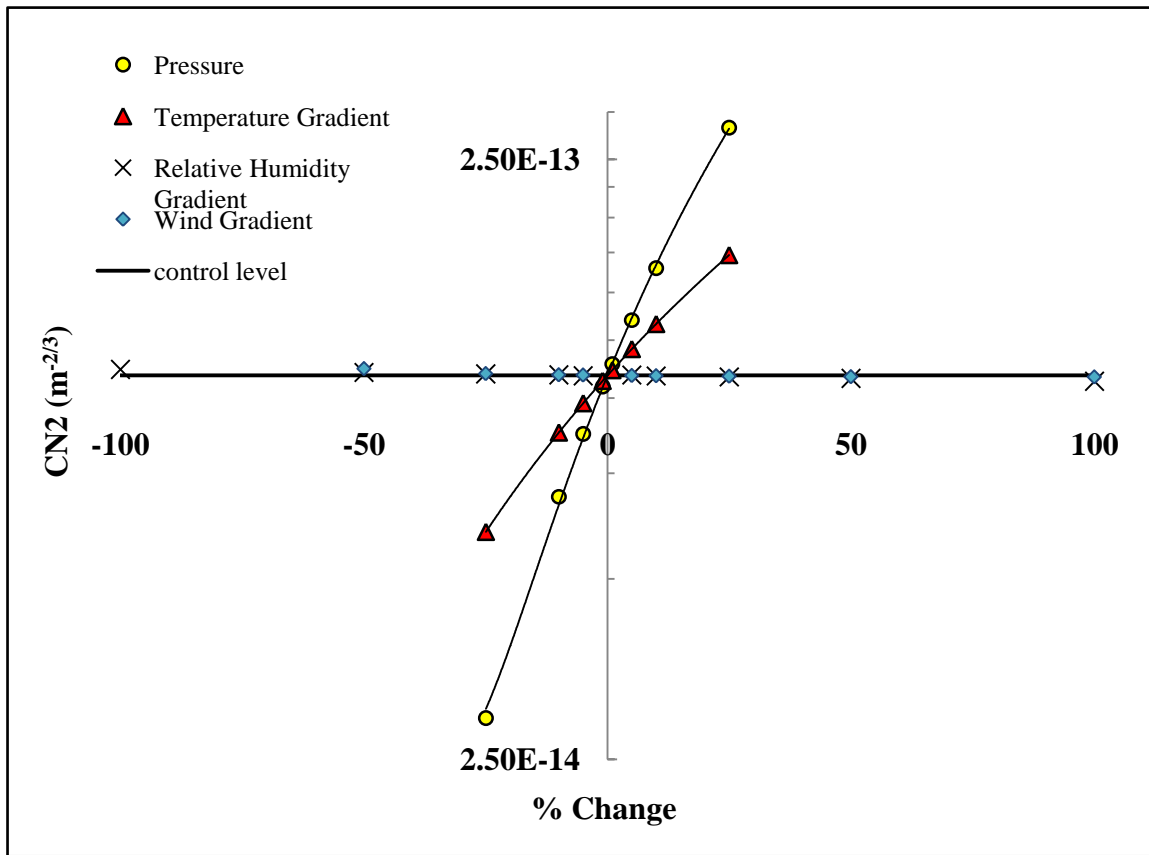


Figure 8. Optical turbulence sensitivity to weather factors. Optical turbulence presented in actual values, not a percentage from a control level. The solid black line is the control level $1.092 \times 10^{-13} m^{-2/3}$. Note the y-axis is logarithmic. Pressure and temperature gradient overshadow other variables.

When looking at the bar chart, Figure 7, it is easy to see that pressure and temperature gradient have the greatest impact on optical turbulence by far. This makes perfect sense, recalling in the literature review Andrews and Phillips stated that fluctuations in the index of refraction were due to small fluctuations in temperature. In both factors, as their error increases, the error in optical turbulence increases at a quadratic or exponential rate. However, for pressure, it is cut off at +/- 25% error because of nonsensical physical meanings beyond 25% error. The original value of pressure was 1010.4mb for WPAFB on a November afternoon. At -25% error, the

pressure read would be 757.8mb or 1.5 miles above sea level, and at +25%, 1263mb or 1.18 miles below sea level for standard day values!

Unlike error in pressure, it is easy to have large errors in the temperature gradient. It is very easy to be off by 100% if not careful. For this small study, the two vertical levels were separated by 1.79m. A reading of 0.8°C was the temperature gradient ($T_1 - T_2$). To be off by 100%, one needs to only be off by 0.8°C! There are two possible solutions to this problem of hypersensitivity to temperature gradient. First, one could extend the vertical difference between the two levels. Secondly, one could acquire highly accurate thermocouples to read the temperature gradient. This last option is surprisingly more cost effective, mobile and will be discussed in the results section as an option to the weather station method.

Weather Station

With the model's sensitivity study performed, the next step involved obtaining atmospheric weather sensors. These sensors would gather the input data for the McClung-Tunick code and compare against the BLS900 scintillometer. Since the BLS900 averages over its path, if one measures over a flat, homogeneous terrain, only one weather station in the middle of the path is needed. It is assumed that optical turbulence at one location in a flat, homogeneous terrain is representative of the entire terrain's optical turbulence when averaged. This is a major assumption in the methodology, that one set of sensors at two vertical levels located in the middle of the path is sufficient.

Knowing that temperature was the primary forcing variable for the model, it was important to obtain sensitive temperature sensors along with the rest of the needed weather sensors. The Davis Weather Station Vantage Pro II Plus is one of the best weather stations commercially available. This weather station was chosen over other weather measurement tools due to its temperature accuracy, data rate output, wireless data logging capability, and dual level temperature and humidity sensors. It provides data for temperature every 10 seconds, suitable to match the BLS900 rate of one data point per minute. The Davis Weather Station's two levels of temperature and humidity, along with a wind and pressure sensor provided all the data needed for the model in one package. However, the accuracy of the temperature sensors, extremely good for commercial purposes, were not, in the author's opinion, as accurate as needed for full validation.

According to industry, such as Davis and Omega Engineering, it is difficult to get temperature sensors accurate to 1°C, and extremely difficult to go beyond that. The first temperature level, T1, located in the integrated sensor suite (ISS), has an accuracy engineered to 1°F or 0.5°C and a resolution of 0.1°F or 0.1°C. The second level of temperature, T2, located in the Temp/Hum system also has a stated accuracy of 0.5°C, but a resolution of only 1°C. Because of this, the highest accuracy obtained in the vertical gradient of temperature would only be 1°C according to specifications. However, it is important to do one's own calibration of sensors used and not solely rely on specification sheets. Calibration results of the weather station temperature sensors, along with several other temperature sensors are presented next.

Temperature Sensors Calibration

Because of the known hypersensitivity to the temperature gradient in the code, an in-depth calibration and study of available temperature sensors were performed. As previously stated, the Davis Vantage Pro2 Weather Station is one of the most accurate weather stations commercially available. From its specification sheet, the ISS containing the T1 sensor has an accuracy of 0.5°C and a resolution 0.1°C . Sensor T2 has an accuracy of 1°C , and outputs in 0.1°C resolution on the console reader (however in reality is calibrated for 1°F resolution).

The following calibration experiment was performed to determine the accuracy of the weather station's T1 and T2 sensors when placed in the same environment. A mercury thermometer, T1, and T2 were placed inside a refrigerator for 2 hours (maintaining the door closed). After two hours passed, to allow for equilibrium, the readings from each sensor are shown in Figure 9.

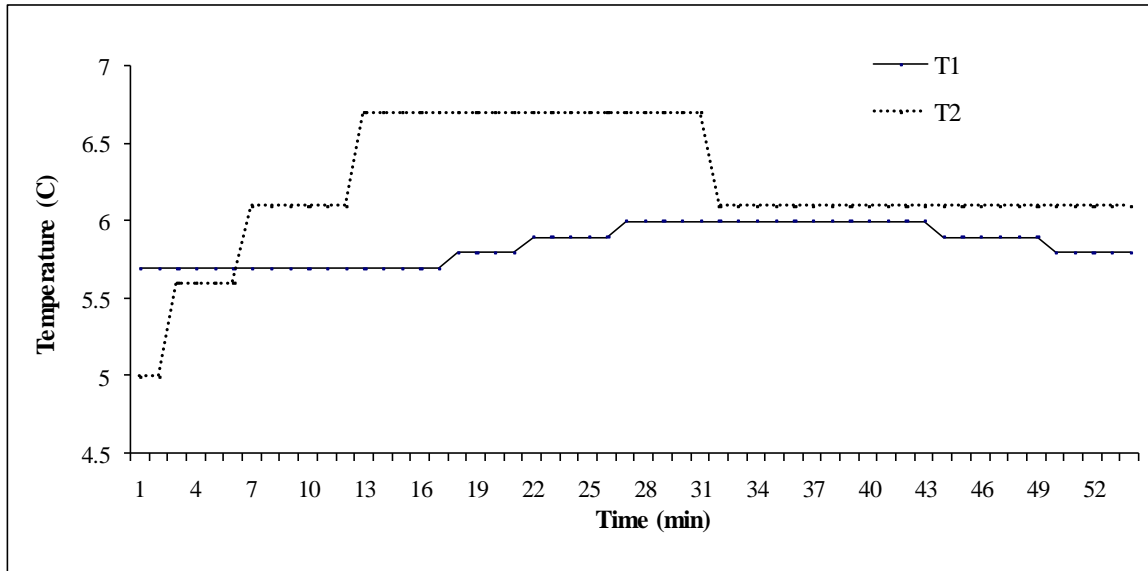


Figure 9. Refrigerator calibration of temperature sensors. T1 and T2 were enclosed for 2 hours before beginning measurement. Average difference between sensors was 0.5C.

Over the span of 53 minutes, the average error between T1 and T2 is 0.45°C or 0.5°C when rounding to the resolution of the system. That was a better value than expected from the specification sheet in this scenario. Next, the sensors were taken out of the closed cold environment and placed at the same level at room temperature.

Surprisingly, after being taken out of the refrigerator, both sensors took approximately an hour and a half to read the correct room temperature (20°C), see the graph below. The temperature response was incredibly slow, especially for a weather station that should be able to respond quickly to fast moving warm or cold fronts. Lack of wind in the room was decidedly a factor. No wind to blow across the temperature sensors, and the internal fan which draws in air across T1 was off due to lack of sunlight (T2 has no fan capability), so the measured temperatures were merely the result of the sensor shielding slowly warming up from the ambient environment. The solar shielding around T1 has more mass, thus explaining why T2 has faster response.

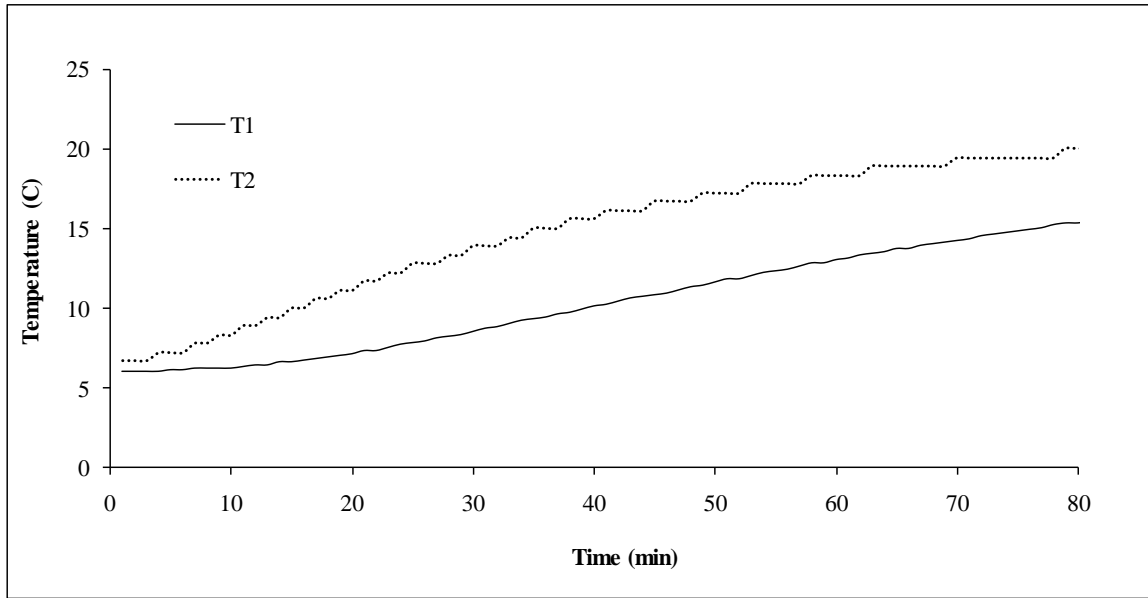


Figure 10. Reaction time of weather station temperature sensors when taken from a 6C refrigerator environment to a 20C room temperature environment. Reaction time would increase with the presence of wind or T1's fan operating. Note the faster response of the T2 due to the lesser shielding mass. Also note the lower resolution of T2 as compared to T1.

After the room temperature test, T1 and T2 were placed outside at the same level, in the presence of wind, overnight (Figure 11). Unlike the other two graphs, the delta between T1 and T2 was observed since I no longer looked for the sensors to read one particular temperature value. After being outside all night, the average error in the gradient was again found to be 0.45°C, with rounding to the resolution of the system 0.5°C. Again, this is a very good value, however it is the minimum error one could expect when the system is working ideally and no fast temperature changes occur.

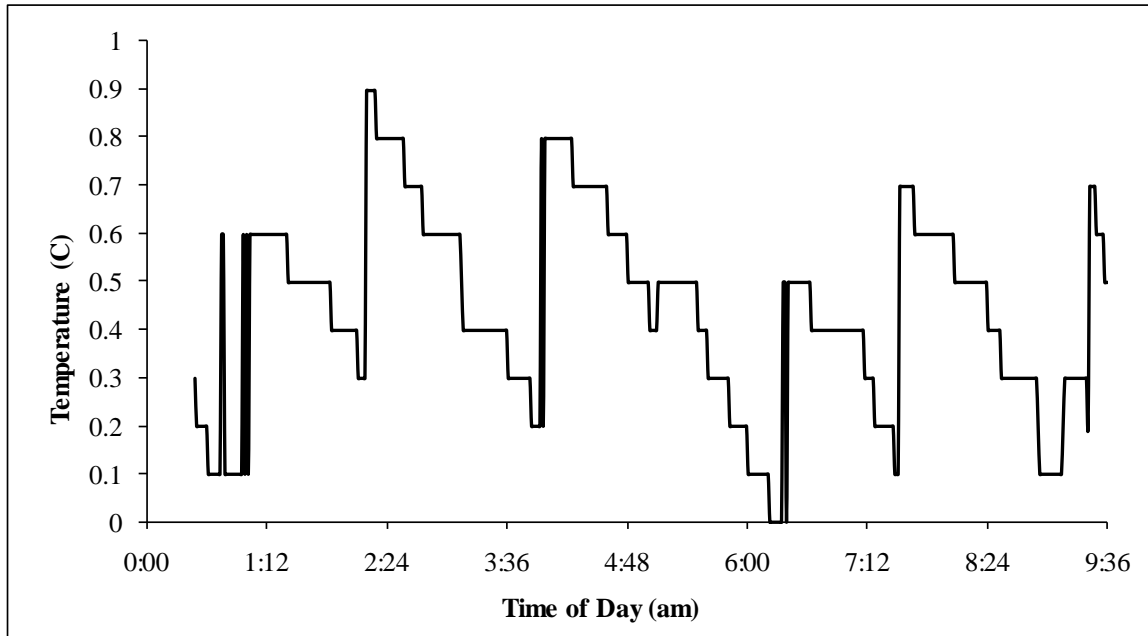


Figure 11. Delta T (T1-T2) data from weather temperature sensors when placed outside overnight at the same vertical level. The weather station’s average temperature gradient error is 0.5C.

In summary of the calibration of the T1 and T2 sensors, 0.5°C was the minimum temperature gradient error found in ideal conditions. Any combinations of low wind, little or no sunlight to run the internal fan, and fast temperature changes will increase error dramatically. Because of this, an alternative to the weather station method was developed using thermocouples and readily available KFFO weather data.

Field Experiment Set-Up

For the field experiment, the Scintec BLS900 scintillometer was used in conjunction with the Davis Vantage Pro2 Weather Station. In this way, scintillometer (intensity variation method) and McClung-Tunick calculations (index of refraction method) were compared against each other. Scintillometer data was treated as the control or “truth” data (as long as it remained within its operational boundaries). The intensity variation method is more robust in the sense it has no hypersensitive input variable that

would cause the output to be orders of magnitude off, as opposed to the index of refraction method. This is a strength of the intensity variation method.

Only one weather station was used in the middle of the scintillometer path range, as the chosen path was homogenous, flat, and contained no obstructions. With these assumptions met, the weather station was placed in the middle of a grassy field, and slightly offset as to not obstruct scintillometer transmission. See the pictures below for a depiction of the field in which the experiments took place, the scintillometer receiver, and the weather station. Data was taken in October, November, and December of 2008. A path range of 800m was chosen because optimal optical turbulence values at this path length are approximately 1.5×10^{-14} to $3.5 \times 10^{-10} \text{ m}^{-2/3}$ (Scintec, 2008). This range of values are appropriate for the WPAFB grassy field environment, minimizing the chance of hitting a floor or ceiling of the BLS900.



Figure 12. Field experiment location, mowed grassy field at WPAFB, next to the Air Force Museum.

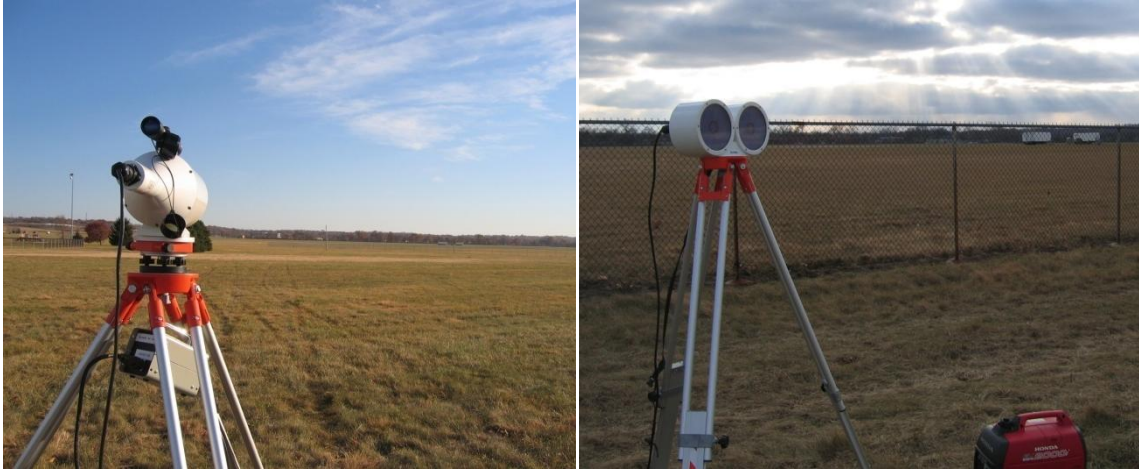


Figure 13. BLS900 receiver and transmitter from left to right. Pictures taken on different days, receiver taken on 7 Nov. 08 and transmitter on 31 Dec. 08.



Figure 14. Scintillometer receiver looking down the path towards the weather station and transmitter. Path length is ~800m. Weather station placed in middle of path range.

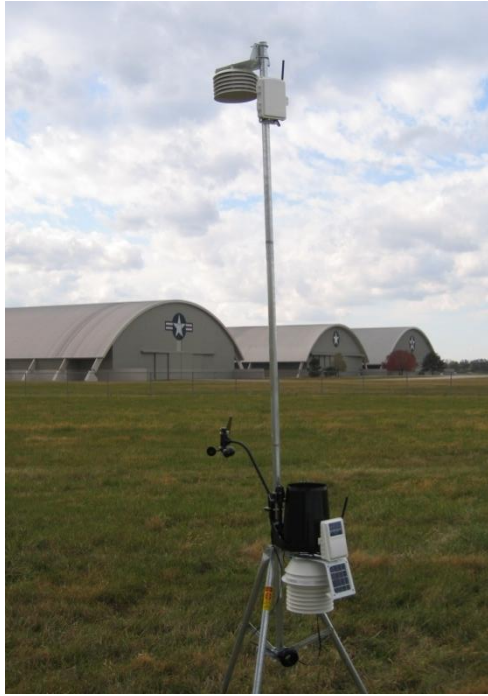


Figure 15. Davis Vantage Pro2 Plus weather station. Two levels of temperature and humidity, one level of pressure and wind are given. Two levels of wind are extrapolated as needed for the model by assuming a linear wind profile and that wind being zero at height zero.



Figure 16. Thermocouple tripod station for two levels of temperature measurements, located in the middle of the BLS900 path, slightly offset, just as weather station set-up. Note lack of shading devices used this day due to overcast.

The same experimental set-up is used for the alternative thermocouple method. Thermocouples (shaded from direct sunlight) are placed at two levels on a tripod, instead of the weather station. Again, the location of the tripod is in the middle of the scintillometer path range. For the other weather inputs, data was taken from the KFFO weather station (located on WPAFB). Pressure, humidity, and wind inputs were used in hourly blocks. The second level of wind was arrived at assuming a linear wind profile, knowing there is zero wind at level zero and the value of the wind given by KFFO is at the standard 10m height.

Omega Engineering's HH506RA, high-accuracy thermocouple data logger was used with both type K and type T thermocouples. Omega engineers were consulted after reviewing accuracy, temperature range, and response charts to come up with the best thermocouple to use with the HH506RA. This was the type T (copper) that can handle moisture well, lower temperatures, and had the least error of the other thermocouples at $\pm 0.8^{\circ}\text{C}$ error $\pm 0.3^{\circ}\text{C}$ for the electronics in the data logger. Type K thermocouples, including the data logger, have a reported error of $\pm 2.5^{\circ}\text{C}$. It is important to note that if some of these reported errors are a constant drift problem (not random noise), and both levels of thermocouples drift at the same rate, then the temperature gradient error is actually reduced significantly.

AFIT Scintillometer

The purpose of building a scintillometer at AFIT was to detect an increase in C_n^2 as an increasing temperature gradient was introduced. The creation of an AFIT scintillometer allowed a deeper look into intensity variation theory and potentially

anomalous dispersion, given the ability to vary wavelength with the tunable laser. An algorithm in MatLab was created using the guidance of Equations 11-13. See Appendix B for the MatLab code, taking intensity variation and converting it to optical turbulence strength. This code was tested by placing a hot plate in the middle of the path of the laser and varying the temperature. The laser was split along two paths and two photodiode detectors were used (D1 and D2). One path went over the hotplate, L1, and the other was kept as a control with no hotplate, L2. The experiment was run at four settings: room temperature, 100°C, 190°C, and 240°C all at $\pm 3^\circ\text{C}$.

The following lists equipment used:

- Tunable Diode Laser #1 (759nm - 771nm) – Model #6312 6000 Vortex Series from New Focus Inc., laser beam $\sim 2\text{mm}$ beam diameter in laboratory
- two photodiode detectors - PDA100A (400nm-1100nm), amplified silicon detectors (gain set to zero), active diameter 9.8mm
- frequency chopper set to 1950Hz $\pm 5\text{Hz}$
- two lock-in amplifiers – Model #SR850 from Stanford Research Systems
- hot plate – area of plate 18.5cm by 18.5cm $\pm 0.5\text{cm}$
- fan – set to 3.0 m/s

Data, in the form of voltage at the detectors, was taken 5000 times a second for three minutes each run. Results are presented in two degrees of averaging, a data point every fifth of a second (every 1000 points averaged), and a data point every second (every 5000 points averaged).

The pictures below illustrate the set-up:

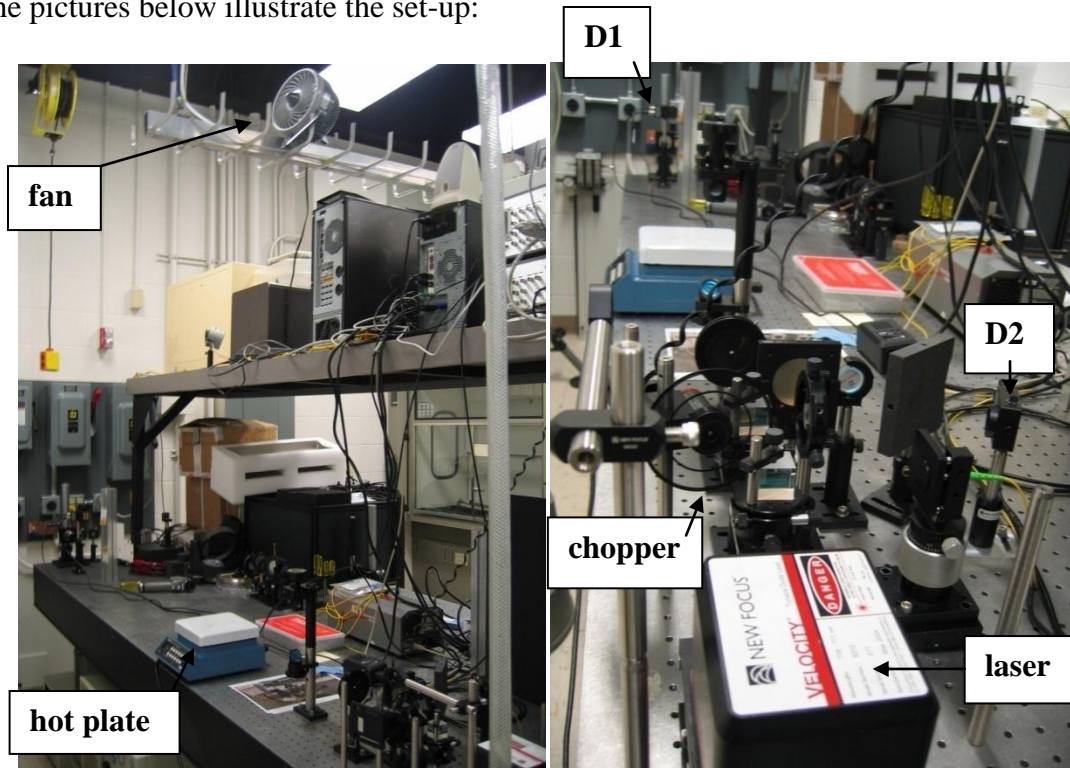


Figure 17. Laboratory built scintillometer experimental set-up.

Control cases were run at room temperature with no hot plate. The laser beam was positioned 26.5cm +/-0.5cm above lab table. Height of hot plate was 12cm +/-0.5cm above table. The two laser path distances used were L1 at 263cm +/- 2cm that went directly over the hot plate, and L2 at 48cm +/- 2cm which went off to the right side and avoided the hot plate. The laser was positioned 112cm +/- 1cm from the hot plate. Laser power was set to 9.0mW at a wavelength of 760.25nm +/- 0.25nm. A fan was located aloft at a height of 155cm +/- 1cm above the lab table in an effort to simulate outside weather and investigate if the McClung-Tunick model would potentially scale with this set-up. Derived C_n^2 values obtained by measuring the laser's intensity fluctuations versus hot plate temperature are presented in Chapter IV.

Communication Laser Sensitivity Study

The general concept of optical turbulence is grasped easily enough, yet its exact implications on system x or application y are more elusive. Questions like, “What does a C_n^2 value of 1×10^{-13} ($\text{m}^{-2/3}$) mean to me in terms my laser’s power in the bucket?” The answer, like the answer to most physics questions is, “It depends.” The true answer depends on the wavelength of one’s laser, and the exact environment it will be used in, i.e. desert, humid, night or day, and so on. It is with this in mind that a communications laser study has been put together to demonstrate the usefulness of the index of refraction method of deriving optical turbulence.

Geographic location, time of day, and season is varied to determine a value of C_n^2 . AFIT/CDE has a large database of weather information for numerous locations around the globe hailed as ExPERT. The ExPERT database is used in this study to find realistic average levels of weather data for the different geographic locations, times of day and season. The levels of weather data are then used as inputs into the McClung-Tunick model and a correlating optical turbulence value is arrived at. This turbulence value is held constant as an input into a HELEEOS laser scenario.

HELEEOS’s laser scenario encompasses a 50kW laser, located 2m off the ground directed horizontally at a 1m square receiver located 2km away, which is also 2m off the ground. Output values of spot size, power in the bucket, and peak irradiance are investigated. Holding C_n^2 constant over the laser path is reasonable since the scenario does not vary, vertical height and terrain for each location is assumed homogenous. Additionally, just as HELEEOS is capable of slant path scenarios, yet for this initial study

vertical height is held constant, so too is the model capable of anomalous dispersion effects, yet this study does not vary wavelength. The common wavelength used for laser communications at $1.55 \mu m$ is held constant.

Tables 1 to 3 below illustrate the run matrix of scenarios. Three different geographic locations, Nellis AFB, WPAFB, and Eglin AFB, were chosen to represent varying climates: desert, mid-latitude, and humid, respectively. June and January represented the two varying seasons, summer and winter.

Table 1. Run matrix for desert scenario at Nellis AFB, NV. Three values for time of day: night, morning, and afternoon are chosen. Two values of season: June and January are chosen.

	Season	
Time of Day	June	January
0000-0300	Nellis_Jun_0300	Nellis_Jan_0300
0900-1200	Nellis_Jun_1200	Nellis_Jan_1200
1200-1500	Nellis_Jun_1500	Nellis_Jan_1500

Table 2. Run matrix for mid-latitude scenario at WPAFB, OH.

	Season	
Time of Day	June	January
0000-0300	WPAFB_Jun_0300	WPAFB_Jan_0300
0900-1200	WPAFB_Jun_1200	WPAFB_Jan_1200
1200-1500	WPAFB_Jun_1500	WPAFB_Jan_1500

Table 3. Run matrix for humid scenario at Eglin AFB, FL.

Time of Day	Season	
	June	January
0000-0300	Eglin_Jun_0300	Eglin_Jan_0300
0900-1200	Eglin_Jun_1200	Eglin_Jan_1200
1200-1500	Eglin_Jun_1500	Eglin_Jan_1500

As previously stated, AFIT/CDE has a large database of weather information (ExPERT) for many locations around the globe. As such, there is a wealth of weather data. As an example, 50% of the time in June, at Nellis AFB, at 1200, the air temperature will be 98°F. However, this data is for one level at 1.25m (4ft) above the ground, a standardized height measurement for air temperature. For the second level at 4.25m, which provides an even 4m difference in levels, educated guesses are used. Please keep in mind this study is merely a demonstration of the tool's usefulness, but is obviously *more* useful with actual data, as opposed to averages.

The educated guesses used are not bad assumptions to make for the following reasons:

1. Temperature² – at this wavelength (1.55 μm), and of all the variables, the temperature gradient impacts C_n^2 the greatest. As such, a range of values is provided so that the user can view the data like a look-up table, i.e. “when my temperature gradient is 2°C in this environment, at this height, my C_n^2 will be x.”

2. Wind2 - being so close to the ground, at 10m (the standard measurement height for wind), wind approximately increases linearly with height. In reality, wind varies logarithmically with height. However, when observing that trend, the height level is much greater. We can also assume that there is zero wind at ground level (0,0), and since we already know one level of wind at 10m (10, x [m/s]) we can calculate through a simple point slope equation the other levels at 1.25m and 4.25m.

3. Humidity2 = Humidity1 + 2%. These values are taken from average differences seen in humidity levels in field research at AFIT. Even if I am wrong on these humidity assumptions (which is likely), at $1.55 \mu\text{m}$, humidity has little impact on C_n^2 as compared to the temperature gradient's impact. For example, being off by 100% in my humidity gradient results in a 2.29% error in C_n^2 . However, the reader should keep in mind that at a different wavelength, such as in the THz region, humidity error will not be as easily hand waved away. Humidity input assumptions should be reassessed if altering wavelength.

Recalling the sensitivity charts produced earlier in Figures 7 and 8, it is notable to mention it is assumed those error trends done at 880nm are valid still for the $1.55 \mu\text{m}$ laser communications wavelength. Sensitivity error charts were not recreated for the different wavelength because both wavelengths have no anomalous dispersion. While the absolute value of optical turbulence is less for all factors at $1.55 \mu\text{m}$ than at 880nm (1.081e^{-13} vs 1.092e^{-13} , respectively), this is due to normal dispersion. Looking at Figure 18 below, the trends in percent error for 880nm should also be valid for the $1.55 \mu\text{m}$.

Both wavelengths are at “clean” lines, with very little absorption and thus little anomalous dispersion. More or less anomalous dispersion at one wavelength than the other would throw off the study. For example, looking at the Terahertz region, the relative humidity gradient should have more of an impact on optical turbulence due to strong water absorption lines present, than the relative humidity gradient would normally have at 880nm.

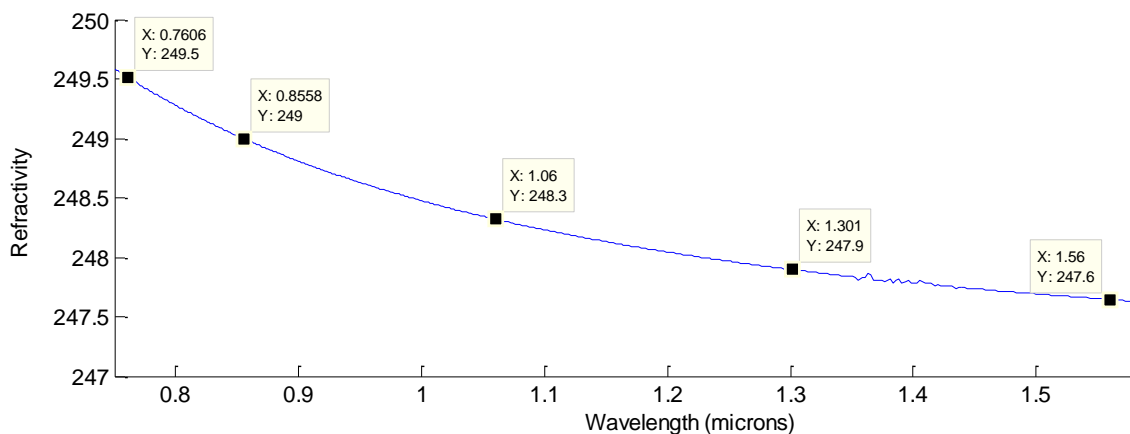


Figure 18. Normal dispersion curve from 760nm – 1560nm. Optical turbulence decreases as the index of refraction decreases. Every box is a depiction of each of AFIT’s five tunable wavelength lasers.

Optical Turbulence Derived with Weather Radar

Akin to the laser communications sensitivity study, the weather radar study demonstrates the far-reaching capabilities of the index of refraction method. In the future, radar and the index of refraction method may potentially be paired together to produce a network of range-gated optical turbulence data. Such an optical turbulence network would have a significant impact on many applications. For example, in wireless communications, being able to stretch the maximum usable range, in imaging, being able

to correct images from further distances away, and in laser weapons, affording better HEL beam propagation correction. In this theorized network, applications have available to them optical turbulence information that is real-time, local, and three dimensional.

As a first step in demonstrating the connection between radar and the index of refraction method, a 10cm S-band weather radar at Wilmington, OH was used in conjunction with the BLS900 and McClung-Tunick model. Using Equations 15-18 together from the literature review chapter and keeping units in mind, an equation relating optical turbulence strength directly to radar reflectivity can be arrived at. See Equation 19. Wavelength is in units of meters and dBz will range from -26 to 0 dBz in the radar's clear air mode.

$$C_n^2 = 2.63\pi^5 \lambda^{-11/3} |K_w|^2 \frac{10^{\left(\frac{dBz}{10}\right)}}{(1000)^6} \quad (19)$$

Equation 19. Optical turbulence strength related to dBz with wavelength in units of meters.

Since the index of refraction for any medium changes with that medium's temperature, it is important to look up values at various temperatures to make a good estimate. Below, in Table 4, the complex index of refraction of water, m_w , was taken from AFIT/CDE's LEEDR/HELEEOS database (Fiorino et al., 2008). With a temperature value of 5°C for the atmosphere estimated and using Equation 18, the resulting value for $|K_w|$ is 0.964 and $|K_w|^2$ is 0.929. These ended up being commonly used values for these variables.

Table 4. Complex index of refraction for water at various temperatures.

Temperature (C)	m_w
0	9.0353+1.3944i
10	8.9832+1.0144i
20	8.8577+0.747108i

Now with the last variable, K_w , needed to find optical turbulence from reflectivity, Equation 19 can be used along with reflectivity data from the Wilmington radar to find optical turbulence. Acquiring reflectivity data from Wilmington is available through weatherTAP.

WeatherTAP required GPS coordinates from the scintillometer location in order to draw a 1 mile diameter ring, labeled AFIT field. The picture below in Figure 19 shows the exact location of the scintillometer during data collection. Figure 20 is example radar reflectivity from weatherTAP for tilt 1 (0.5°) and tilt 2 (1.5°), respectively. Tilt 1 gives reflectivities lower to the ground than tilt 2. AFIT field is approximately 30 miles away from Wilmington, OH. This means the optical turbulence derived is for the atmosphere above the field within approximately a few thousand feet.

In the AFIT field ring are nine pixels correlating to a specific reflectivity. Reflectivity is denoted by pixel color. The entire ring was averaged to provide one value for reflectivity. Black or null values were treated as -26 dBz instead of zero. This value corresponds to the minimum radar reflectivity that can be received.

Lat: Lon: Combo: [Set Pin Here](#) [How to use this page](#)

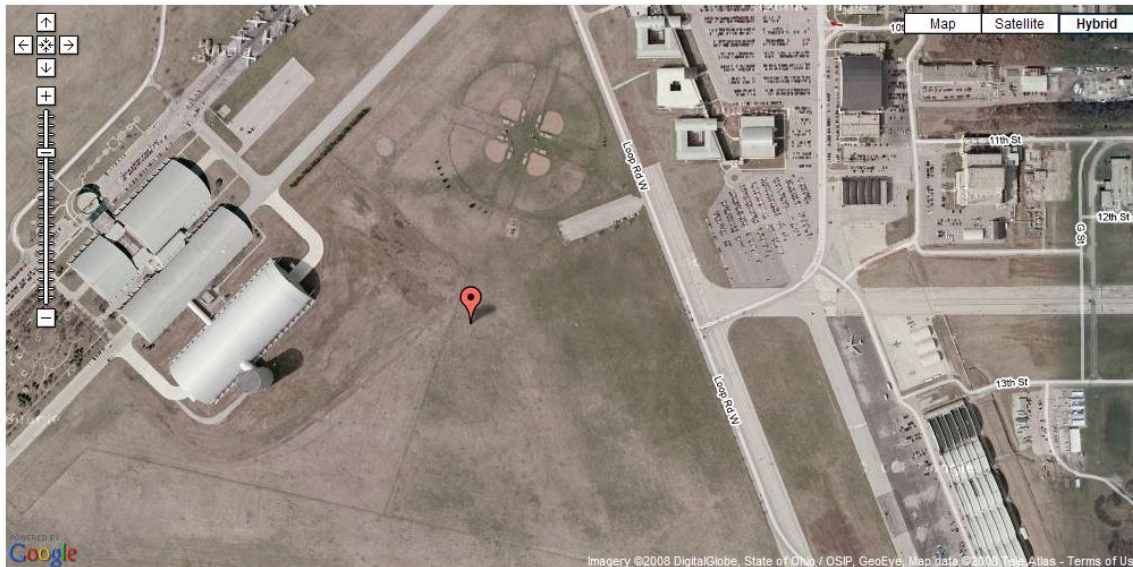


Figure 19. GPS coordinates of scintillometer location available through Google.

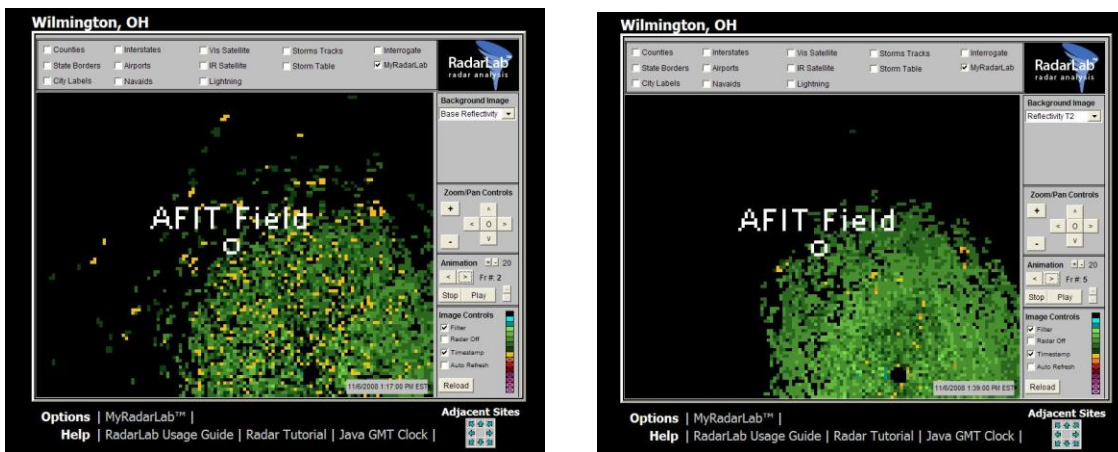


Figure 20. Example of reflectivity data from weatherTAP radar analysis model.

Results of optical turbulence derived from weather radar are unveiled in the next section.

IV. Analysis and Results

This results section is organized into four parts: modeling and simulation, laboratory experiment, field experiment, and demonstration results.

Modeling and Simulation Across Wavelengths

In preparation for the laboratory and field scintillometer experiments, the McClung-Tunick model was used to investigate the amount of expected anomalous and normal dispersion within the regions of AFIT's five tunable wavelength lasers and the BLS900 scintillometer. Refractivity versus wavelength plots were created by running 10,000 point calculations in the code across the stated ranges of the tunable lasers and the BLS900. For example, the BLS900 transmits at a wavelength of 880nm +/- 20nm, therefore, a wavelength range from 860nm-900nm was graphed. Figures 21 and 22 are of tunable lasers #1 and #5, respectively. The plots for tunable lasers #2-4 had no discernable absorption features, looking similar to Figure 23 of the BLS900 refractivity.

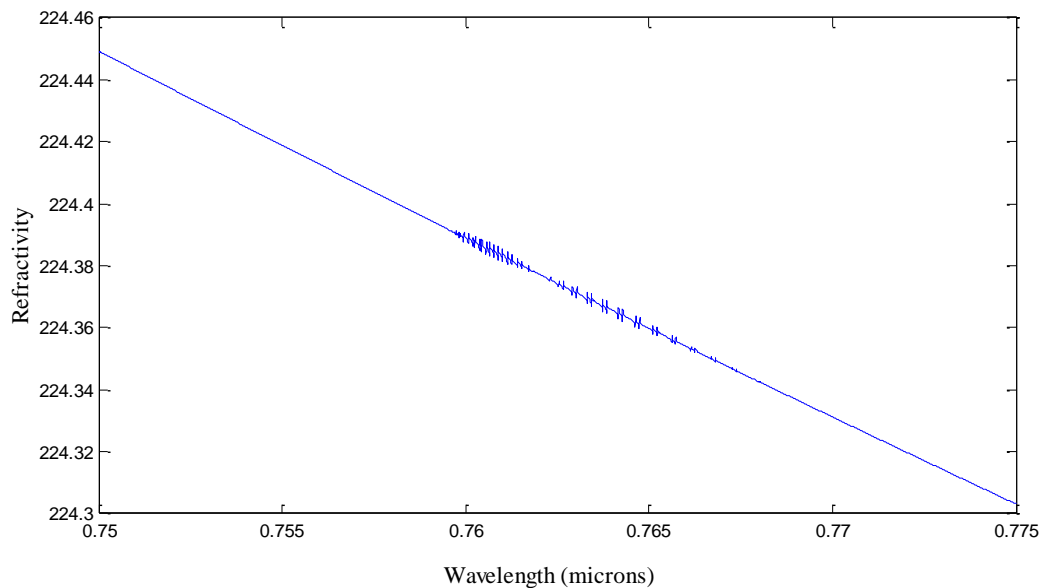


Figure 21. Theorized refractivity of tunable wavelength laser #1. 10,000 point calculation performed in the McClung-Tunick tool. Note the absorption features of O₂. If sensitive enough, the laboratory scintillometer could theoretically measure a distinction in optical turbulence when the laser's wavelength is at an absorption line or not.

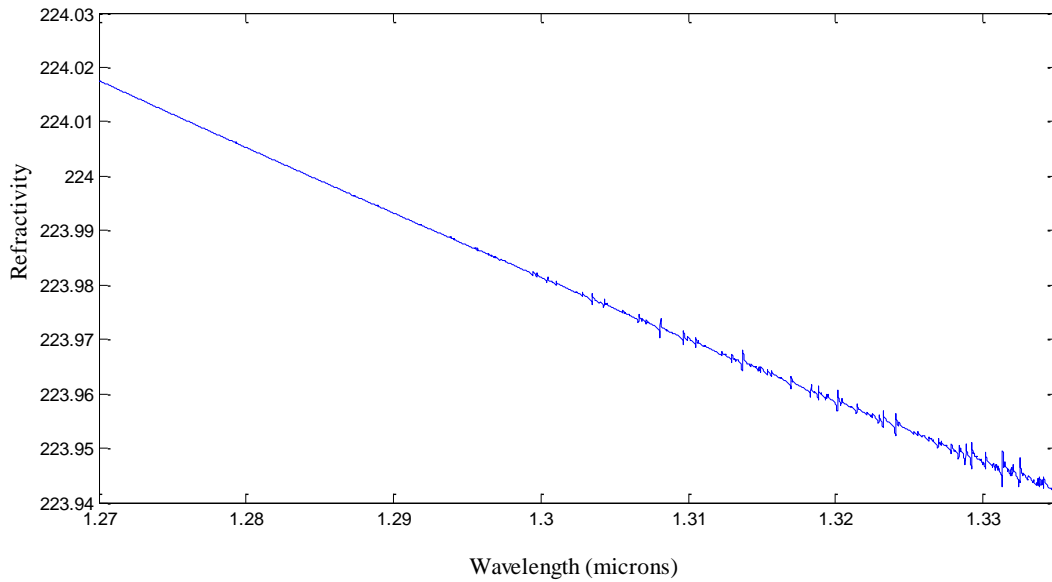


Figure 22. Theorized refractivity of tunable wavelength laser #5. 10,000 point calculation performed in the McClung-Tunick tool. Absorption features are seen around the 1.33 micron wavelength, and are most likely around the same strength as laser #1. Note the scale of each axis. To prove that optical turbulence has different values at absorption lines than not, one need find lasers that cross stronger absorption lines. These features are not strong enough to discern that the difference in optical turbulence is only due to anomalous dispersion and not system error.

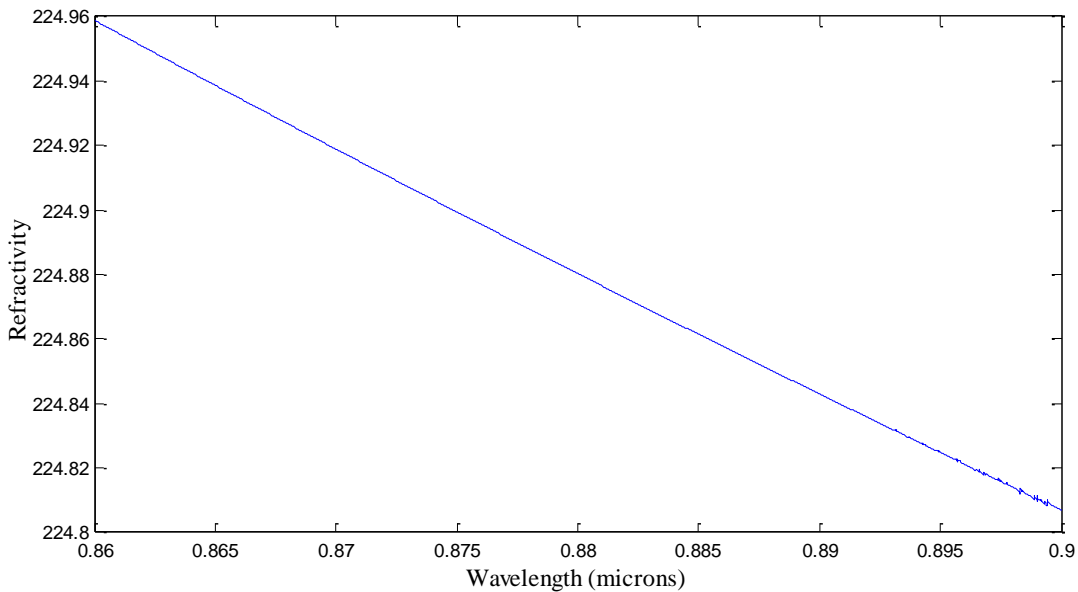


Figure 23. Theorized refractivity of BLS900 scintillometer. 10,000 point calculation performed in the McClung-Tunick tool. There are little to no absorption features present at this wavelength range. This is perfect for the scintillometer as they are not currently capable of accounting for anomalous dispersion.

Additional plots across wavelengths were created to investigate the tool and compare its graphs to other plots in literature, like the Mathar curves from Figure 5. Figures 24 and 25 recreate the Mathar curves while Figure 26 provides a broader spectral range.

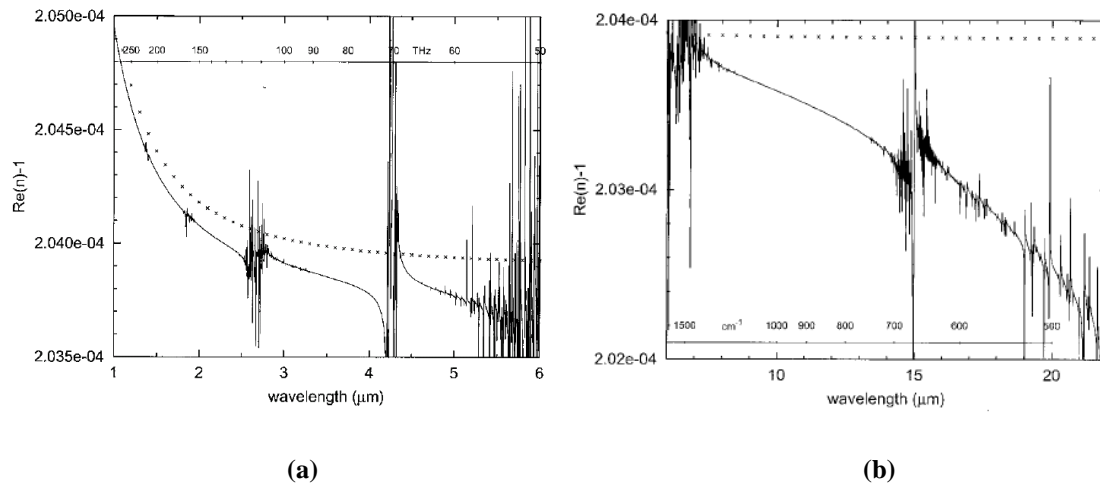


Figure 5. Mathar curves showing anomalous dispersion for various wavelengths.

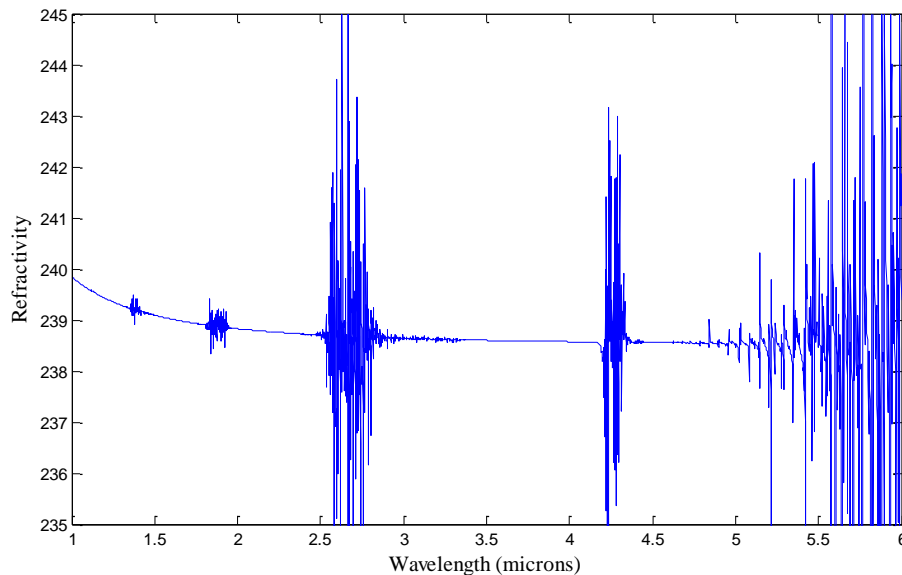


Figure 24. Recreation of Mathar curve (a) from 1 to 6 microns. 10,000 point calculation in McClung-Tunick, from 0.3 – 6 microns. Notable differences are the stronger downward curve in Mathar's figure due to ozone dispersion in his method. The crosses in his graphs are refractivity of wet air using Ciddor equations (widely accepted laboratory derived refractivity equations). The McClung-Tunick model extends the range of the Ciddor equations into absorption regions as a baseline, adding anomalous dispersion effects to this baseline. For this reason, the re-creation will not curve as sharply down. Also, the strength of the absorption lines around 2.6 and 4.3 microns appear reversed from Figure 5 (a). Mathar used the HITRAN 2001 database, accounting for 8 molecular species, while AFIT uses the 2004 database taking into account 13 molecules.

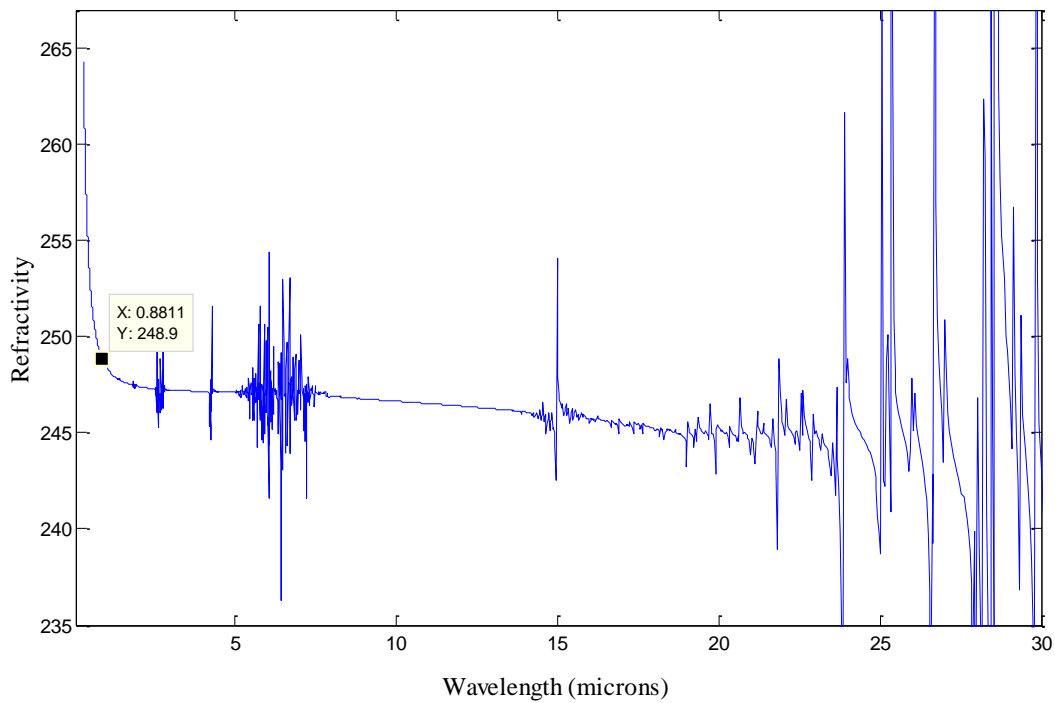


Figure 25. Re-creation of Mathar curve (b) from 0.3 – 30 microns. 10,000 point calculation however performed for 0.3 microns to 8m and zoomed in. Data tip represents where the BLS900 falls on the refractivity curve. Both Mathar curves and recreation show strong absorption around 6 microns, however the 15 micron feature shown here appears smaller only due to scaling. Also, the original curves show a steep drop down in refractivity from 10-20 microns that is not present here. There is a downward slope, but not steep at all. Again, this is due to the McClung-Tunick adding anomalous dispersion onto a baseline level.

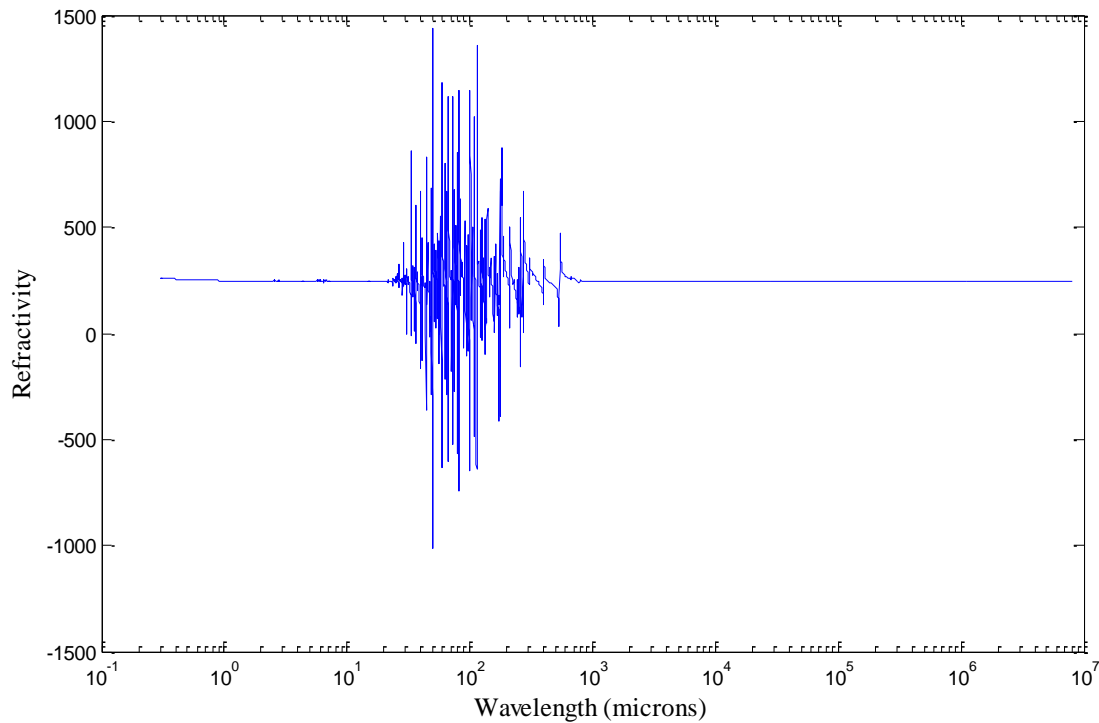


Figure 26. Broad spectrum view of refractivity from UV to RF. Wavelength is put on a logarithmic scale to fit figure. Here it is easy to see the baseline onto which the anomalous dispersion effects are added. The normal dispersion curve in the visible is indistinguishable due to the incredibly large refractivity scale.

The McClung-Tunick model has the capability to plot refractivity across wavelengths, but this ability has not been validated yet. Re-created plots of the Mathar curves do not completely agree, but were not expected to be exact re-creations since AFIT used a slightly different method than Mathar. AFIT treated the Ciddor equations as a baseline and adding absorption line effects to that baseline. Validation of the anomalous dispersion portion of the McClung-Tunick model could be done with a tunable laser near strong absorption lines, stronger lines than where the AFIT tunable lasers are currently.

AFIT Laboratory Built Scintillometer

As expected, Figures 27 and 28 show trends which show as hot plate temperature increases, so does the derived optical turbulence. Recall that each run contained two paths, L1 and L2, with respective detectors D1 and D2. D1 received a laser beam whose path was over the hot plate, whereas D2 did not. Figure 27 below shows the significant difference in turbulence at the two detectors.

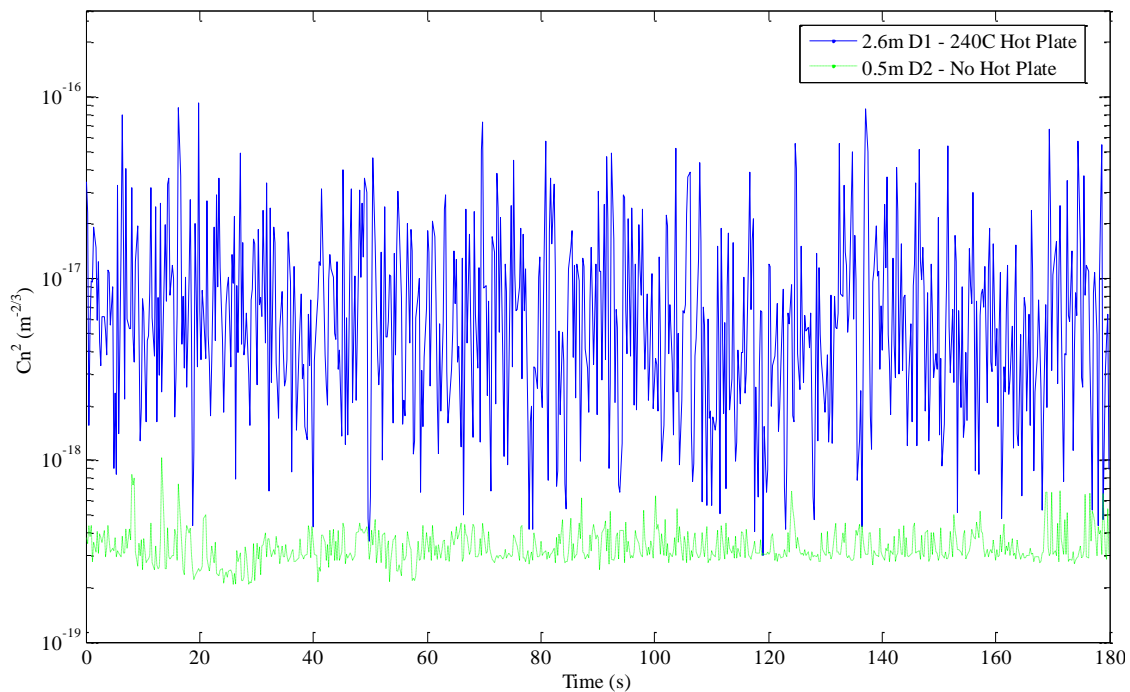


Figure 27. AFIT scintillometer showing optical turbulence versus time for three minutes or 180 seconds. Hot plate for L1 was set to 240C. Despite the hot plate not taking up much of the path length, it still made a significant impact on optical turbulence. This plot's trend showed the algorithm qualitatively worked. 5000 data points a second of voltage were taken at the two detectors, D1 and D2. The graph is showing a running average of 1000 points, meaning this figure shows a data point for every fifth of a second.

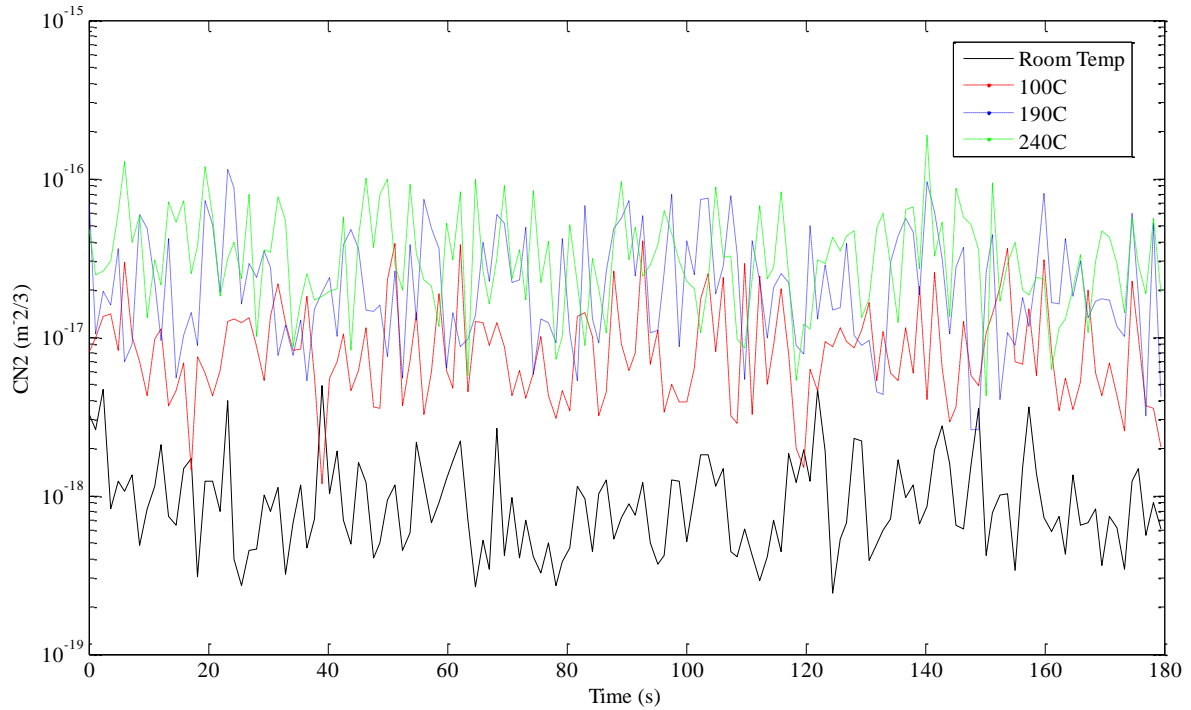


Figure 28. AFIT scintillometer with all four hot plate temperatures. Graph is showing optical turbulence derived for three minutes of run time. An increase in hot plate temperature corresponds to a higher optical turbulence value. Outside the laboratory, a value of $1 \times 10^{-16} \text{ (m}^{-2/3}\text{)}$ would be very low, yet here is very high compared to the normal value of $1 \times 10^{-18} \text{ (m}^{-2/3}\text{)}$ at room temperatures. There is a limitation to the scintillation index method used here, in that only “weak” turbulence conditions are valid. The entire C_n^2 range shown can be considered weak turbulence. Data was gathered at a rate of 5000 points a second. This graph shows a running average of 5000 points, meaning every there is one data point per second.

The laboratory built scintillometer was successful in demonstrating the scintillation index method of deriving optical turbulence. Notably, this method cannot be scaled in the McClung-Tunick model. What is meant by not scalable is that the laboratory set up, for example, was not $1/50^{\text{th}}$ the scale of a field experiment outside. Perhaps a different laboratory set-up would scale if the entire path length was at a certain temperature radiating upwards, simulating how the earth re-radiates energy from the sun. The laboratory scintillometer is a good step towards validation of the anomalous dispersion portion of the McClung-Tunick model.

Field Experiments

Data was collected in October, November, and December of 2008. Right away it was observed that the McClung-Tunick model does not work in rainy day conditions. The similarity theory upon which the model is based on requires that humidity, temperature, and wind gradients exist, and in a storm, some of these will go away or reverse. For example, when it rained during one of the experiment dates, the temperature at both levels was the same. Field experiments always involved the scintillometer, but not always the Davis weather station. Thermocouples were used in November and December.

Weather Station and BLS900

The weather station, without sunlight or batteries to run its internal fan, has a very slow response time to temperature variations. This being so, it was observed that in the mornings when the sun is low or clouds are overcast combined with the winds being very low, large errors in optical turbulence were found. In most cases when this occurred, the weather station either needed a few hours to adjust to the ambient temperatures or because of low wind, incorrectly reads temperature and be largely off in value. Figure 29 below depicts both of the concerns when using the weather station to gather the data for the model. This data was collected on 23 Oct. Figure 30 is a zoomed-in view of Figure 29 with added error bars. Figure 31 graphs data collected on 6 November.

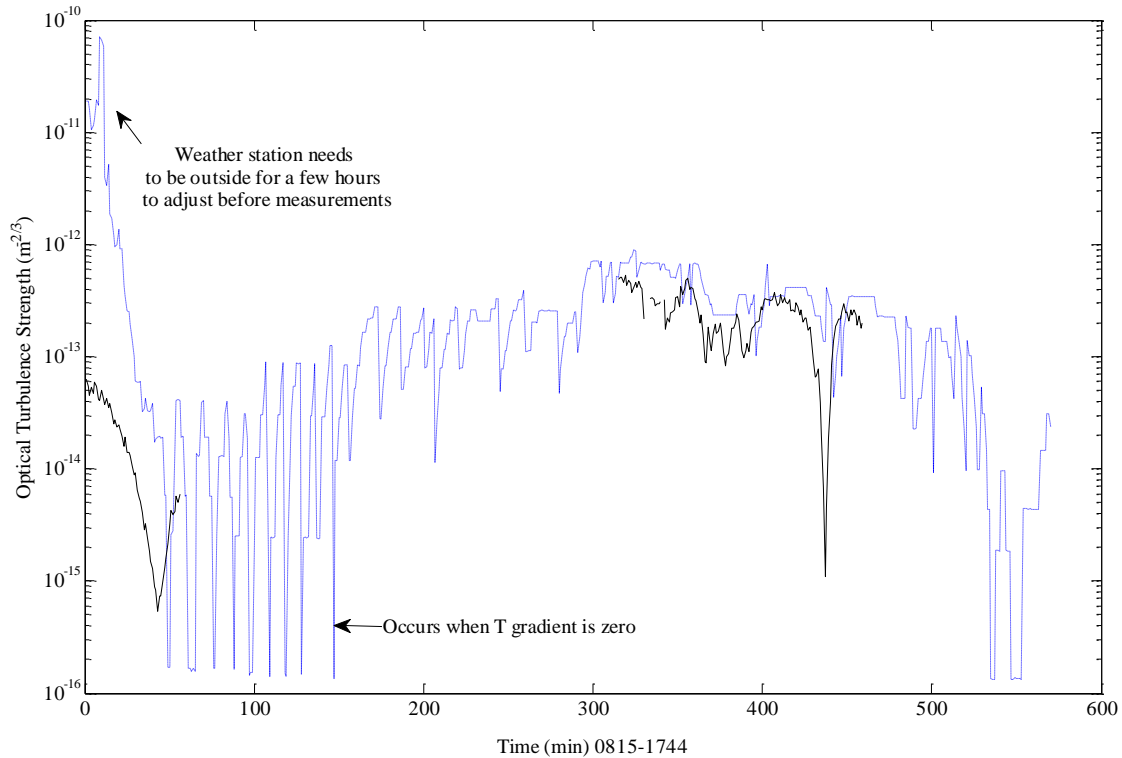


Figure 29. 23 Oct 08 BLS900 compared to McClung-Tunick model, optical turbulence versus time. As an initial observation the weather station needed to be in the field a few hours before taking measurements. Also, in the code, at this wavelength, whenever the temperature gradient is zero turbulence sharply drops. All the sharp drops in the model in the morning are due to a lack of wind across the temperature sensors and a lack of sunlight to run the internal fan. This routinely happened from 0800-1000 at WPAFB. A minimum gradient can be inputted into the code in the future, never allowing the temperature gradient to be zero. Model trends well with scintillometer in afternoon conditions.

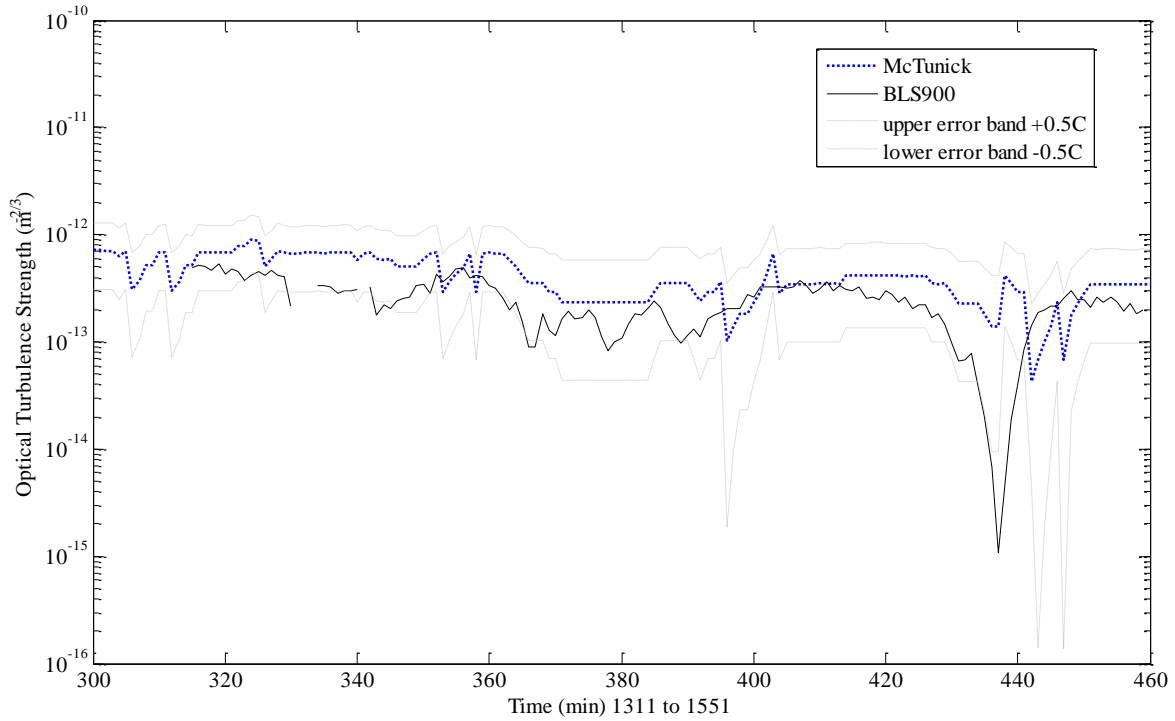


Figure 30. Zoomed-in 23 Oct 08 BLS900 compared to McClung-Tunick model, afternoon optical turbulence values versus time. Upper and lower error bands are added by adding or subtracting 0.5C from the temperature gradient. Model is able to trend well with the scintillometer unless a sharp drop in temperature occurs. Recall that the weather station is unable to respond to rapid temperature changes. The thermocouple method will fix the response issue. Also note around minute 440, the model's lower error band sharply drops, this is again a result of a zero temperature gradient in the model.

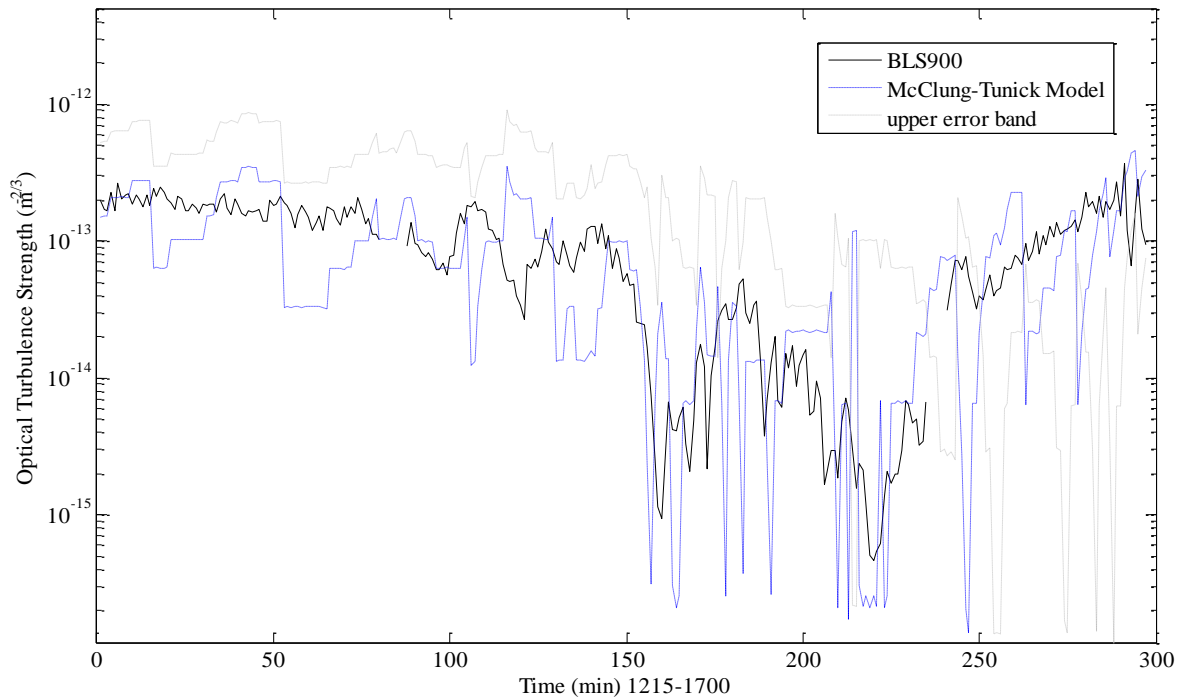


Figure 31. 6 Nov 08 BLS900 compared to McClung-Tunick model, optical turbulence versus time. Upper error band represent +0.5C, the minimum error in T1-T2 during calibration. Lower band is not shown as it would clutter the graph. Note the upper error band crosses down and becomes the lower band around minute 240. This is due to a temperature inversion that is happening as the sun goes down. Drop outs in value occur when temperature gradient is zero. Overall the model trends well around the scintillometer data, treated as truth data.

In summary of the weather station method, the model trends well in afternoon, non-rainy conditions. Order of magnitude of the optical turbulence is captured correctly in the model, however, finer details shown by the scintillometer cannot be seen using inputs from the weather station. A faster temperature response is needed to capture the quick temperature fluctuations. The thermocouple method, discussed next, attempts to capture the finer details.

Thermocouples and BLS900

Types K and T thermocouples were used in field experiments in November and December of 2008 and used as weather inputs along with hourly KFFO weather data. The first run was 21 November using Type K. Thermocouples were calibrated each time before a data collection run by putting the sensors in frozen purified water (water that had been through a reverse osmosis process) and ensuring they read 0°C. Figure 32 is created using Type K, while Figures 33 and 34 use Type T.

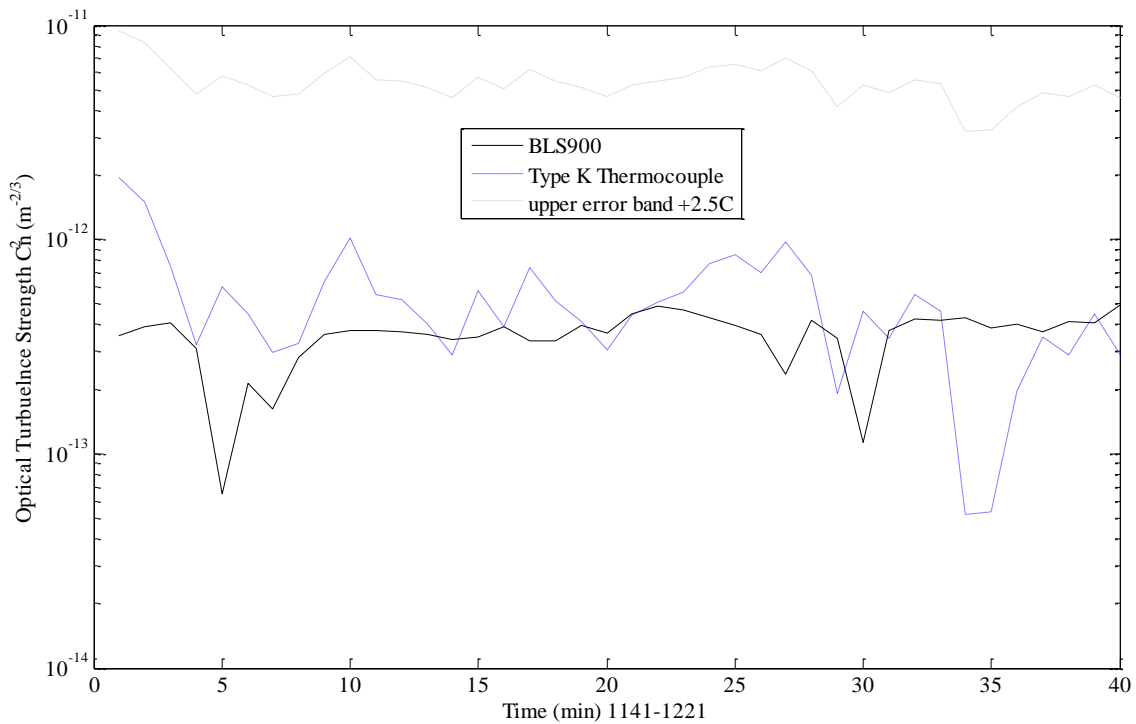


Figure 32. 21 Nov 08 BLS900 compared to McClung-Tunick model using Type K thermocouples. Thermocouples were calibrated before hand and kept away from direct sunlight during data collection. Very large error band due to inherent error in Type K wire and HH506RA logger electronics being 2.5C. Lower error band not shown because 2.5C is a greater value than the overall temperature gradient, which would make the “lower” error band higher than original modeled data. It can be assumed that the lower error band is $3.5e^{-16}$, as this would be the lowest value given by the model if the temperature gradient were zero.

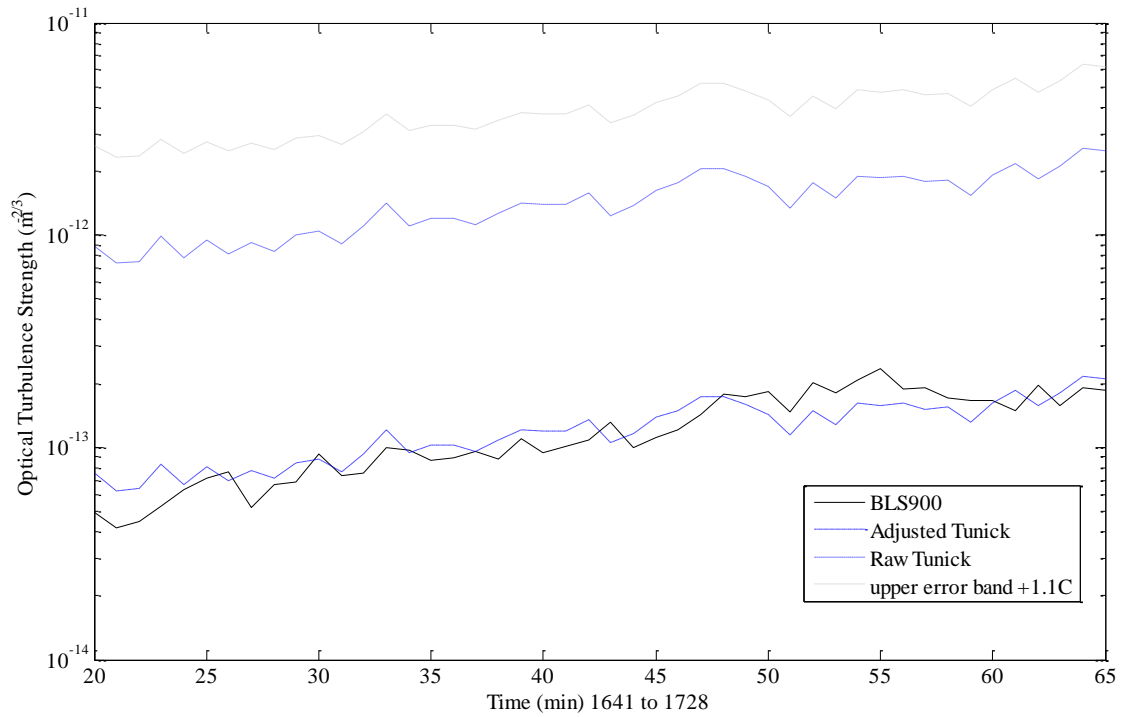


Figure 33. 30 Dec 08 BLS900 compared to McClung-Tunick model using Type T thermocouples. Type T thermocouples were used due to their lower error, at +/-0.8C, another +/-0.3C must be added due to the logger electronics. Data was taken with the logger in the incorrect Type K mode, which is why the “raw” data looks the way it does. Raw data was adjusted down by multiplying the optical turbulence derived by 0.085.

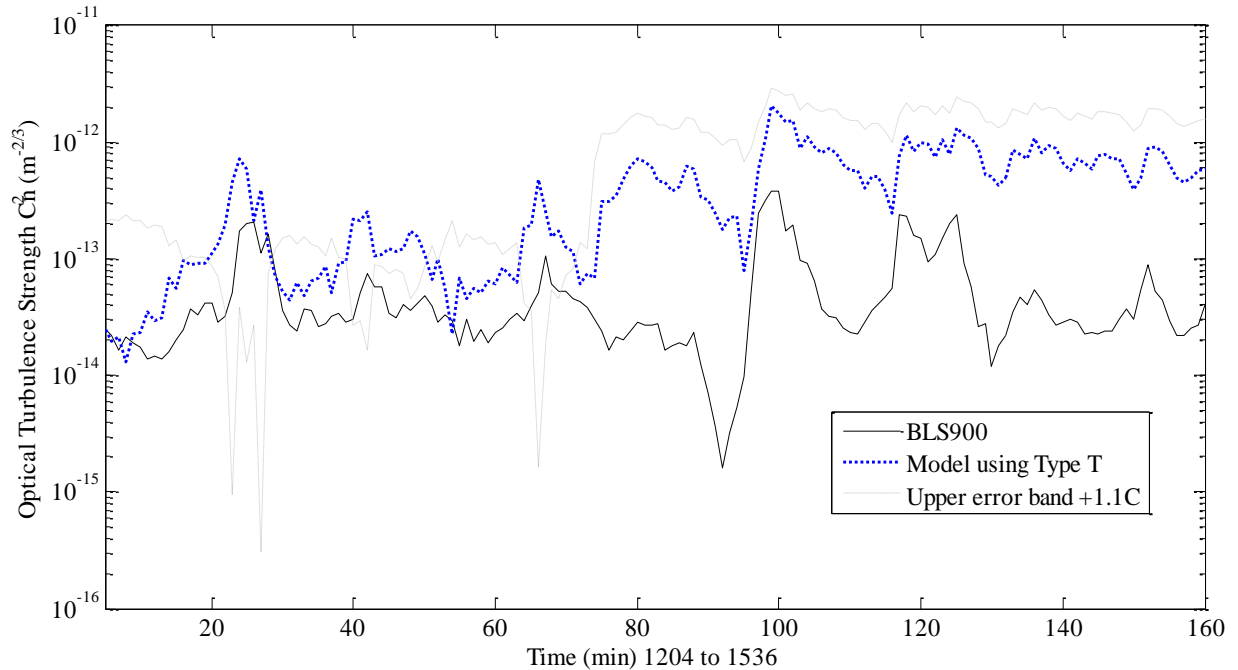


Figure 34. 31 Dec 08 BLS900 compared to McClung-Tunick model using Type T thermocouples. Model trends very well with scintillometer data. Finer details in trends are being captured. Solar contamination may be an explanation for higher values after min 75. A temperature inversion occurs at min 75, made apparent by the error band. This day was extremely cold (below freezing) and heavily overcast most of the time with intermittent light snowfall. Type T (copper) thermocouples are a good type for moisture and cold environments. The sun did randomly peak through in some areas. Figures 13 and 14 are pictures taken during this day's data collection.

In summary, with further improvements to the thermocouple method, the McClung-Tunick model can be validated at the 880nm wavelength. Specifically, type Ts should be used to reduce error. This method is superior to the weather station method because it is less cumbersome, requiring only a hand held data logger, a laptop, and access to free and readily available common weather station data off the internet. The largest hurdle to overcome using this method is the extremely large database incurred because temperature values are gathered every second. Figure 34 was created from a temperature database of over 13,000 lines. A visual basic macro in Excel can be written to perform a running average every 60 lines. The macro used for this method is located in Appendix C, with credit being given to Capt Allen Cohen (AFIT/ENS) for its creation.

Laser Communications Sensitivity Study

Optical turbulence values and laser performance for humid, mid-latitude, and desert environments are presented, respectively. Exact inputs used for the sensitivity study can be found in Appendix D. Table 5 displays optical turbulence values while Table 6 characterizes the laser after traveling its path. Figure 35 provides a 3D look at the irradiance of the laser beam for the worst case scenario (WCS) of turbulence. Figures 36 and 37 compare seasons, showing optical turbulence profiles for June 1200-1500 and January 1200-1500. Results are provided for stable and unstable atmospheric conditions. As a reminder, stable means T1, which is lower to the ground, is at a lower temperature than T2. Stable conditions are common at night, right after sunset or sunrise, and during fog or rainy conditions. Unstable conditions occur when T1 is higher than T2.

HUMID

Table 5. Optical turbulence values for stable and unstable atmospheres for the humid Eglin, FL scenario. As expected, turbulence increases as temperature gradient increases. Bolded values indicate highest C_n^2 for the given scenario. Usually highest values of turbulence occur in the unstable and afternoon conditions. However, there is an outlier for June nights, indicating one of three things. Either 1.5C is too high for a reasonable temperature gradient at night in humid conditions, a glitch in the code has been found, or it is correct. The order of magnitude jumps from 0.5C to 1.0C may indicate the next gradient at 1.5 really is increased by an order of magnitude.

HUMID	Temp Gradient	Stable C_n^2 at 2m	Unstable C_n^2 at 2m
Eglin AFB, FL	(C)	($m^{-2/3}$)	($m^{-2/3}$)
June_0000-0300	0.5, 1.0, 1.5	1.42e-13, 1.07e-12, 1.17e-11	2.06e-13, 1.06e-12, 2.70e-12
June_0900-1200	1.0, 1.5, 2.0	3.04e-13, 6.83e-13, 1.23e-12	3.84e-13, 9.71e-13, 1.89e-12
June_1200-1500	1.5, 2.0, 2.5	6.76e-13, 1.21e-12, 1.91e-12	9.14e-13, 1.77e-12, 2.97e-12
JAN_0000-0300	0.5, 1.0, 1.5	1.25e-13, 5.01e-13, 1.18e-12	1.67e-13, 8.95e-13, 2.37e-12
JAN_0900-1200	1.0, 1.5, 2.0	3.99e-13, 9.01e-13, 1.62e-12	5.60e-13, 1.44e-12, 2.83e-12
JAN_1200-1500	1.5, 2.0, 2.5	9.00e-13, 1.62e-12, 2.57e-12	1.44e-12, 2.83e-12, 4.78e-12

Table 6. Laser characterization for worst case scenario (WCS) in humid environment. Peak irradiance and power in the bucket decrease as C_n^2 increases. Spot size increases as C_n^2 increases. Laser started at 50kW of power with an exit aperture diameter of 0.5m. Beam quality was assumed to be 1, wavefront errors at zero, and relative obscuration at 0.1. Power in the bucket values at the square 1m² target are the result of the laser traveling 2km horizontally through the WCS turbulence. In turbulence on the order of 10^{-11} , approximately 12% of initial laser power is left after traveling 2km. 64% of initial laser power is left after traversing path in turbulence on the order of 10^{-12} . This shows that modulating initial power out of a ground based laser as optical turbulence fluctuates, is worthwhile in regards to efficiency and energy conservation purposes.

HUMID	Peak Irradiance (W/m ²)	Spot Size - 1/e (m)	Power In Bucket (W)
Eglin AFB, FL			
June_0000-0300	6.62E+03	2.83	6.01E+03
June_0900-1200	5.91E+04	0.97	3.20E+04
June_1200-1500	3.60E+04	1.25	2.43E+04
JAN_0000-0300	3.11E+04	1.31	2.17E+04
JAN_0900-1200	2.81E+04	1.41	2.05E+04
JAN_1200-1500	1.65E+04	1.86	1.37E+04

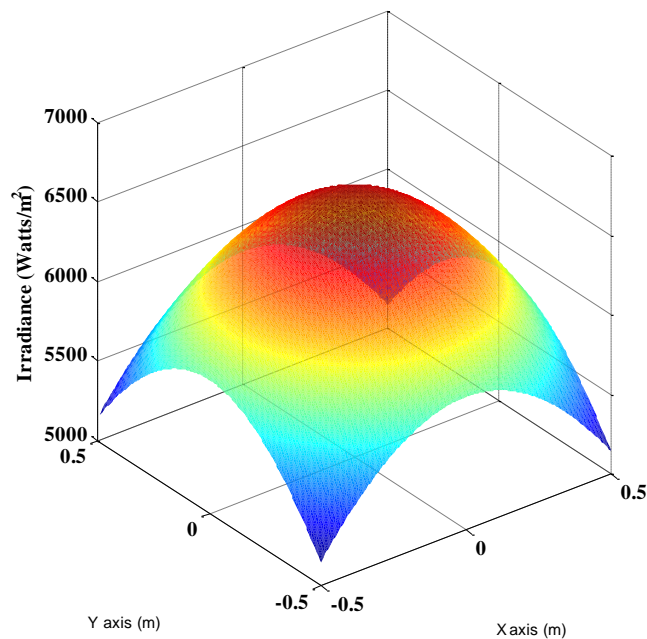


Figure 35. Humid, Eglin AFB, 3D irradiance (all effects) plot of the laser beam.

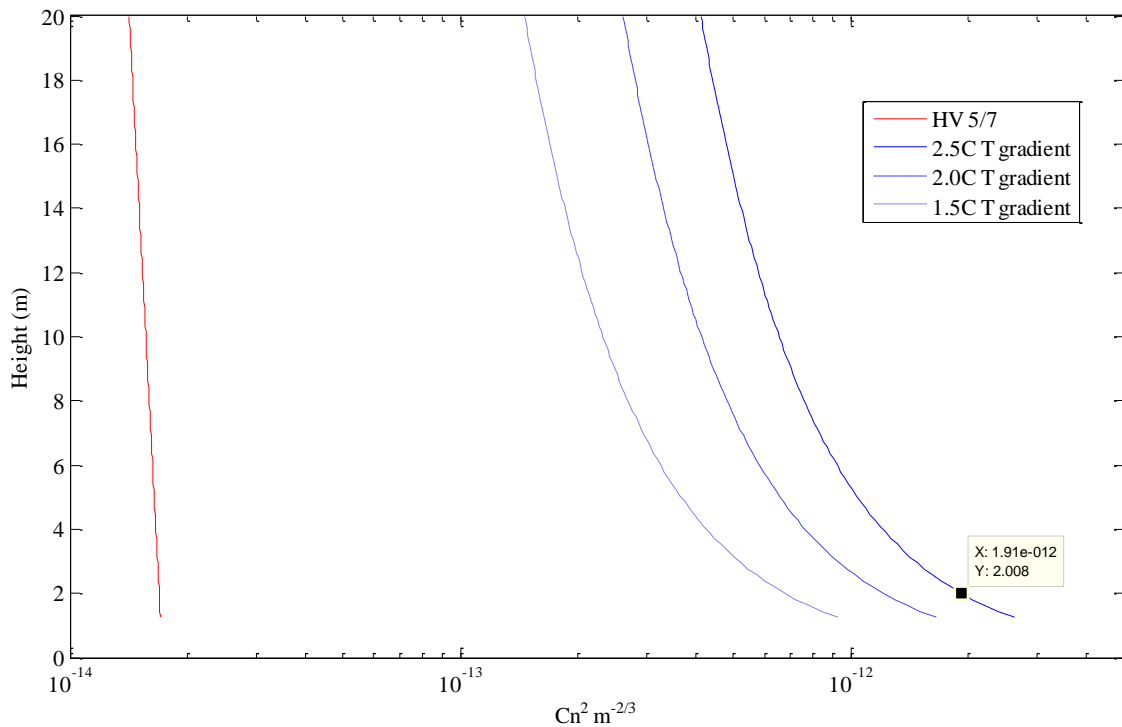


Figure 36. Humid, Eglin AFB, FL scenario at 1200-1500 in June. Plot is for a stable atmosphere. Turbulence trends nicely with increasing gradient. Datatip represents the 2m level. Recall that the McClung-Tunick model (in blue) is designed for use within the first 50m of the surface boundary layer, explaining why the height goes up to 20m. It is important to note the large differences in values given by the regularly used Hufnagel-Valley (HV 5/7 in red to the far left) profile versus the McClung-Tunick. HV 5/7 profiles were taken using radiosonde (weather balloon) data at night to avoid solar contamination, explaining the much lower turbulence values. The McClung-Tunick gives realistic turbulence values within the surface boundary layer, while HV 5/7 provides a good profile to be used at heights greater than 50m. When looking at the blue McClung-Tunick values, note the drop off in turbulence, nearly an order of magnitude, as one travels vertically 20m. This graph illustrates the already known importance of placing laser communication devices higher up from the ground, i.e. on top of a building.

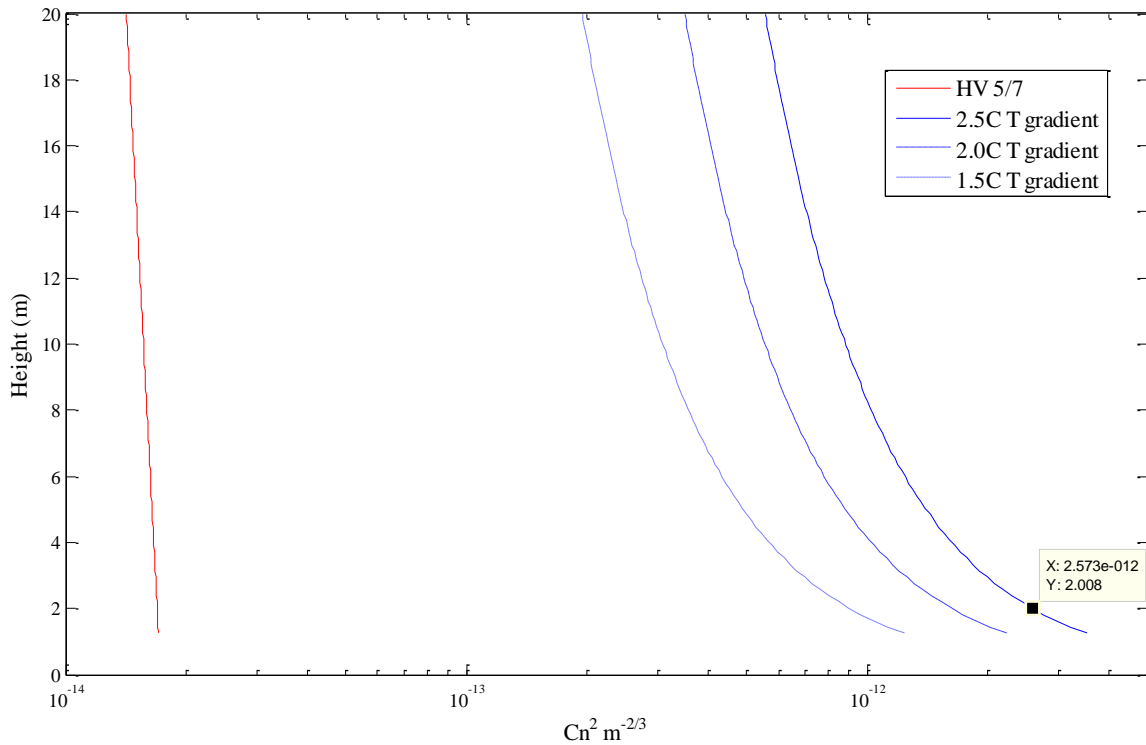


Figure 37. Humid, Eglin AFB, FL scenario at 1200-1500 in January. Plot is for a stable atmosphere. While it seems unlikely a gradient of 2.5C will occur within a 4m layer of the atmosphere in January, it's not impossible. In fact, a sunny day against the cold air of wintertime creates large (10^{-12}) values of optical turbulence. For the humid scenario in January, the trends in the graph look nearly identical to the trends in June.

MID-LATITUDE

Tables 7 and 8 depict the optical turbulence values and laser performance for the mid-latitude, WPAFB, OH scenarios. Figure 38 is a 3D irradiance plot for the mid-latitude WCS, while Figure 39 is a turbulence profile for unstable conditions for January 0900-1200, illuminating the differences between stable and unstable profiles.

Table 7. Optical turbulence values for stable and unstable atmospheres for the mid-latitude WPAFB, OH scenario. Bolded values indicate WCS turbulence. As expected, unstable atmospheres at the same temperature gradient will have a greater optical turbulence. There is more mixing and upward motion in an unstable atmosphere. Another outlier, like the one seen in the humid environment, occurs during the summer night scenario. There are higher jumps in optical turbulence from smaller gradients, i.e. 0.5C to 1.0C than from 1.0C to 1.5C. This proves again, a non-linear correlation of optical turbulence to temperature gradient. On average WPAFB experiences higher optical turbulence than Elgin, AFB. Highest values occur in the afternoon and in January. The 10^{-12} values correspond nicely to scintillometer values taken outside in winter at WPAFB.

MID-LAT	Temp Gradient	Stable C_n^2 at 2m	Unstable C_n^2 at 2m
WPAFB, OH	(C)	($m^{-2/3}$)	($m^{-2/3}$)
June_0000-0300	0.5, 1.0, 1.5	1.52e-13, 1.10e-12, 9.76e-12	2.40e-13, 1.25e-12, 3.18e-12
June_0900-1200	1.0, 1.5, 2.0	3.26e-13, 7.37e-13, 1.33e-12	4.57e-13, 1.18e-12, 2.31e-12
June_1200-1500	1.5, 2.0, 2.5	7.26e-13, 1.31e-12, 2.10e-12	1.16e-12, 2.29e-12, 3.88e-12
JAN_0000-0300	0.5, 1.0, 1.5	1.55e-13, 6.10e-13, 1.40e-12	1.93e-13, 1.01e-12, 2.66e-12
JAN_0900-1200	1.0, 1.5, 2.0	5.28e-13, 1.19e-12, 2.13e-12	7.24e-13, 1.85e-12, 3.63e-12
JAN_1200-1500	1.5, 2.0, 2.5	1.18e-12, 2.12e-12, 3.35e-12	1.85e-12, 3.62e-12, 6.13e-12

Table 8. Laser characterization for worst case scenario (WCS) for mid-latitude environment. When comparing geographic locations, optical turbulence at one location does not necessarily degrade laser performance the same at another. For example, one can have a larger value for C_n^2 at Eglin on a summer afternoon, and have better laser performance than a lower value for C_n^2 at WPAFB on a summer morning. (Compare Eglin June 1200-1500 to WPAFB June 0900-1200). Higher pressure in an area will cause the laser to shoot through a denser atmosphere than a lower pressure area.

MID-LAT	Peak Irradiance	Spot Size - 1/e	Power In Bucket
WPAFB, OH	(W/m^2)	(m)	(W)
June_0000-0300	5.60E+03	3.12	5.24E+03
June_0900-1200	3.04E+04	1.36	2.17E+04
June_1200-1500	1.69E+04	1.83	1.40E+04
JAN_0000-0300	3.55E+04	1.25	2.40E+04
JAN_0900-1200	2.48E+04	1.5	1.87E+04
JAN_1200-1500	1.37E+04	2.02	1.17E+04

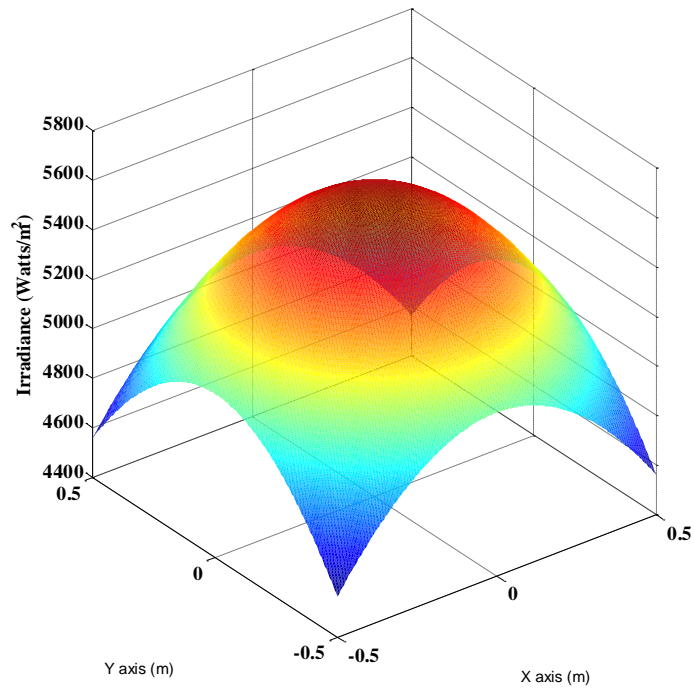


Figure 38. 3D irradiance plot (all effects) of the laser beam for the mid-latitude WCS. WPAFB has a much lower peak irradiance than Eglin, despite Eglin having the highest turbulence value.

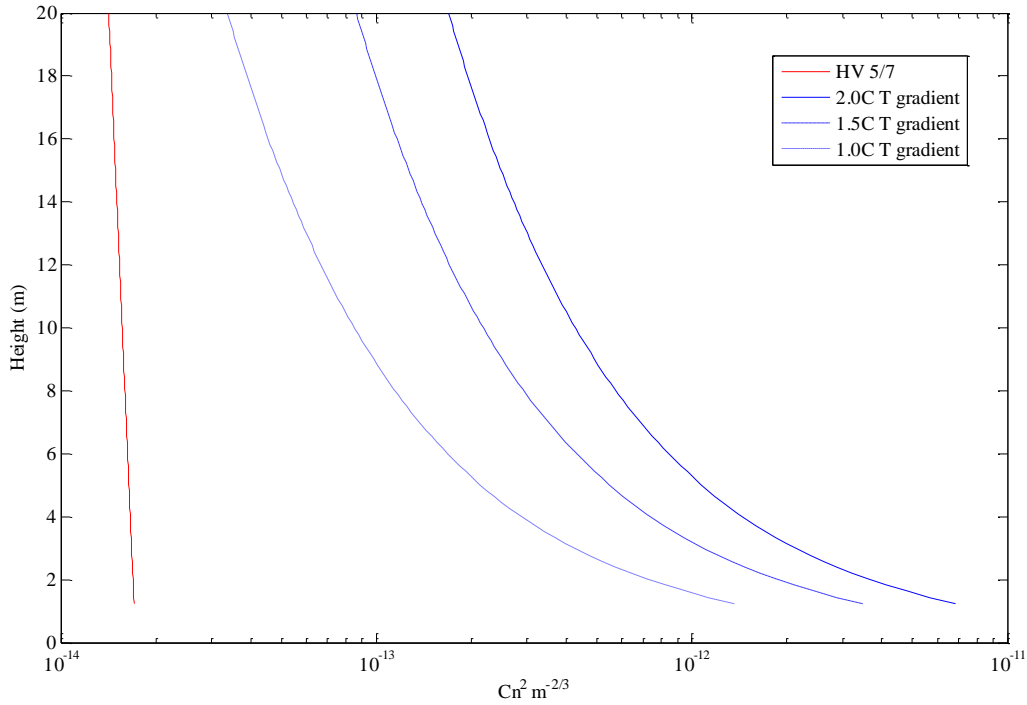


Figure 39. Optical turbulence vertical profile for mid-latitude, January 0900-1200 scenario with unstable atmospheric conditions. When comparing this graph to Figure 37, note the increased drop off in C_n^2 (in blue) as one travels vertically to 20m. This is characteristic for all unstable plots vs stable plots. This may indicate it is uncommon for stable atmospheres to experience the same temperature gradients as unstable atmospheres. The large drop in C_n^2 and eventual “meshing” with HV 5/7 at higher altitudes, as seen in this plot is expected. This also indicates that should the same temperature gradients be experienced for both stable and unstable environments: stable environments have a higher average C_n^2 throughout the vertical profile, while unstable environments have a higher C_n^2 at lower vertical levels, i.e at 2m, yet have an overall lower average value throughout the surface boundary layer.

DESERT

Tables 9 and 10 depict the optical turbulence values and laser performance for the desert, Nellis AFB, NV scenarios. Figure 40 is a turbulence profile for unstable conditions for the WCS of optical turbulence, while Figure 39 is a 3D irradiance plot for the WCS.

Table 9. Optical turbulence values for stable and unstable atmospheres for the desert Nellis AFB, NV scenario. While humid and mid-lat temperature gradients remained the same, desert temperature gradients were increased due to the increased potential for direct sunlight and little cloud cover. Surprisingly, even with this increase, optical turbulence remained on the order of the other two scenarios at 10^{-12} . With the hotter desert environment, especially during the summer there is a less dense atmosphere, contributing to the lower C_n^2 .

DESERT	Temp Gradient	Stable CN2 at 2m	Unstable CN2 at 2m
Nellis AFB, LV	(C)	($m^{-2/3}$)	($m^{-2/3}$)
June_0000-0300	0.5, 1.0, 1.5	9.25e-14, 3.77e-13, 9.06e-13	1.25e-13, 7.00e-13, 1.88e-12
June_0900-1200	1.5, 2.0, 2.5	5.87e-13, 1.05e-12, 1.65e-12	8.74e-13, 1.74e-12, 2.98e-12
June_1200-1500	2.0, 2.5, 3.0	1.00e-12, 1.57e-12, 2.27e-12	1.49e-12, 2.52e-12, 3.88e-12
JAN_0000-0300	0.5, 1.0, 1.5	1.99e-13, 1.36e-12, 9.81e-12	3.42e-13, 1.79e-12, 4.55e-12
JAN_0900-1200	1.5, 2.0, 2.5	1.14e-12, 2.19e-12, 3.77e-12	2.39e-12, 4.73e-12, 7.98e-12
JAN_1200-1500	2.0, 2.5, 3.0	1.89e-12, 3.12e-12, 4.76e-12	4.03e-12, 6.84e-12, 1.05e-11

Table 10. Laser characterization for worst case scenario (WCS) for desert environment. The expected highest degradation occurs in winter afternoons.

DESERT	Peak Irradiance	Spot Size - 1/e	Power In Bucket
Nellis AFB, LV	(W/m^2)	(m)	(W)
June_0000-0300	5.31E+04	0.96	2.86E+04
June_0900-1200	3.15E+04	1.26	2.14E+04
June_1200-1500	2.32E+04	1.47	1.73E+04
JAN_0000-0300	7.15E+03	2.64	6.51E+03
JAN_0900-1200	9.16E+03	2.33	8.13E+03
JAN_1200-1500	6.70E+03	2.73	6.13E+03

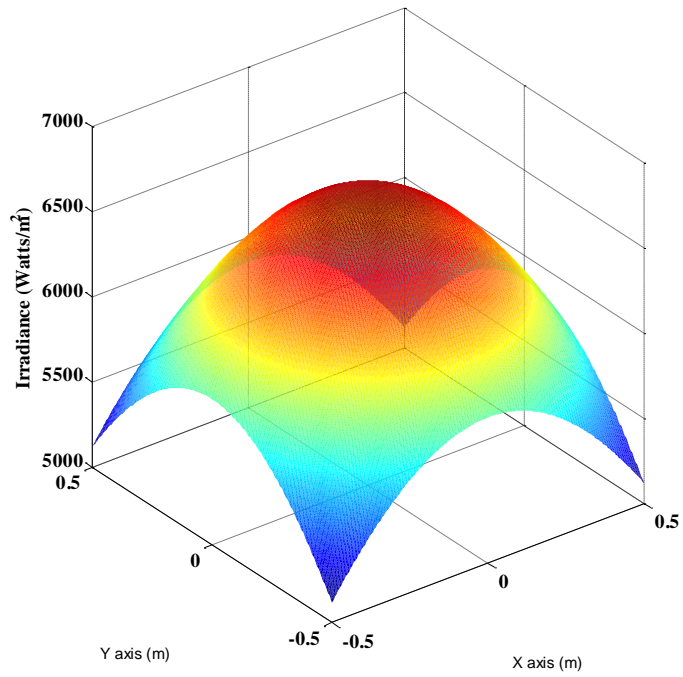


Figure 40. 3D irradiance plot (all effects) of the laser beam for the desert WCS.

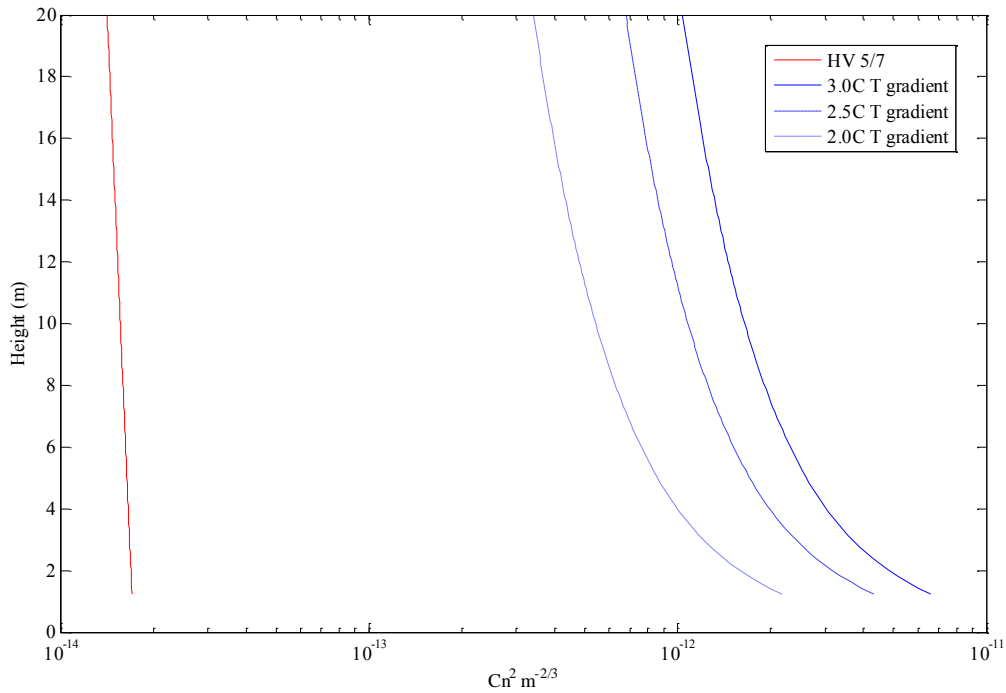


Figure 41. Optical turbulence vertical profile for desert, January 1200-1500 scenario with stable atmospheric conditions. Turbulence is severe and remains so throughout the profile for a stable atmosphere. The above is WCS, most likely an unstable atmosphere will be encountered.

Weather Radar Proof of Concept

The derivation of optical turbulence using radar is an entirely separate method of deriving optical turbulence from the refractive index method. However, combining the two methods together makes it possible to calculate optical turbulence at multiple wavelengths. The following study demonstrates that turbulence can be calculated from 10cm weather radar and compares it to 880nm scintillometer measurements. Figure 42 below shows data collected on 6 Nov 08. Figures 43 and 44 show data for 21 Nov 08. Figure 44 shows optical turbulence from the thermocouples (in red) overlaid for an additional comparison.

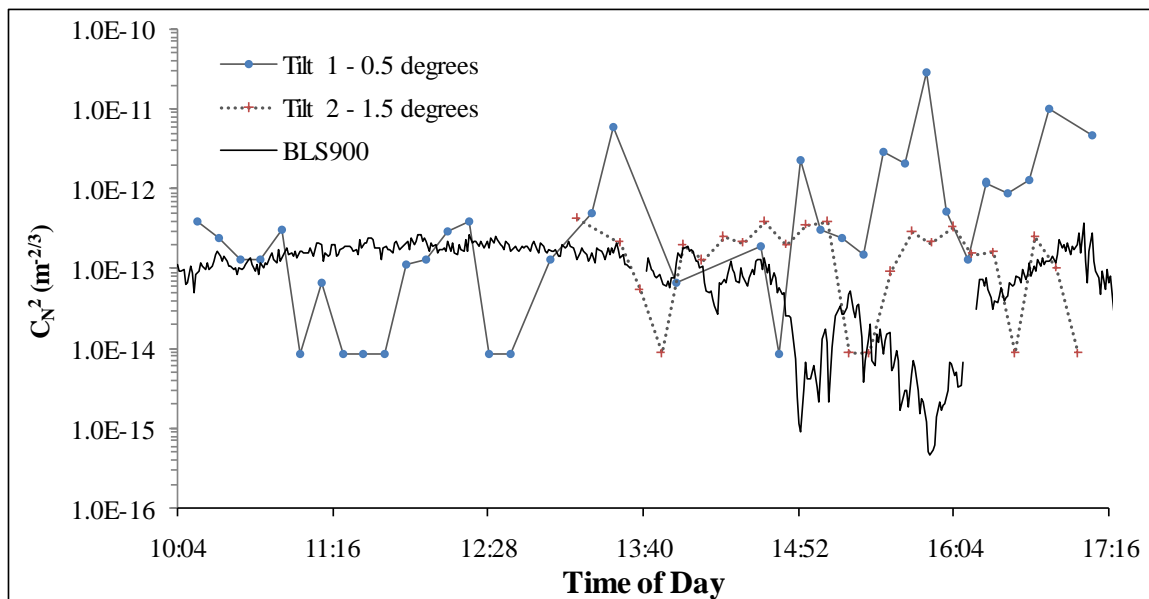


Figure 42. 6 Nov 08 BLS900 data compared to weather radar method of deriving optical turbulence. Null values of reflectivity, as seen at 11:17 cause derived turbulence values to be extremely low. This is due to the fact AFIT is located near the edge of usability for this radar. This problem is solved if a location is chosen closer to the radar. 10cm radars do not have extensive range, AFIT is ~30 miles away. Note that in the late afternoon tilt 1 rises up (opposite the BLS900 trend). This is due to “ground clutter” reflectivities seen in the morning when the sun rises and at dusk when the sun sets. Tilt 2 does not follow tilt 1’s trend because it reflects off atmosphere higher up.

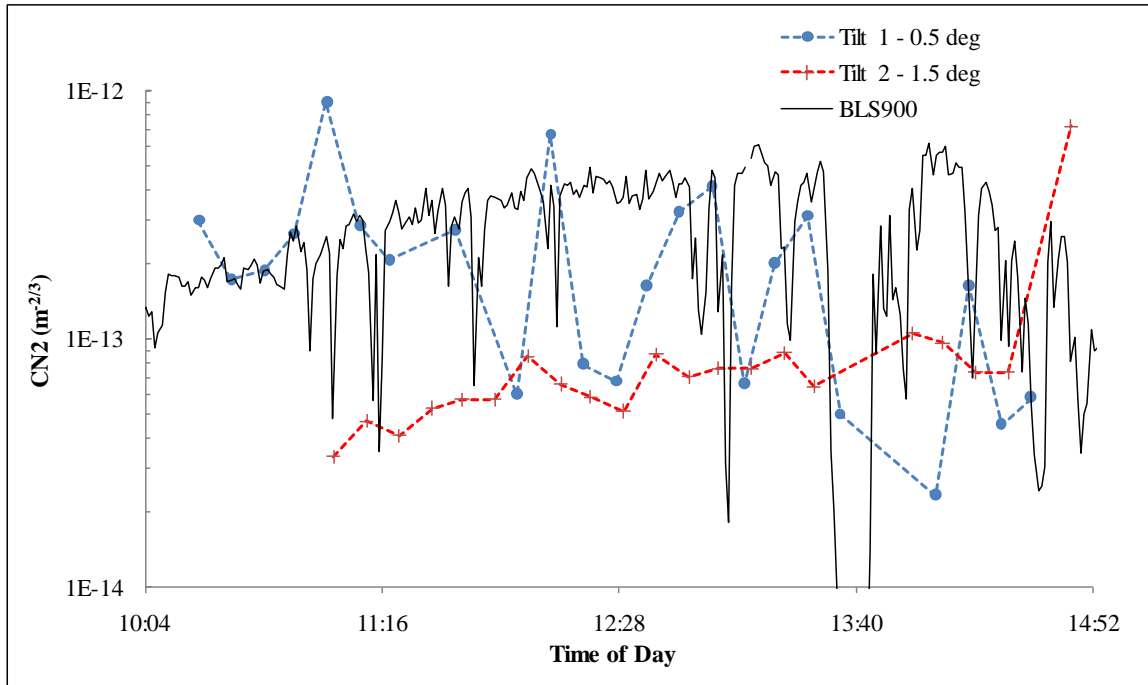


Figure 43. 21 Nov 08 BLS900 data compared to weather radar derived optical turbulence. Note tilt 2 sharply increases towards the end. A cold front started to move in and it had just started to snow. Tilt 2 is higher up and reflected off the precipitation, while tilt 1 stayed underneath the cloud layer.

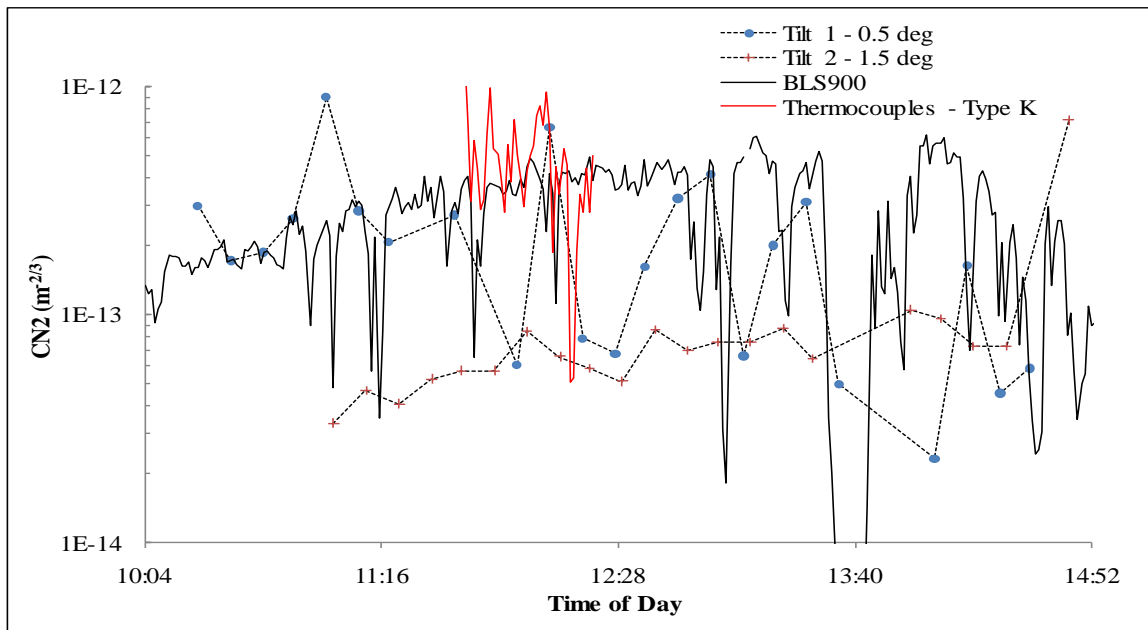


Figure 44. 21 Nov 08 with overlay of Type K thermocouple trend for an additional comparison of methods. Three methods are shown here, intensity variation (BLS900), index of refraction (thermocouples), weather radar (tilts 1 and 2).

V. Conclusions and Recommendations

Conclusions

It is the opinion of the author that the objectives of verification and demonstration of the index of refraction method for deriving optical turbulence have been met. Theory behind the McClung-Tunick tool has been vetted and verified with its exact equations made available in Appendix A. Verification was achieved through field experiments, comparing model values against scintillometer field measurements. Optical turbulence values derived using the model trend well against scintillometer measurements, particularly in the afternoon using thermocouples and the KFFO weather station. Based on this research, the tool cannot be said to be “validated” due to the extreme accuracy needed in the temperature sensors, but is a good goal for future work. For validation, the tool should be tested against other scintillometer measurements of various wavelengths in a variety of geographic locations, seasons, and times of day.

The use of the weather station was a good step towards validation as it gave the correct rate of data needed, but was usable only in the afternoon. It was invalid early in the morning because of the combined effect of low sun and little wind, causing large errors in the weather station temperature sensors. For an accuracy of $\pm 0.5^{\circ}\text{C}$, the sensors needed wind to blow or be drawn across them, since they are sheltered by large solar shield casings. This can be overcome by replacing the current T2 sensor that does not contain a fan (Temp/Hum unit), with two integrated sensor suites (ISS) units running on batteries. However, this is a more cumbersome solution as opposed to using the type T thermocouples in conjunction with any nearby weather station.

Based on the results, the thermocouple method shows promise as a means of validation. Care needs to be taken to calibrate the sensors often and to protect data against solar contamination by shading the junctions and wires from direct sunlight. From the type T thermocouple results, problems in accuracy may occur when temperature inversions happen in the boundary layer (meaning $T1 < T2$, then flip to $T1 > T2$, or visa versa). The concern that temperature inversions increase error is uncertain, but should be investigated. In the type T experiment, it is unknown whether the increased error was due to a temperature inversion or solar contamination. It was heavily overcast with brief intermittent snow and sun the day of the experiment and therefore no shading devices were used.

Regarding the second part of this thesis's objective, the McClung-Tunick's far-reaching utility in the realm of electro-optics, astronomy, directed energy weapons, and wireless communications has been demonstrated. Two proof-of-concept demonstrations have been performed, the laser communications sensitivity study, and the radar weather study. As expected in the laser communications study, highest values of optical turbulence occur in the afternoon and in January (if the same temperature gradient as summer is experienced). All locations showed C_n^2 values on the order of 10^{-12} , with Eglin at the highest overall value at $1.17e^{-11}$ for summer nights. Nellis AFB had the second highest C_n^2 value at $1.05e^{-11}$ for winter afternoons. WPAFB had the overall highest C_n^2 average when comparing apples-to-apples (same temperature gradients), than either humid or desert geographic locations. Vertical profiles of optical turbulence were

created in the study and can be used in the future as look up graphs of optical turbulence strength for a given geographic location experiencing various temperature gradients.

As a proof of concept, weather radar was used to calculate optical turbulence and was compared against scintillometer measurements. Optical turbulence in three layers of the atmosphere was shown, and for two different wavelengths, 10cm and 880nm. It is important to note corrections were not made to the 10cm derived turbulence, in order to exactly compare against the 880nm wavelength. Humidity impacts the 10cm wavelength more than the 880nm wavelength. As future work, this correction factor can be added to more accurately compare the 880nm scintillometer to the 10cm weather radar.

Additionally, the weather radar method works only in its clear air mode (no precipitation) and during the afternoon. Due to the experiments' location at AFIT near the radar's range of usability, this method was only valid in the afternoon in November. If an experiment took place in the summer, the usable time range would be extended. Approximately, before 11am and after 4pm ground clutter problems or null reflectivity values occur (shown in results section, Figure 37, tilt 1). Lastly regarding weather radar, expected trends involving optical turbulence and height above ground were shown. Optical turbulence values decreased as atmospheric height increased.

Lastly, this research not only impacts the Air Force, but its sister services as well. AFIT's model builds upon the Army and Navy's individual similarity theory based optical turbulence tools, enhancing the broad spectrum capability. Previously, optical turbulence models were limited to narrow regions of the spectrum, visible and infrared. Expanding the usable spectrum has been a significant improvement for turbulence tools.

Recommendations for Future Work

Research in the future should focus on validation of the McClung-Tunick tool as a refractive index method of deriving optical turbulence. Validation of the code should be broken up into two areas: single wavelength and across wavelength. Focus should be put upon testing the code in multiple environments, times of day, across time, and across wavelength. Improvement upon the thermocouple method will help towards the goal of validation for single wavelength scenarios. Improvement upon the laboratory scintillometer will help towards validation of the across wavelength or anomalous dispersion scenarios.

The laboratory scintillometer method can be improved upon in two ways immediately: quantitatively finding the noise floor of the scintillometer and finding the time average where steady state occurs for optical turbulence. This last value delineates between short-term and long term optical turbulence exposure. Expected values for short term turbulence calculations are on the order of 10s of milliseconds or less. This can be achieved by taking the data already gathered at 5000 points per second, and graphing optical turbulence values versus time averaged intervals. For example one data point will be the optical turbulence average for the first two data points, then first ten, and so on until the turbulence values converge to a steady state value.

As of the date of this thesis, AFIT's electro-optics lab will be acquiring a tunable wavelength laser around $6.3\mu\text{m}$; strong water absorption lines exist here! This is a great opportunity to run experiments with the laboratory scintillometer to validate the anomalous dispersion portion of this thesis. The tunable wavelength lasers previously

available tuned through weak absorption lines, making it hard to claim any differences in optical turbulence were from absorption rather than merely noise. This concern goes away with the new tunable laser being around strong absorption lines.

It is also recommended that work be continued towards the creation of a 3D optical turbulence density information network. Weather radars, with their range-gating ability can be used in a network, providing local, real-time updates of optical turbulence. Imaging, directed energy weapons, wireless communication, and astronomy applications that tap into the network may receive updates, correcting for atmospheric distortion. The weather radar method can be improved upon by taking data closer to the Wilmington radar, AFIT is near the end of its usable range. Also, as stated before, additional improvements to the weather radar method can immediately be made by automating the correction factor needed for the wavelength differences between the scintillometer and radar, accounting for humidity. Lastly, as an additional immediate improvement, robustness to the model can be achieved by adding a minimum temperature gradient, i.e. 0.01°C or 0.05°C , so that sharp, incorrect drops in optical turbulence are avoided.

Appendix A

MatLab source code for runTunickModel.m

```
%This function is the function that runs the Tunick model. It
%determines if the atmosphere is stable and then calls a pre defined
%function based on the stability. The inputs of this function are the
%standard meteorological data at the specified heights. The wavelength
%is in microns, pressure in millibars, height in meters, temperature in
%Kelvin, and windspeed in m/s. the variable variousHeight is the array
%of the heights of the atmosphere, or an array of heights from the
%initial level, to the specified height of the surface boundary layer.
```

```
function out = runTunickModel(wavelength, pressure, height1, temp1,
wspd1, rhum1, height2, temp2, wspd2, rhum2, variousHeight)
```

```
%% calculate the potential temperature difference
deltaPotTemp = (temp2-temp1)+(height2-height1).*0.0098;
```

```
%% calculate the specific humidities at each level
```

```
%convert the relative humidities to decimals
```

```
RH1 = rhum1./100;
RH2 = rhum2./100;
```

```
%find the saturation vapor pressure at each level
```

```
es1 = 6.11.*exp((2.453e6/461).*(1/273.15-1./temp1));
es2 = 6.11.*exp((2.453e6/461).*(1/273.15-1./temp2));
```

```
%find the vapor pressure at each level
```

```
e1=(RH1.*es1).*100;
e2=(RH2.*es2).*100;
```

```
%calculate the mixing ratio
```

```
mixRatio1 = .622.*e1./(pressure.*100-e1);
mixRatio2 = .622.*e2./(pressure.*100-e2);
```

```
%solve for the specific humidity
```

```
q1 = mixRatio1./(1+mixRatio1);
q2 = mixRatio2./(1+mixRatio2);
```

```
%find the difference
```

```
deltaq = q2-q1;
if(deltaq<0)
    deltaq=-deltaq;
end
```

```
%% calculate the virtual potential temperatures
```

```
virtPotTemp1 = temp1.*(1+.61.*q1);
```

```
%% calculate change in wind speed
```

```
deltaWind = wspd2-wspd1;
if(deltaWind<0)
```

```

        deltaWind=-deltaWind;
end

%% calculate scaling height used in similarity theory
scalingHeight = (height2-height1)./log(height2./height1);

%% calculate the scaling length used in similarity theory
scalingLength =
(virtPotTemp1.*deltaWind.^2)./(log(height2./height1).*9.81.*(deltaPotTemp+
.61.*temp1.*deltaq));

if(temp2>temp1)%the atmosphere is stable
    isStable=true;

    %calculate the change in the scaling length
    scalingLength = scalingLength.*(1-5.*scalingHeight);
else%the atmosphere is unstable
    isStable=false;
end

%% calculate the scaling ratio
scalingRatio = scalingHeight./scalingLength;

%% calculate the dimensionless lapse rates
if(isStable)%stable
    temperatureLapseRate = 1+5.*scalingRatio;
    windLapseRate = 1+5.*scalingRatio;
else%unstable
    temperatureLapseRate = (1-15.*scalingRatio).^-.5;
    windLapseRate = (1-15.*scalingRatio).^-.25;
end

%% calculate the friction velocity, temperature and humidity scaling
%% constants
    fricVel = .4.*deltaWind./(windLapseRate.*log(height2./height1));
    tempScaleConst =
.4.*deltaPotTemp./(temperatureLapseRate.*log(height2./height1));
    humScaleConst =
.4.*deltaq./(temperatureLapseRate.*log(height2./height1));

%% calculate the surface and latent heat fluxes
surfHeat = -1004.*tempScaleConst.*fricVel;
latentHeat = -2.5116e06.*fricVel.*humScaleConst;

%% obtain the gradients needed to calculate dndz
dThetadz =
tempScaleConst./(.4.*scalingHeight).*temperatureLapseRate;
dqdz = (humScaleConst./(.4.*scalingHeight)).*temperatureLapseRate;

%% calculate the dndz value for both anomalous dispersion and not
%% anomalous dispersion

%if the wavelength is greater than 19 microns, we only want the
%refractivity at 19 microns, thus we need to check

```



```

if wavelength>19
    sigma = 1./19;
    X=10./19;
else
    sigma = 1./wavelength;
    X=10./wavelength;
end

%calculate the variables used in the Ciddor/Tunick Equations
%dispersion formulas for CO2 and H2O
M1 = 23.7134+(6839.397./(130-sigma.^2))+(45.473/(38.9-sigma.^2));
M2 = 64.8731+(.58058.*sigma.^2)-
(.007115.*sigma.^4)+(.0008851.*sigma.^6);

alpha=temp1./273.15;
A = (-1.359.*alpha.^(-.6).*(X-1))./(1.03.*alpha.^17-
19.8.*X.^2+8.2.*X.^4-1.7.*X.^8)+(.5949.*alpha.^(-.43).*(X-
1))./((1.03.*alpha.^17-19.8.*X.^2+8.2.*X.^4-
1.7.*X.^8)+3.747E6./(12499-X.^2).^2);
B = ((957-928.*alpha.^4.*(X-1))./(1.03.*alpha.^17-
19.8.*X.^2+8.2.*X.^4-1.7.*X.^8)+3.747E6./(12499-X.^2));

%set the paths to include the HELEEOS files so the HITRAN database can
%be accessed
addpath(genpath('L:\enp students\HELEEOS\Heleeeos'));
heleeeosSetDefaults
heleeeosCalc

%initialize any arrays to be used
realIndex = zeros(size(wavelength));
baseRefract = zeros(size(wavelength));
realIndex2 = zeros(size(wavelength));
baseRefract2 = zeros(size(wavelength));

%get the base refractivity and anomalous dispersion data for the first
%level
for i = 1:length(wavelength)
    [abs sca realIndex(i) baseRefract(i) ] =
heleeeosCalcMolecularEffects2(wavelength(i)*1e-6,temp1,rhum1,pressure);
end

%get the base refractivity and anomalous dispersion data for the second
%level
for i = 1:length(wavelength)
    [abs2 sca2 realIndex2(i) baseRefract2(i)] =
heleeeosCalcMolecularEffects2(wavelength(i)*1e-6,temp2,rhum2, pressure);
end

%calculate the total refractivity including anomalous dispersion for
%both levels
refractivity=baseRefract;
refractivity2 = baseRefract2;
refractAnomDisp = baseRefract+realIndex;
refractAnomDisp2 = baseRefract2 + realIndex2;

```

```

    %using a derived pde from the original ciddor equation, substitute
in the refractivity for
    %anomalous dispersion
    if(wavelength>=.3 && wavelength<7.8)%visible to near infrared

        %calculate dn/dz without anomalous dispersion
        term1 = -refractivity./temp1;
        term1 = term1.*dThetadz;
        term2 = refractivity-M1.*pressure./temp1;
        term2 = term2.*dqdz;
        dndz = (term1+term2).*1e-6;

        %calculate dn/dz with anomalous dispersion
        termAnomDisp1 = -refractAnomDisp./temp1.*dThetadz;
        termAnomDisp2 = refractAnomDisp-M1.*pressure./temp1;
        termAnomDisp2 = termAnomDisp2.*dqdz;
        dndzAnomDisp = (termAnomDisp1+termAnomDisp2).*1e-6;
    else %anything beyond 7.8 microns

        %calculate dn/dz without anomalous dispersion
        termInf1 = (-
refractivity./temp1)+(1.60948.*M2.*pressure.*q1./(temp1.^2))+(.34875.*p
ressure.*q1.*A./temp1)-(.34875.*B.*pressure.*q1./(temp1).^2)-
(pressure.*q1./(2.87.*temp1)).*(.6135.*alpha.^(-
.83)./(1.03.*alpha.^17-19.8.*X.^2+8.2.*X.^4-1.7.*X.^8));
        termInf1 = termInf1.*dThetadz.*1e-6;
        termInf2 = refractivity-(M1.*pressure./temp1)-
(1.60948.*M2.*pressure./temp1)+.34875.*B.*pressure./temp1;
        termInf2 = termInf2.*dqdz.*1e-6;
        dndz = termInf1+termInf2;

        %calculate dn/dz with anomalous dispersion
        termAnomDispInf1 = (-
refractAnomDisp./temp1)+(1.60948.*M2.*pressure.*q1./(temp1.^2))+(.34875
.*pressure.*q1.*A./temp1)-(.34875.*B.*pressure.*q1./(temp1).^2)-
(pressure.*q1./(2.87.*temp1)).*(.6135.*alpha.^(-
.83)./(1.03.*alpha.^17-19.8.*X.^2+8.2.*X.^4-1.7.*X.^8));
        termAnomDispInf1 = termAnomDispInf1.*dThetadz.*1e-6;
        termAnomDispInf2 =refractAnomDisp-(M1.*pressure./temp1)-
(1.60948.*M2.*pressure./temp1)+.34875.*B.*pressure./temp1;
        termAnomDispInf2 = termAnomDispInf2.*dqdz.*1e-6;
        dndzAnomDisp = termAnomDispInf1+termAnomDispInf2;
    end

%% calculate the turbulent exchange coefficient for heat, and the
energy
%% dissipation rate
tecf = fricVel.*.4.*scalingHeight./temperatureLapseRate;
edr = fricVel.^3.*(windLapseRatescalingRatio)./(.4.*scalingHeight);

%% calculate the Cn2 value for the different heights

```

```

%calculate Cn2 based on the scaling height
Cn2 = 3.2.*(tecf./(edr.^(1/3))).*(dndz.^2);
Cn2AnomDisp = 3.2.*(tecf./(edr.^(1/3))).*(dndzAnomDisp.^2);

%using a known equation, apply the different heights in the atmosphere
if(isStable)
    Cn2 = Cn2.*(variousHeight./scalingHeight).^(-2/3);
    Cn2AnomDisp = Cn2AnomDisp.*(variousHeight./scalingHeight).^(-
2/3);
else
    Cn2 = Cn2.*(variousHeight./scalingHeight).^(-4/3);
    Cn2AnomDisp = Cn2AnomDisp.*(variousHeight./scalingHeight).^(-
4/3);
end

%create a cell array so both values can be returned
Cn2CellArray = {Cn2, Cn2AnomDisp};

    out = {dThetadz, dqdz, surfHeat, latentHeat, Cn2CellArray,
refractivity, refractivity2, refractAnomDisp, refractAnomDisp2};

```

MatLab source code for tunickGUI2.m

```
function tunickGUI2(varargin)
persistent hufnagelHandle noAnomHandle anomHandle handles;
global tunickData

if nargin == 0

    %% create the parent figure
    parent = figure('Name', 'McClung - Tunick Model', 'NumberTitle',
'Off');

    %% create the panels used in the GUI, one for the parameters,
level one and two data, the output data, the model options and the
graphs
    param = uipanel(parent, 'Title', 'Parameters',
'Units','normalized', 'Position', guiSubdivide(4, 3, 1, 1,.01,.01),
'tag', 'param');
    level1 = uipanel(parent, 'Title', 'Level 1 Meteorology','Units',
'normalized', 'Position', guiSubdivide(4, 3, 2, 1,.01,.01), 'tag',
'level1');
    level2 = uipanel(parent, 'Title', 'Level 2 Meteorology','Units',
'normalized', 'Position', guiSubdivide(4, 3, 3, 1, .01,.01), 'tag',
'level2');
    output = uipanel(parent, 'Title', 'Output/Results','Units',
'normalized', 'Position', guiSubdivide(4, 3, 4, 1, .01,.01), 'tag',
'output');
    models = uipanel(parent, 'Title', 'Model Options','Units',
'normalized', 'Position', guiSubdivide(4, 3, 4, 2:3, .01,.01), 'tag',
'models');
    graphs = uipanel(parent, 'Title', 'Graphs', 'Units', 'normalized',
'Position', guiSubdivide(4, 3, 1:3, 2:3,.01,.01), 'tag', 'graphs');

    %% create static text boxes labeling the edit text boxes for the
atmospheric parameters
    handles.st1 = uicontrol(param,'Style','text','String','Boundary
Layer Depth (m)','Units', 'normalized', 'Position', guiSubdivide(3, 2,
1:1, 1:1, .03, .03), 'tag', 'st1');
    handles.st2 = uicontrol(param,'Style','text','String','Wavelength
(microns)','Units', 'normalized', 'Position', guiSubdivide(3, 2, 2:2,
1:1, .03, .03), 'tag', 'st2');
    handles.st3 = uicontrol(param,'Style','text','String','Pressure
(mb)','Units', 'normalized', 'Position', guiSubdivide(3, 2, 3:3, 1:1,
.03, .03), 'tag', 'st3');

    %% create the edit boxes allowing for input of the atmospheric
parameters
    handles.et1 = uicontrol(param,'Style','edit','String','50','Units',
'normalized', 'Position',guiSubdivide(3, 2, 1:1, 2:2, .03, .03),
'callback', [mfilename, '('callback_et')'], 'backgroundcolor',
'white', 'tag', 'et1');
    handles.et2 =
uicontrol(param, 'Style', 'edit', 'String', '1.3153', 'Units',
```

```

'normalized','Position',guiSubdivide(3, 2, 2:2, 2:2, .03, .03),
'callback', [mfilename, '('callback_et')'], 'backgroundcolor',
'white', 'tag', 'et2');
handles.et3 =
uicontrol(param, 'Style', 'edit', 'String', '1000', 'Units',
'normalized', 'Position', guiSubdivide(3, 2, 3:3, 2:2, .03, .03),
'callback', [mfilename, '('callback_et')'], 'backgroundcolor',
'white', 'tag', 'et3');

%% create the static text boxes labeling the edit boxes for the
level 1 meteorology
handles.st4 = uicontrol(level1, 'Style', 'text', 'String', 'Height
(m)', 'Units', 'normalized', 'Position', guiSubdivide(4, 2, 1:1, 1:1,
.03, .03), 'tag', 'st4');
handles.st5 = uicontrol(level1, 'Style', 'text', 'String', 'Temperature
(K)', 'Units', 'normalized', 'Position', guiSubdivide(4, 2, 2:2, 1:1,
.03, .03), 'tag', 'st5');
handles.st6 = uicontrol(level1, 'Style', 'text', 'String', 'Relative
Humidity (%)', 'Units', 'normalized', 'Position', guiSubdivide(4, 2,
3:3, 1:1, .03, .03), 'tag', 'st6');
handles.st7 = uicontrol(level1, 'Style', 'text', 'String', 'Wind Speed
(m/s)', 'Units', 'normalized', 'Position', guiSubdivide(4, 2, 4:4, 1:1,
.03, .03), 'tag', 'st7');

%% create the edit text boxes for input of the level meteorology
data
handles.et4 = uicontrol(level1, 'Style', 'edit', 'String', '1', 'Units',
'normalized', 'Position', guiSubdivide(4, 2, 1:1, 2:2, .03, .03),
'callback', [mfilename, '('callback_et')'], 'backgroundcolor',
'white', 'tag', 'et4');
handles.et5 =
uicontrol(level1, 'Style', 'edit', 'String', '306.59', 'Units',
'normalized', 'Position', guiSubdivide(4, 2, 2:2, 2:2, .03, .03),
'callback', [mfilename, '('callback_et')'], 'backgroundcolor',
'white', 'tag', 'et5');
handles.et6 =
uicontrol(level1, 'Style', 'edit', 'String', '30.2', 'Units', 'normalized',
'Position', guiSubdivide(4, 2, 3:3, 2:2, .03, .03), 'callback',
[mfilename, '('callback_et')'], 'backgroundcolor', 'white',
'tag', 'et6');
handles.et7 =
uicontrol(level1, 'Style', 'edit', 'String', '5.39', 'Units', 'normalized',
'Position', guiSubdivide(4, 2, 4:4, 2:2, .03, .03), 'callback',
[mfilename, '('callback_et')'], 'backgroundcolor', 'white',
'tag', 'et7');

%% create the static text boxes labeling the edit boxes for the
level 2 meteorology
handles.st8 = uicontrol(level2, 'Style', 'text', 'String', 'Height
(m)', 'Units', 'normalized', 'Position', guiSubdivide(4, 2, 1:1, 1:1,
.03, .03), 'tag', 'st8');
handles.st9 = uicontrol(level2, 'Style', 'text', 'String', 'Temperature
(K)', 'Units', 'normalized', 'Position', guiSubdivide(4, 2, 2:2, 1:1,
.03, .03), 'tag', 'st9');

```

```

handles.st10 = uicontrol(level2,'Style','text','String','Relative
Humidity (%)','Units','normalized','Position',guiSubdivide(4,2,
3:3,1:1,.03,.03),'tag','st10');
handles.st11 = uicontrol(level2,'Style','text','String','Wind Speed
(m/s)','Units','normalized','Position',guiSubdivide(4,2,4:4,1:1,
.03,.03),'tag','st11');

%% create the edit text boxes allowing for the input of the level 2
meteorology
handles.et8 = uicontrol(level2,'Style','edit','String','4','Units',
'normalized','Position',guiSubdivide(4,2,1:1,2:2,.03,.03),
'callback',[mfilename,('callback_et')],'backgroundcolor',
'white','tag','et8');
handles.et9 =
uicontrol(level2,'Style','edit','String','304.57','Units',
'normalized','Position',guiSubdivide(4,2,2:2,2:2,.03,.03),
'callback',[mfilename,('callback_et')],'backgroundcolor',
'white','tag','et9');
handles.et10 =
uicontrol(level2,'Style','edit','String','32.9','Units','normalized',
'Position',guiSubdivide(4,2,3:3,2:2,.03,.03),'callback',
[mfilename,('callback_et')],'backgroundcolor','white',
'tag','et10');
handles.et11 =
uicontrol(level2,'Style','edit','String','6.35','Units','normalized',
'Position',guiSubdivide(4,2,4:4,2:2,.03,.03),'callback',
[mfilename,('callback_et')],'backgroundcolor','white',
'tag','et11');

%% create the static text boxes labeling the output edit text
boxes
handles.st12 =
uicontrol(output,'Style','text','String','Temperature Lapse Rate
(K/m)','Units','normalized','Position',guiSubdivide(4,2,1:1,1:1,
.03,.03),'tag','st12');
handles.st13 = uicontrol(output,'Style','text','String','Moisture
Lapse Rate (g/g/m)','Units','normalized','Position',guiSubdivide(4,
2,2:2,1:1,.03,.03),'tag','st13');
handles.st14 = uicontrol(output,'Style','text','String','Surface
Heat Flux (W/m^{2})','Units','normalized','Position',guiSubdivide(4,
2,3:3,1:1,.03,.03),'tag','st14');
handles.st15 = uicontrol(output,'Style','text','String','Latent
Heat Flux (W/m^{2})','Units','normalized','Position',guiSubdivide(4,
2,4:4,1:1,.03,.03),'tag','st15');

%% create the edit text boxes that will display the output of the
model
handles.et12 = uicontrol(output,'Style','edit','String','Edit
Text','Units','normalized','Position',guiSubdivide(4,2,1:1,2:2,
.03,.03),'callback','callback_et12','backgroundcolor','white',
'enable','off','tag','et12');
handles.et13 = uicontrol(output,'Style','edit','String','Edit
Text','Units','normalized','Position',guiSubdivide(4,2,2:2,2:2,
.03,.03),'callback','callback_et13','backgroundcolor',
'white','enable','off','tag','et13');

```

```

handles.et14 = uicontrol(output, 'Style', 'edit', 'String', 'Edit
Text', 'Units', 'normalized', 'Position', guiSubdivide(4, 2, 3:3, 2:2,
.03, .03), 'callback', 'callback_et14', 'backgroundcolor',
'white', 'enable', 'off', 'tag', 'et14');
handles.et15 = uicontrol(output, 'Style', 'edit', 'String', 'Edit
Text', 'Units', 'normalized', 'Position', guiSubdivide(4, 2, 4:4, 2:2,
.03, .03), 'callback', 'callback_et15', 'backgroundcolor',
'white', 'enable', 'off', 'tag', 'et15');

%% create the check boxes that allow the user to choose which model
to run
handles.checkBox1 =
uicontrol(models, 'Style', 'checkbox', 'String', 'Hufnagel Valley
(red)', 'Value', 0, 'Units', 'normalized',
'Position', guiSubdivide(3, 2, 1:1, 1:1, .03, .03), 'callback',
[mfilename, ('checkboxCallback')], 'tag', 'checkBox1');
handles.checkBox2 =
uicontrol(models, 'Style', 'checkbox', 'String', 'Model w/o Anom Disp
(blue)', 'Value', 0, 'Units', 'normalized',
'Position', guiSubdivide(3, 2, 2:2, 1:1, .03, .03), 'callback',
[mfilename, ('checkboxCallback')], 'tag', 'checkBox2');
handles.checkBox3 =
uicontrol(models, 'Style', 'checkbox', 'String', 'Model w/ Anom Disp
(green)', 'Value', 0, 'Units', 'normalized',
'Position', guiSubdivide(3, 2, 3:3, 1:1, .03, .03), 'callback',
[mfilename, ('checkboxCallback')], 'tag', 'checkBox3');

%% create the printable plot and write to excel buttons
handles.printPlot = uicontrol(models, 'Style', 'pushbutton',
'String', 'Printable Plot', 'Units', 'normalized', 'Position',
guiSubdivide(4, 2, 1:1, 2:2, .03, .03), 'callback',
[mfilename, ('printPlotCallback')], 'tag', 'printPlot');
handles.excelWrite = uicontrol(models, 'Style', 'pushbutton',
'String', 'Write to Excel', 'Units', 'normalized', 'Position',
guiSubdivide(4, 2, 2:2, 2:2, .03, .03), 'callback',
[mfilename, ('excelWriteCallback')], 'tag', 'excelWrite');
handles.refractPlot = uicontrol(models, 'Style', 'pushbutton',
'String', 'Plot Across Wavelengths', 'Units', 'normalized', 'Position',
guiSubdivide(4, 2, 3:3, 2:2, .03, .03), 'callback',
[mfilename, ('refractPlotCallback')] );
handles.sendToHeleeeos = uicontrol(models, 'Style', 'pushbutton',
'String', 'Send to HELEEOS', 'Units', 'normalized', 'Position',
guiSubdivide(4, 2, 4:4, 2:2, .03, .03), 'callback',
[mfilename, ('heleeeosCallback')]);

%% create axes such that the model and refractivity values can be
plotted
handles.tunick = axes('Parent', graphs, 'Units', 'normalized',
'Position', guiSubdivide(1, 10, 1:1, 1:4, .05, .07),
'tag', 'tunick', 'nextplot', 'add', 'xscale', 'log');
handles.refract = axes('Parent', graphs, 'Units', 'normalized',
'Position', guiSubdivide(1, 10, 1:1, 7:10, .05, .07),
'tag', 'refract', 'nextplot', 'add');

```

```

elseif nargin == 1
    switch lower(varargin{1})
        %% whenever an input is changed in an edit box, the axes need
to be
        %% cleared, the checkboxes need to be unchecked, and the output
edit boxes need to be disabled
        case 'callback_et'
            set(handles.checkBox1, 'value', 0);
            set(handles.checkBox2, 'value', 0);
            set(handles.checkBox3, 'value', 0);

            %clear the axes
            delete(get(handles.tunick, 'children'))
            delete(get(handles.refract, 'children'))

            set(handles.et12, 'string', 'Edit Text', 'enable', 'off');
            set(handles.et13, 'string', 'Edit Text', 'enable', 'off');
            set(handles.et14, 'string', 'Edit Text', 'enable', 'off');
            set(handles.et15, 'string', 'Edit Text', 'enable', 'off');

        case 'checkboxcallback'
            useHV = get(handles.checkBox1, 'value');
            useNoAnom = get(handles.checkBox2, 'value');
            useAnom = get(handles.checkBox3, 'value');

            %clear the axes
            delete(get(handles.tunick, 'children'))
            delete(get(handles.refract, 'children'))

            %Plot the first Axis
            if useHV == 1
                %get the heights from the edit boxes of the boundary
layer
                minHeight = str2double(get(handles.et4, 'string'));
                maxHeight = str2double(get(handles.et1, 'string'));

                %create an array of the heights for the Cn2 values to
be calculated
                variousHeight = linspace(minHeight, maxHeight);

                %calculate the Cn2 profile
                hufnagelValley = HufnagelValley(variousHeight,
21, 1.7E-14);

                hufnagelHandle = plot(handles.tunick,
hufnagelValley, variousHeight, 'r');
                xlabel(handles.tunick, 'Cn^{2} m^{-2/3}');
                ylabel(handles.tunick, 'Height (m)');
                title(handles.tunick, 'Cn^{2} profile');
            end

            %get the data for anom and no anom
            if useAnom || useNoAnom

```



```

        %get the data in order to make the plots
        data = getData(handles);
end

if useNoAnom == 1
    refract = data{8};
    anomRefract = data{9};

    noAnomHandle = plot(handles.tunick, data{6}, data{1});
    xlabel(handles.tunick, 'Cn^{2} m^{-2/3}');
    ylabel(handles.tunick, 'Height (m)');
    title(handles.tunick, 'Cn^{2} profile');

end

if useAnom == 1
    refract = data{8};
    anomRefract = data{9};

    anomHandle = plot(handles.tunick, data{7}, data{1}, 'g');
    xlabel(handles.tunick, 'Cn^{2} m^{-2/3}');
    ylabel(handles.tunick, 'Height (m)');
    title(handles.tunick, 'Cn^{2} profile');
end

%Plot the second axis and set the edit text boxes
if useAnom || useNoAnom
    height1 = str2double(get(handles.et4, 'string'));
    height2 = str2double(get(handles.et8, 'string'));

    plot(handles.refract, refract, [height1 height2]);
    plot(handles.refract, anomRefract, [height1 height2], 'g');
    xlabel(handles.refract, 'Refractivity');
    ylabel(handles.refract, 'Height (m)');

    legend(handles.refract, 'Base Refractivity', 'Anomalous Dispersion');
    title(handles.refract, 'Refractivity Between the Two Levels');

    %set the appropriate text boxes to display the flux results
    set(handles.et12, 'string', num2str(data{2}), 'enable', 'on');
    set(handles.et13, 'string', num2str(data{3}), 'enable', 'on');
    set(handles.et14, 'string', num2str(data{4}), 'enable', 'on');
    set(handles.et15, 'string', num2str(data{5}), 'enable', 'on');

end
case 'printplotcallback'
    figure

    useHV = get(handles.checkBox1, 'value');
    useNoAnom = get(handles.checkBox2, 'value');
    useAnom = get(handles.checkBox3, 'value');

```

```

        if useHV == 1
%get the heights from the edit boxes of the boundary layer
        minHeight = str2double(get(handles.et4,'string'));
        maxHeight = str2double(get(handles.et1,'string'));

%create an array of the heights for the Cn2 values to be calculated
        variousHeight = linspace(minHeight, maxHeight);

%calculate the Cn2 profile
        hufnagelValley = HufnagelValley(variousHeight, 21,1.7E-14);

        semilogx(hufnagelValley,variousHeight, 'r');
        hold on;
        xlabel('Cn^{2} m^{-2/3}');
        ylabel('Height (m)');
        title('Cn^{2} profile');
        end

        if useAnom || useNoAnom
%get the data in order to make the plots
                data = getData(handles);
        end

        if useNoAnom == 1
                semilogx(data{6}, data{1});
                hold on;
                xlabel('Cn^{2} m^{-2/3}');
                ylabel('Height (m)');
                title('Cn^{2} profile');
        end

        if useAnom == 1
                semilogx(data{7}, data{1}, 'g');
                hold on;
                xlabel('Cn^{2} m^{-2/3}');
                ylabel('Height (m)');
                title('Cn^{2} profile');

        end
        hold off;
        case 'excelwritecallback'
%get all of the data that needs to be exported to excel
                data = getData(handles);

%create cell arrays for labels of the data once it is in excel
        excelLabel = {'Height (m)', 'Cn2 w/o Anom Disp', 'Cn2 w/ Anom Disp'};
        excelLabel1 = {'Temp Gradient K/m'; 'Humidity Gradient g/g/m';
'Surface Heat Flux W/m^2'; 'Latent Heat Flux W/m^2'};

                height = data{1}';
                Cn2NoAnomColumn = data{6}';
                Cn2AnomColumn = data{7}';

```

```

        excelData = [height, Cn2NoAnomColumn, Cn2AnomColumn];
        excelData = num2cell(excelData);
        excelData = vertcat(excelLabel, excelData);
        xlswrite('Model Output', excelData);

        fluxes = [data{2}; data{3}; data{4}; data{5}];
        fluxes = num2cell(fluxes);
        fluxes = horzcat(excelLabel1, fluxes);
        xlswrite('Model Output', fluxes, 'Sheet1', 'E6:F9');

        msgbox('Thanks for waiting, the write to excel is
complete!', 'Excel Write');

    case 'refractplotcallback'
        pressure = str2double(get(handles.et3, 'string'));
        temp1 = str2double(get(handles.et5, 'string'));
        rhum1 = str2double(get(handles.et6, 'string'));
        refractivityPlot(pressure, temp1, rhum1);

    case 'heleeoscallback'
        data = getData(handles);
        Cn2Anom = data{7};
        height = data{1};
        tunickData.Cn2Anom = Cn2Anom;
        tunickData.height = height;
        close(gcf)
        pause(.05)
    end%switch
end%if-else statement

%% This function obtains all of the data from the text boxes. Then
gets the results from the model run.

function out = getData(handles)

persistent save
if isempty(save)
    save.minHeight = nan;
    save.maxHeight = nan;
    save.wavelength = nan;
    save.pressure = nan;
    save.height1 = nan;
    save.temp1 = nan;
    save.rhum1 = nan;
    save.wspd1 = nan;
    save.height2 = nan;
    save.temp2 = nan;
    save.rhum2 = nan;
    save.wspd2 = nan;
    save.out = nan;
end

%get the min and max heights for the surface boundary layer

```

```

minHeight = str2double(get(handles.et4,'string'));
maxHeight = str2double(get(handles.et1,'string'));

%obtain all of the parameters from the edit fields to send
%to the tunick model
wavelength = str2double(get(handles.et2,'string'));
pressure = str2double(get(handles.et3,'string'));
height1 = str2double(get(handles.et4,'string'));
temp1 = str2double(get(handles.et5,'string'));
rhum1 = str2double(get(handles.et6,'string'));
wspd1 = str2double(get(handles.et7,'string'));
height2 = str2double(get(handles.et8,'string'));
temp2 = str2double(get(handles.et9,'string'));
rhum2 = str2double(get(handles.et10,'string'));
wspd2 = str2double(get(handles.et11,'string'));

if (save.minHeight == minHeight)&&(save.maxHeight ==
maxHeight)&&(save.wavelength == wavelength)&&(save.pressure ==
pressure)&&(save.height1 == height1)&&(save.temp1 ==
temp1)&&(save.rhum1 == rhum1)&&(save.wspd1 ==wspd1)&&(save.height2 ==
height2)&&(save.temp2 == temp2)&&(save.rhum2 == rhum2)&&(save.wspd2 ==
wspd2)

    %if the inputs are the same
    out = save.out;
else
    %do the calculation (different input)
    %perform checks on the parameters to make sure the
    %model will run accurately
    if(height1<.5)
        errordlg('Sorry, the Tunick model does not run
correctly on initial heights less than .5 meters. Please enter an
initial height greater than .5');
        return;
    end

    if(height2<height1)
        errordlg('The second height must be greater than
the first. ');
        return;
    end

    if(pressure<5)
        errordlg('The Tunick model does not function
properly at the pressure specified. Please enter a pressure between
700 and 1060 millibars (hectoPascals). ');
        return;
    end

%create an array of the heights for the Cn2 values to be calculated
variousHeight = linspace(minHeight, maxHeight);

%calculate the Cn2, flux and lapse rate values using the tunick model

```

```

tunickResults = runTunickModel(wavelength, pressure,
height1, temp1, wspd1, rhum1, height2, temp2, wspd2,
rhum2, variousHeight);
dThetadz = tunickResults{1};
dqdz = tunickResults{2};
sfcHeat = tunickResults{3};
latentHeat = tunickResults{4};
Cn2 = tunickResults{5};
Cn2NOAnom = Cn2{1};
Cn2Anom = Cn2{2};
baseRefractivity1 = tunickResults{6};
baseRefractivity2 = tunickResults{7};
anomRefractivity1 = tunickResults{8};
anomRefractivity2 = tunickResults{9};

refract = [baseRefractivity1 baseRefractivity2];
anomRefract = [anomRefractivity1 anomRefractivity2];

out = {variousHeight, dThetadz, dqdz, sfcHeat,
latentHeat, Cn2NOAnom, Cn2Anom, refract, anomRefract};

%save the variables for later
save.out = out;
save.minHeight = minHeight;
save.maxHeight = maxHeight;
save.wavelength = wavelength;
save.pressure = pressure;
save.height1 = height1;
save.temp1 = temp1;
save.rhum1 = rhum1;
save.wspd1 = wspd1;
save.height2 = height2;
save.temp2 = temp2;
save.rhum2 = rhum2;
save.wspd2 = wspd2;
end

```

MatLab source code for McTunick.m

(only additions to runTunickModel.m are provided below)

```
function out = McTunick(time, wavelength, pressure, height1, temp1,
wspd1, rhum1, height2, temp2, wspd2, rhum2)
%%
                    McTunick
%
                    Optical Turbulence Model
%
    Plots CN2 vs time from thermocouple or weather station data
%
    Founded on principles from Tatarski & Similarity Theory
%
%
                    AFIT Fall 2008
%
                    V 2.1
%
% Acknowledgements: LtCol Steven Fiorino, Dr. Arnold Tunick, Brandon
% McClung, Matthew Krizo, Kenneth Moore, Thomas Harris, Rick Bartell
%
%
                    Jannette.Cohen@afit.edu
                    Steven.Fiorino.afit.edu

close all;
clear all;
%%

%%
                    Import Data from .xls file
numeric = xlsread('2008-31DEC-ALLDATA.xlsx', 'A4:O216');
time      = numeric(:,1);
wavelength = numeric(:,2);
pressure  = numeric(:,3);
height1   = numeric(:,4);
temp1     = numeric(:,6);
wspd1     = numeric(:,7);
rhum1     = numeric(:,8);
height2   = numeric(:,9);
temp2     = numeric(:,11);
wspd2     = numeric(:,12);
rhum2     = numeric(:,13);
CN2_BLS900 = numeric(:,14);
% Enables code to graph any adjustments to calculated CN2 -biasing
%CN2_Tunick = numeric(:,15);
.
.
.
%% calculate the Cn2 value for the different heights

%calculate Cn2 based on the scaling height
Cn2 = 3.2.*(tecf./(edr.^(1/3))).*(dndz.^2);
Cn2AnomDisp = 3.2.*(tecf./(edr.^(1/3))).*(dndzAnomDisp.^2);

%declare height variation interested in, linspace(a,b,n) creates an
%array of linearly spaced vectors with n values in the array
```

```

%    variousHeight = linspace(.6, 3,length(wavelength))';

%    %using a known equation, apply the different heights in the
atmosphere
%    if(isStable)
%        Cn2 = Cn2.*(variousHeight./scalingHeight).^(-2/3);
%        Cn2AnomDisp = Cn2AnomDisp.*(variousHeight./scalingHeight).^(-2/3);
%    else
%        Cn2 = Cn2.*(variousHeight./scalingHeight).^(-4/3);
%        Cn2AnomDisp = Cn2AnomDisp.*(variousHeight./scalingHeight).^(-4/3);
%    end
%I'm concerned with one height, the height of scintillometer-1.65m
if(isStable)
    Cn2 = Cn2.*(1.65./scalingHeight).^(-2/3);
    Cn2AnomDisp = Cn2AnomDisp.*(1.65./scalingHeight).^(-2/3);
else
    Cn2 = Cn2.*(1.65./scalingHeight).^(-4/3);
    Cn2AnomDisp = Cn2AnomDisp.*(1.65./scalingHeight).^(-4/3);
end

%create a cell array so both values can be returned
Cn2CellArray = {Cn2, Cn2AnomDisp};
Cn2

    out = {dThetadz, dqdz, surfHeat, latentHeat, Cn2CellArray,
refractivity, refractivity2, refractAnomDisp, refractAnomDisp2};
%% Graph CN2 vs Time
figure('visible','on');
semilogy(time,Cn2);
figure(2)
semilogy(time,CN2_BLS900);
%Plots adjusted CN2
%figure(3)
%semilogy(time,CN2_Tunick);

```

Appendix B

AFIT Scintillometer

```
%
%           A COHEN CODE
%           CN2 Intensity Variation - Rytov variance
%           Code based on Arnold Tunick (ARL) Journal Article
%           AFIT FALL 2008
%
%           Tunable Laser #1
%           Data Taken: 30 SEP, 7 OCT 2008
%
%           Jannette.Cohen@afit.edu           Christopher.Rice@afit.edu
%%%%%%%%%%%%%%%%%%%%%%%%%%%%%%%%%%%%%%%%%%%%%%%%%%%%%%%%%%%%%%%%%%%%%%%%
close all;
clear all;
%%
%%           Define Variables

% wavelength [meters]
lambda=760*10^-9;
% propogation path length [meters]
L1 = 2.62;
L2 = 0.5;
% aperture diameter
%D=0.0113; % use for 30 SEP data, use lower value for 7 OCT
D=0.0098;
%%           Import Data from .mat file
%load('2008-09-30-Jean3.mat');
load('2008-10-07-Jean-BE-3.mat');

volts1 = data(:,1);
volts2 = data(:,2);
time    = data(:,4);

%%           Find Scintillation Index
% 5000 data points per second
% intensity data taken for 180 seconds
for n = 1:1000:length(volts1);
    if n+999 <= length(volts1);
        a((n+999)/1000) = mean(volts1(n:(n+999)).^2);
        b((n+999)/1000) = (mean(volts1(n:(n+999)))).^2;
    else
        a((n+999)/1000) = mean(volts1(n:length(volts1)).^2);
        b((n+999)/1000) = (mean(volts1(n:length(volts1)))).^2;
    end;
end;
sigmaI = ((a-b)./b)';

for n = 1:1000:length(volts2);
    if n+999 <= length(volts2);
        c((n+999)/1000) = mean(volts2(n:(n+999)).^2);
        d((n+999)/1000) = (mean(volts2(n:(n+999)))).^2;
    else
        c((n+999)/1000) = mean(volts2(n:length(volts2)).^2);
```



```

        d((n+999)/1000) = (mean(volts2(n:length(volts2))))).^2;
    end;
end;
sigmaI2 = ((c-d)./d)';

%%           Aperature Averaging Correction
% Needs correction when D/2 is larger than Sqrt(L/k)
k = (2*pi)/lambda;
X1 = (1+0.33*(k*D^2/(4*L1))^(5/6))^(7/5);
X2 = (1+0.33*(k*D^2/(4*L2))^(5/6))^(7/5);

newsigmaI=X1*sigmaI;
newsigmaI2=X2*sigmaI2;
%%           For Weak Turbulence Case Find CN2

CN2=2*k^-(7/6)*L1^-(11/6)*newsigmaI

CN2_2=2*k^-(7/6)*L2^-(11/6)*newsigmaI2

noncorrectedCN2=2*k^-(7/6)*L1^-(11/6)*sigmaI;

noncorrectedCN2_2=2*k^-(7/6)*L2^-(11/6)*sigmaI2;

%%           Graph Figure of CN2 vs Time
%figure('visible','on');
x = time(1:1000:length(time));
%xlabel('Time (s)');
%ylabel('CN2 (m^-2/3)');
semilogy(x,CN2);
figure(2)
semilogy(x,CN2_2)

```

Appendix C

Running Average Macro in Excel

```
Sub GetT2()  
Dim i As Integer  
i = 0  
  
'Averages for the first T1 and T2'  
Range("E2").Value = "=AVERAGE(B2:B14)+$I$3"  
Range("F2").Value = "=AVERAGE(C2:C14)+$I$3"  
  
'Calculating averages for the remaining 59 cells of T1 and T2'  
For Each c In [F3:F217]  
    c.Offset(0, -1).Value = "=AVERAGE(B" & (i + 15) & ":B" & (i + 74) & ")+$I$3"  
    c.Value = "=AVERAGE(C" & (i + 15) & ":C" & (i + 74) & ")+$I$3"  
    c.Offset(0, -2).Value = "=A" & (15 + i)  
'This will shift the cells down 60 at a time in the B and C cols for every'  
'cell in E and F'  
    i = i + 60  
Next  
  
End Sub
```

Appendix D

Input Values for Laser Comm Sensitivity Study												
DESERT												
	Pressure	Wind ExPERT (kts)	Wind (m/s)	Level1 (m)	T1 (K)	Hum1 (%)	W1 (m/s)	Level2 (m)	T2 grad	Hum2 (%)	W2 (m/s)	
Nellis AFB, LV												
June_0000-0300	1009.82	4.08	2.09893152	1.25	295.9278	21	0.2623664	4.25	.5, 1, 1.5	23	0.8920459	
June_0900-1200	1011.5	7.97	4.10011868	1.25	309.8167	11	0.5125148	4.25	1.5, 2, 2.5	13	1.74255044	
June_1200-1500	1009.33	9.91	5.09814004	1.25	310.3722	10	0.6372675	4.25	2, 2.5, 3	12	2.16670952	
JAN_0000-0300	1019.98	1.94	0.99802136	1.25	277.0389	55	0.1247527	4.25	.5, 1, 1.5	57	0.42415908	
JAN_0900-1200	1019.3	4.08	2.09893152	1.25	286.4833	28.5	0.2623664	4.25	1.5, 2, 2.5	30.5	0.8920459	
JAN_1200-1500	1018.3	5.05	2.5979422	1.25	287.0389	27	0.3247428	4.25	2, 2.5, 3	29	1.10412544	
MID-LAT												
WPAFB, OH												
June_0000-0300	1015.917	1.94	0.99802136	1.25	290.9278	84	0.1247527	4.25	.5, 1, 1.5	86	0.42415908	
June_0900-1200	1016.255	6.99	3.59596356	1.25	299.2611	53	0.4494954	4.25	1, 1.5, 2	55	1.52828451	
June_1200-1500	1015.239	6.99	3.59596356	1.25	299.8167	48	0.4494954	4.25	1.5, 2, 2.5	50	1.52828451	
JAN_0000-0300	1018.964	6.02	3.09695288	1.25	269.8167	81	0.3871191	4.25	.5, 1, 1.5	83	1.31620497	
JAN_0900-1200	1011.852	8.94	4.59912936	1.25	273.15	69	0.5748912	4.25	1, 1.5, 2	71	1.95462998	
JAN_1200-1500	1011.175	8.94	4.59912936	1.25	273.15	67	0.5748912	4.25	1.5, 2, 2.5	69	1.95462998	
HUMID												
Eglin AFB, FL												
June_0000-0300	1015.577	1.94	0.99802136	1.25	297.0389	87	0.1247527	4.25	.5, 1, 1.5	89	0.42415908	
June_0900-1200	1017.271	7.97	4.10011868	1.25	303.15	62	0.5125148	4.25	1, 1.5, 2	64	1.74255044	
June_1200-1500	1015.577	8.94	4.59912936	1.25	302.5944	64	0.5748912	4.25	1.5, 2, 2.5	66	1.95462998	
JAN_0000-0300	1020.657	4.86	2.50019784	1.25	280.9278	85	0.3125247	4.25	.5, 1, 1.5	87	1.06258408	
JAN_0900-1200	1016.932	7.97	4.10011868	1.25	287.5948	59.5	0.5125148	4.25	1, 1.5, 2	61.5	1.74255044	
JAN_1200-1500	1019.98	7.97	4.10011868	1.25	288.15	60	0.5125148	4.25	1.5, 2, 2.5	62	1.74255044	

Bibliography

- Andrews, L. C., & Phillips, R. L. (2005). *Laser beam propagation through random media* (2nd ed.). Bellingham, WA: SPIE.
- Born, M., & Wolf, E. (1975). *Principles of optics* (5th ed.). Oxford: Pergamon.
- Bradshaw, P. (1996). Of cream and clouds. *TimesHigherEducation*. Retrieved December 10, 2008, from <http://www.timeshighereducation> Last updated November 8, 1996. Emeritus professor of engineering, Stanford University.
- Ciddor, P. E. (1996). Refractive index of air: new equations for the visible and near infrared. *Applied Optics*, 35(9), 1566-1573.
- Ciddor, P. E. (1999). Refractive index of air. 2. group index. *Applied Optics*, 38(9), 1663-1667.
- Ciddor, P. E. (2002). Refractive index of air: 3. the roles of CO₂, H₂O, and refractivity virials. *Applied Optics*, 41(12), 2292-2298.
- Doviak, R. J., & Zrnic, D. S. (2006). Measurements of turbulence and observations of fair weather. *Doppler radar and weather observations* (2nd ed., pp. 386-505). Mineola, NY: Dover Publications.
- Fiorino, S. T., Bartell, R. J., Krizo, M. J., Caylor, G. L., Moore, K. P., Harris, T. R., et al. (2008). A first principles atmospheric propagation & characterization tool - the laser environmental effects definition and reference (LEEDR). *SPIE*, 6878 (68780B).
- Fitzgerald, J. W., & Hoppel, W. A. (1982). The size and scattering coefficient of urban aerosol particles at Washington, DC as a function of relative humidity. *Journal of Atmospheric Sciences*, 39, 1838-1852.
- Good, E. R., Watkins, B. J., Quesada, A. F., Brown, J. H., Loriot, G. B. (1982). Radar and optical measurements of C_n². *Applied Optics*, 21 (18), 3373-76.
- Gravley, L. E., Fiorino, S. T., Bartell, R. J., Perram, G. P., Drizo, M. J., & Le, K. B. (Fall 2007). Comparison of climatological optical turbulence profiles to standard, statistical, and numerical models using HELEEOS. *Journal of Directed Energy*, 2(4), 347-362.
- Jumper, G. Y., Vernin, J., Azoit, M., & Trinquet, H. (2005). Comparison of recent measurements of atmospheric optical turbulence. Toronto, Ontario. , 4778
- Kohsiek, W. (1985). A comparison between line-averaged observation of C_n² from scintillation of a CO₂ laser beam and time-averaged *in situ* observations. *Journal of Climate and Applied Meteorology*, 24, 1099-1103.

- Lemery, J. M. (2006). Electro-optic sensor detection via optically augmented retroreflections. (M.S., Air Force Institute of Technology).
- Liou, K. N. (2002). An introduction to atmospheric radiation. (2nd ed.,). San Diego, CA: Academic Press.
- Martin, F., et al. (2000). Optical parameters relevant for high angular resolution at Paranal from GSM measurement and surface layer contribution. *Astron. Astrophys. Suppl. Ser.*, 144, 39-44.
- Mathar, R. J. (2004). Calculated refractivity of water vapor and moist air in the atmospheric window at 10 micrometers. *Applied Optics*, 43(4), 928-932.
- Max, C. (2008). *Lecture 4: Propagation of light through atmospheric turbulence*. Retrieved August 21, 2008, from http://www.ucolick.org/~max/289C/Lectures/Lecture%204/Lecture4_v1.ppt
- McClung, B. et al. (Summer 2008). *Optical turbulence: accurately modeling the index of refraction structure parameter in the surface boundary layer*. AFIT/CDE Internal Report.
- Mishchenko, Y. V. (1998). Laser interference refractometer for monitoring the absolute index of refraction of air. *Measurement Techniques*, 41(4), 334-342.
- Moene, A. F., Meijninger, W. M. L., Hartogensis, O. K., Kohsiek, W., & de Bruin, H. A. R. (2005). *A review of the relationships describing the signal of a large aperture scintillometer*. No. 2004/2. Wageningen Universiteit, The Netherlands: Meteorology and Air Quality Group.
- Morgan, Laura. (2006). *Spectrometers*. Retrieved November 15, 2008, from <http://www.abdn.ac.uk/~u20lm5/px2013/app2.htm>. Last updated December 19, 2006. Department of Physics, University of Aberdeen, Scotland.
- Owens, J. C. (1967). Optical refractive index of air: dependence on pressure, temperature and composition. *Applied Optics*, 6(1), 51-59.
- Panofsky, H. A. (1968). The structure constant for the index of refraction in relation to the gradient of index of refraction in the surface layer. *J. Geophys. Res.*, 73, 6047-6049.
- Petty, G. W. (2006). *A first course in atmospheric radiation* (2nd ed.). Madison, WI: Sundog Publishing.
- Poggio, L. P., Furger, M., Prevot, Andre S. H., & Graber, W. K. (2000). Scintillometer wind measurements over complex terrain. *Journal of Atmospheric and Oceanic Technology*, 17, 17-26.

- Rachele, H., Tunick, A., & Hansen, F. A. (1995). MARIAH - A similarity-based method for determining wind, temperature, and humidity profile structure in the atmospheric surface layer. *J. Appl. Meteor.*, 34, 1000-1005.
- Rothman, L. S. et al. (2005). The HITRAN molecular spectroscopic database and HAWKS (HITRAN atmospheric workstation) 2004 edition. *Journal of Quantitative Spectroscopy & Radiative Transfer*, 96, 139-204.
- Tatarski, V. I. (1961). *Wave propagation in a turbulent medium*. New York - Toronto - London: McGraw-Hill Book Company, Inc.
- Tatarski, V. I. (1971). *The effects of the turbulent atmosphere on wave propagation*. (NIST Technical Translation 68-50464 Trans.). Jerusalem: Israel Program for Scientific Translations.
- Tunick, A., Rachele, H., & Miller, W. B. (1991). C_n^2 estimates in the boundary layer for damp unstable conditions. *SPIE Propagation Engineering: Fourth in a Series*, 1487, 51-62.
- Tunick, A., & Rachele, H. (1992). Estimating effects of temperature and moisture on C_n^2 in the damp unstable boundary layer for visible, infrared, radio, and millimeter wavelengths. *SPIE Atmospheric Propagation and Remote Sensing*, 1688, 465-476.
- Tunick, A. (2003). CN2 model to calculate the micrometeorological influences on the refractive index structure parameter. *Environmental Modeling & Software*, 18, 165-171.
- Tunick, A. (2005). Improving future optical turbulence calculations. *SPIE proceedings* 5981.
- Tunick, A., Vorontsov, M., Carhart, G., & Tikhonov, N. (2005). *Characterization of optical turbulence (C_n^2) data measured at the ARL A_Lot facility*. Report No. ARL-MR-625. Adelphi, MD: Army Research Laboratory.
- Tunick, A. (2007). Statistical analysis of measured free-space laser signal over a 2.33 km optical path. *Optics Express*, 15(21) 14115-22.
- Tunick, A. (2008a). *Army overland optical turbulence (C_n^2) model*. Report No. ARL-TN-0318). Adelphi, MD: Army Research Laboratory.
- Tunick, A. (2008b). Optical turbulence parameters characterized via optical measurements over a 2.33 km free-space laser path. *Optics Express*, 16(19) 14645-54.
- Scintec. (2008). *Boundary layer scintillometer user's manual: BLS450, BLS900, BLS2000*. Tübingen, Germany: Scintec Co.

- Wallace, J. M., & Hobbs, P. V. (2006). The atmospheric boundary layer. *Atmospheric science: An introductory survey* (2nd ed., pp. 375-417). Burlington, MA: Academic Press.
- Yee, Y. P., Sutherland, R. A., Rachele, H., & Tunick, A. (1993). Effect of aerosol induced radiative interactions of atmospheric stability and optical turbulence. *SPIE Atmospheric Propagation and Remote Sensing II*, 1968, 192-201.

REPORT DOCUMENTATION PAGE				<i>Form Approved OMB No. 074-0188</i>	
<p>The public reporting burden for this collection of information is estimated to average 1 hour per response, including the time for reviewing instructions, searching existing data sources, gathering and maintaining the data needed, and completing and reviewing the collection of information. Send comments regarding this burden estimate or any other aspect of the collection of information, including suggestions for reducing this burden to Department of Defense, Washington Headquarters Services, Directorate for Information Operations and Reports (0704-0188), 1215 Jefferson Davis Highway, Suite 1204, Arlington, VA 22202-4302. Respondents should be aware that notwithstanding any other provision of law, no person shall be subject to a penalty for failing to comply with a collection of information if it does not display a currently valid OMB control number.</p> <p>PLEASE DO NOT RETURN YOUR FORM TO THE ABOVE ADDRESS.</p>					
1. REPORT DATE (DD-MM-YYYY) 26-03-2009		2. REPORT TYPE Master's Thesis		3. DATES COVERED (From – To) March 2008 – March 2009	
4. TITLE AND SUBTITLE Demonstration and Verification of a Broad Spectrum Anomalous Dispersion Effects Tool for Index of Refraction and Optical Turbulence Calculations				5a. CONTRACT NUMBER	
				5b. GRANT NUMBER	
				5c. PROGRAM ELEMENT NUMBER	
6. AUTHOR(S) Cohen, J. Jean, Captain, USAF				5d. PROJECT NUMBER	
				5e. TASK NUMBER	
				5f. WORK UNIT NUMBER	
7. PERFORMING ORGANIZATION NAMES(S) AND ADDRESS(S) Air Force Institute of Technology Graduate School of Engineering and Management (AFIT/EN) 2950 Hobson Way, Building 640 WPAFB OH 45433-7765				8. PERFORMING ORGANIZATION REPORT NUMBER AFIT/GAP/ENP/09-M03	
9. SPONSORING/MONITORING AGENCY NAME(S) AND ADDRESS(ES) Intentionally left blank.				10. SPONSOR/MONITOR'S ACRONYM(S)	
				11. SPONSOR/MONITOR'S REPORT NUMBER(S)	
12. DISTRIBUTION/AVAILABILITY STATEMENT APPROVED FOR PUBLIC RELEASE; DISTRIBUTION UNLIMITED.					
13. SUPPLEMENTARY NOTES					
14. ABSTRACT An atmospheric optical turbulence strength model with a broad wavelength range of 355nm (ultraviolet) to 8.6m (radio frequencies) has been created at AFIT and implemented into the High Energy Laser End-to-End Operational Simulation tool (HELEEOS). This modeling and simulation tool is a first principles atmospheric propagation and characterization model. Within HELEEOS lies the High-Resolution Transmission Molecular Absorption (HITRAN) database, containing 1,734,469 spectral lines for 37 different molecules as of version 12.0 (2004). HITRAN affords HELEEOS incredible accuracy for electromagnetic (EM) propagation prediction. A full understanding of optical turbulence is needed to successfully predict EM radiation propagation, particularly within the application of high energy laser weapon systems. Existing models for optical turbulence do not encompass wide ranges of wavelengths, nor do they include anomalous dispersion effects. Both of these additions have been incorporated into AFIT/CDE's new optical turbulence strength model. This thesis's objective is to verify and demonstrate the optical turbulence prediction tool. This tool enables predictions to occur in notoriously difficult regions of the spectrum to measure (i.e. Terahertz). One can measure optical turbulence at one wavelength and accurately determined optical turbulence at a different wavelength based on the relation of the vertical gradient of the index of refraction to optical turbulence.					
15. SUBJECT TERMS Index of Refraction, Optical Turbulence, Anomalous Dispersion, Scintillometers, High Energy Laser (HEL), Modeling and Simulation					
16. SECURITY CLASSIFICATION OF:			17. LIMITATION OF ABSTRACT UU	18. NUMBER OF PAGES 106	19a. NAME OF RESPONSIBLE PERSON LtCol Steven T. Fiorino (ENP)
REPORT U	ABSTRACT U	c. THIS PAGE U			19b. TELEPHONE NUMBER (Include area code) (937) 255-3636 x 4506 steven.fiorino@afit.edu

Standard Form 298 (Rev: 8-98)
Prescribed by ANSI Std. Z39-18